Montanuniversität Leoben
Department Product Engineering
Lehrstuhl für Allgemeinen Maschinenbau

Competence Centers for Excellent Technologies

Crack propagation analysis of welded joints by numerical and experimental investigations

Diplomarbeit

FAHEEM SHAH

Leoben, 2015

Eidesstattliche Erklärung

Ich erkläre an Eides statt, dass ich diese Arbeit selbständig verfasst, andere als die angegebenen Quellen und Hilfsmittel nicht benutzt und mich auch sonst keiner unerlaubten Hilfsmittel bedient habe.

AFFIDAVIT

I declare in lieu of oath, that I wrote this thesis and performed the associated research myself, using only literature cited in this volume.

Datum Unterschrift

Acknowledgements

This master thesis (Diplomarbeit) has been conducted at the Chair of Mechanical Engineering of the Montanuniveristät Leoben Austria, since summer 2014. I would like to acknowledge all those brains that have been a kind support in completion of this thesis. It is therefore of my greatest pleasure to express my gratitude to all of them in this acknowledgement.

First and foremost I wish warmest gratitude to the head of the institute, Univ.-Prof. Dipl.-Ing. Dr.mont Florian Grün, who has given me the opportunity to conduct my diploma thesis in his research group under his excellent leadership and friendly working environment.

My heart full thanks go to my advisor Associate.-Prof. Dipl.-Ing. Dr.mont. Michael Stoschka for his guidance, generous contribution of knowledge, experience, valuable comments and encouragement from the start till the end of my diploma thesis.

I would like to pay special thanks to my co-advisor Dipl.-Ing.Dr.mont Martin Leitner for his kind cooperation, friendly guidance with a great care, discussions and comments which helped me to bring this thesis successfully to an end.

Special thank to my co-advisors Dipl.-Ing. David Simunek. He is a person, who was always there to help me learning to work with software's, literature survey, experimental and microscopic work.

I want to use this opportunity to say words of thanks to Dipl.-Ing. Dr.mont. István Gódor, Dr.mont. MSc. Kartik Pondicherry, Dipl.-Ing. Markus Ottersböck, Dipl.-Ing. Tim Haslinger, Dipl.-Ing. Florian Summer, Martina Höfler, Stefan Gerstbrein, Melanie Waltritsch and Edith Wolfgruber for their courage and kind support.

I would like to acknowledge the financial support from the Bundesministerium für Europa, Integration und Äußeres (BMEIA) for considering me for their Scholarship program.

Special thanks for financial support by the Austrian Federal Government (in particular from Bundesministerium für Verkehr, Innovation und Technologie and Bundesministerium für Wirtschaft, Familie und Jugend) represented by Österreichische Forschungsförderungsgesellschaft mbH and the Styrian and the Tyrolean Provincial Government, represented by Steirische Wirtschaftsförderungsgesellschaft mbH and Standortagentur Tirol, within the framework of the COMET Funding Programme is gratefully acknowledged.

My parents, Syed Fida Shah and Bushra Fatima receive my deepest gratitude and love for their dedication and the many years of support during my studies that provided the foundation for this work.

Last, but not least, I would like to thank my wife Asta SHAH for her understanding and love during the past few years. Her support and encouragement was in the end what made this thesis possible.

Kurzfassung

Das Ermüdungrisswachstum ist wesentlich zur Bewertung und Beurteilung der Bauteilfestigkeit und Lebensdauer maschinenbaulicher Komponenten. Das Ziel dieser Diplomarbeit ist eine numerische, analytische und experimentelle Analyse des Rissfortschritts bei geschweißten Verbindungen. Eine vergleichende Studie unter Anwendung der SoftwarePakete Franc2D und nCode erfolgt für unterschiedliche strukturelle Details. Besonderer Fokus liegt dabei auf einem Kantenriss in einer Platte und Schweißverbindungen mit nicht-tragenden und last-tragenden Quersteifen. Dies ermöglicht einen Vergleich zu kürzlich veröffentlichten IIW-Ergebnissen. Die Bewertung mit Franc2D führt dabei aufgrund benutzerabhängiger Integrationseinstellungen zu etwas konservativeren Werten. Im Fall von nCode ist eine genaue analytische Berechnung des Spannungintensitätsfaktors SIF Voraussetzung, wobei auch hier die Resultate eine gute Übereinstimmung zeigen.

Die experimentelle Arbeit konzentriert sich auf die Durchführung und mikroskopische Analyse von Ermüdungsversuchen bei variablen Blocklasten, mit und ohne Überlast. Die untersuchten T-Stoß Proben weisen dabei eine Grundmaterialfestigkeit von niederfestem Baustahl S355 bis zu höherfestem Feinkornstahl S690 auf. Einzelne Überlasten führen zu makroskopische Rastlinien, welche im Lichtmikroskop gut zu erkennen sind. Um die Schwingstreifen innerhalb der polykristallinen Mikrostruktur zu detektieren, wurde Rasterelektronmikroskopie eingesetzt. Die charakteristischen Rastlinien und Schwingstreifen sind gut erkennbar und entsprechen den Ergebnissen der numerisch ermittelten Rissfortschrittsanalyse.

Abschließend erfolgt eine umfangreiche Parameterstudie von numerischen Franc2D Berechnungen unter Berücksichtigung zahlreicher verschiedener Materialparameter aus Richtlinien und der Literatur. Es zeigt sich, dass die Anfangsrisslänge der wesentlichste Faktor für den weiteren Rissfortschritt und die Lebensdauer ist. Eine detaillierte Studie über die Anfangsrisslänge zeigt, dass ein Wert von 0,01mm für die Ermüdungsversuche der hochfesten Stahlverbindung gut anwendbar ist. Ein Vergleich zwischen den Simulationen und experimentellen Ergebnissen beweist, dass alle Rissfortschrittsparameter zu einer sicheren Auslegung führen, wenn die Anfangsrisslänge nicht kleiner als dieser Wert gewählt wird. Zusammengefasst kann festgehalten werden, dass die ausgewerteten Materialparameter eine Lebensdauerspanne aufweisen, welche innerhalb des empfohlenen Streubereichs für geschweißte Verbindungen ist.

Abstract

The study of fatigue crack growth is an important issue to assess the fatigue strength of engineering components and service life. The aim of this master thesis is a numerical, analytical and experimental analysis of crack propagation in welded joints. A comparative study by the aid of the software packages Franc2D and nCode is performed for different structural details. Special focus is laid on a standard single edge crack plate, and welded joints ranging from non-load carrying to partial penetrated load-carrying transversal stiffeners. This enables a direct comparison to recently published results by the IIW-community. Thereby, the assessment based on Franc2D is slightly conservative because of the user-dependent internal integration procedure settings. In case of the tool nCode, an accurate analytical calculation of the stress intensity factor SIF is necessary and the results are in good accordance to the Round robin IIW-results.

The experimental work focuses on testing and microscopic evaluation of block constant amplitude fatigue tests with and without overloads. The investigated material ranges from common construction steel S355 to high-strength steel S690. Single overloads cause macroscopic beachmarks which are detectable by LOM, but striation markers within the polycrystalline microstructure are only recognisable by SEM. For the investigated specimens characteristic striation markers are evaluated and basically match the numerically obtained crack propagation results.

Finally, an extensive set of numerical Franc2D calculations are performed using numerous different material parameters given by state-of-the-art guidelines, recommendations and published literature. Thereby, it is shown that the initial crack length is the most important factor for crack propagation and total life time. A detailed study of the initial crack length exhibited that a value of 0.01mm is well applicable for the fatigue-tested high strength steel specimens. A comparison between simulation and experimental results proves that all crack growth parameters lead to a safe design if the initial crack length is not lower than this value. Summarized, for such a defined minimum crack length, all evaluated material parameters exhibit a fatigue life which is below the recommended scatter range of welded structures and therefore the investigated methods are well applicable for a conservative fracture mechanical assessment.

Contents

Nomenclature

Notation	Meaning
B	Plate thickness
C	Compliance
da	Crack extension
E	Total energy
F	Work
f	Frequency
G	Energy release rate
G_c	Fracture toughness
K_I	Stress intensity factor mode I
K_{II}	Stress intensity factor mode II
K_{III}	Stress intensity factor mode III
n	Strain-hardening exponent
P	Load
S_{max}	Maximum elastic stress
U*	Complimentary strain energy
U	Strain energy
Ws	Work done
W_f	Fracture energy
Y	Geometry factor
Υ_p	Plastic work per unit area
Υ_s	Surface energy
Δ	Displacement
σ_{YS}	Remote tensile stress
σ_a	Applied Stress
τ	Shear stress
ε	Strain

σ	Stress
ρ	Root radius
υ	Poison's ratio
Π	Potential energy
Π_o	Potential energy of uncracked plate

1. Introduction and aim of the work

Introduction

Fracture mechanics characterizes the fracture behaviour of defective structural components based on stress analysis in the vicinity of a notch or crack. Many large, complex structures such as bridges, ships, buildings, aircraft, and pressure vessels can have cracks, imperfections, sharp notches or various kinds of discontinuities. Using the basic concept of liner elastic fracture mechanics, the stress field ahead a sharp crack is characterized with a single parameter known as the stress intensity factor K_I. Cyclic loading causes local weakening of the material, for example by means of persistent slip bands leading to crack initiation at the microscopic level, coalescence of such microcracks to a macroscopic crack and subsequent propagation as long-crack growth until failure burst failure. A microscopic crack starts at mostly stressed areas to grow, when the applied load reaches a certain threshold value. Mostly stressed concentrated areas are surfaces, where failure mechanism can be deduced to originating of slip bands out of the smooth surface, or microscopic discontinuities such as grain boundaries or existence of inclusions such as carbides or heterogeneous weak material zones such as manganese-sulfides in carbon-steels. The study of fatigue crack growth is therefore important in fatigue strength of engineering components and their service life.

Welded joints are used as an integral part in many complex loaded carrying structures. The geometrical discontinuity of weld joints enforces a high stress concentration factor at the weld notch. In addition, the weld process induces in general high tensile residual stresses which support crack growth due to the influence of stress ratio on the effective stress intensity factor. Finally, welded joints – even produced in good-workmanship - always possess a statistically observed amount of imperfections or defects. In technical engineering, these defects are not always measurable because such failures are often below the non-destructively measureable characteristic length of one millimetre. Hence, it is of interest to determine the amount of lifetime spent until the crack propagates to a characteristic length of one millimetre, especially for thin-walled sheets.

Fatigue failures of welded joints originate at high stress concentration points, such as the weld toe and weld root. Cyclic loading and stress concentration cause crack initiation and propagation in the vicinity of welds during service life. A crack can initiate and propagate even if the applied stress is well below the yield strength. The weld toe and weld roots are the region where high stress concentration occur which make these points weak to initiate a crack (Motarjemi et al. 2000).

The peak stresses at the weld toe can be calculated using stress concentration factors, available in the literature, and appropriate reference stresses of the structural weld detail. These stress concentration factors are unique for given geometry and mode of loading. The fracture mechanical approach is the most local design concept and enables the design engineer to study both the remaining life time as well as the influence of local geometry property such as weld root radius or wall thickness in a unique manner. This gathered information can be used to derive thickness or misalignment factors for more global approaches such as the notch stress, structural and nominal stress approach. The state-of-the-art design concepts for the design and analysis of welded components under cyclic loading are given by the IIW-recommendations (Hobbacher 2009) or the fracture mechanical guideline published by the FKM (Forschungskuratorium Maschinenbau 2001).

Aim of the work

This work summarizes the author's investigaiton to the application of fracture mechanics to high-strength steel joints. The application of numeric crack propagation analysis has to be shown for non-load carrying transversal attachments made of common construction and high-strength steel.

- At first, the chosen numerical tools have to be verified against the fracture-mechanical IIW Round-Robin test results.
- Second, the influence of material parameters on crack propagation has to be benchmarked against the experimental work, leading to a recommendation about initial crack size for high-quality welds.
- Finally, some fatigue tests on T-joints have to be carried out to compare the theoretically derived crack propagation lifetime to experimentally observed constant-amplitude fatigue test results.

2. State of the art

2.1. Fundamentals of fracture mechanics

Fracture mechanics is a field of mechanics that deals with crack propagation under loading in a material of a structure. To improve performance of mechanical components fracture mechanics plays a big role in modern material science and mechanical engineering. It correlates analytical investigation of crack propagation with related experimental work and characterizes material resistance to fracture. Such analytical investigation is done by calculating parameters like stress intensity factor at the crack tip. Stress intensity factor is further used to determine the crack growth rate. Each applied cyclic load cause an increase in crack length.

Fracture mechanics is divided into linear elastic fracture mechanics (LEFM) and elasto-plastic fracture mechanics (EPFM). LEFM is a design methodology applicable under elastic conditions to deal with brittle-elastic materials such as high-strength steel, glass, ice, and concrete (Shukla 2005). On the other hand, EPFM is valid for materials that exhibit non-linear stress-strain behaviour, as for example low-carbon steel, stainless steel, and certain aluminium alloys (Anderson 2005).

2.1.1. Crack propagation modes

A crack is propagated according to the way a force is applied to material. There are basically three crack propagation modes, as shown in Fig. 2.1.

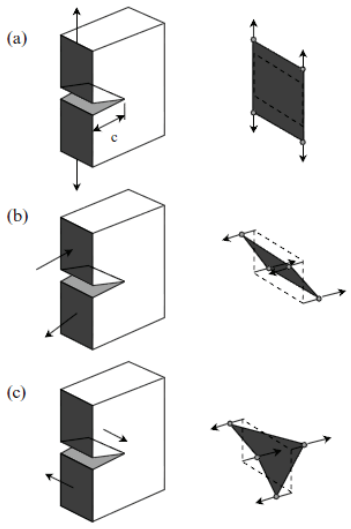

Fig. 2.1: The three fracture modes (Fischer-Cripps 2007)

- **Mode I - Opening mode**

The applied force acts perpendicularly to the fracture surface and pulls the crack surfaces away from each other. The crack extends horizontally while the force acts in vertical direction. This kind of fracture mode is called opening mode (Schmid 2013).

- **Mode II - Sliding mode**

In this mode, the applied force acts parallel to the crack. One force pushes the lower part of crack surface and other pulls the upper part or vice versa. These forces cause a shear crack and tend the crack to propagate in its own direction. This mode of crack propagation is also known as in–plane shear (Schmid 2013).

- **Mode III - Tearing mode**

In this mode, forces acts parallel to the crack surface and pulls the upper and lower half parts in opposite directions (left, right). These forces cause the material to separate and slide out of its original plane. For this reason this mode of crack propagation is also called out-of-plane shear (Schmid 2013).

2.1.2. Linear elastic fracture mechanics (LEFM)

2.1.2.1. Stress concentration

Inglis (Inglis 1913) was first who provided the evidence of stress concentration due to a corner or a hole. He showed that the local stress around a corner or a hole in a stressed plate is much higher than the average applied stress. Inglis used the theory of elasticity to show that a stress increases around a hole depending on the radius of the curvature of a hole. His theoretical investigations give a design formula for an elliptical hole, described by Equ. (2.1). This formula is as well applicable with reasonable accuracy to openings such as portholes and hatchways (Shukla 2005).

$$S_{max} = S[1 + 2(h/\rho)^{1/2}] \qquad \text{Equ. (2.1)}$$

Where S_{max} is the maximum elastic stress at the tip of the hole in this equation, S the nominal stress, h the major semi axis of the ellipse, and ρ the root radius. Additionally, this root radius is defined as for an elliptic hole:

$$\rho = b^2/h \qquad \text{Equ. (2.2)}$$

Furthermore, ρ can also be described as the local radius of curvature at the tip of the ellipse. Fig. 2.2 shows the notation of the elliptical hole for Inglis formula.

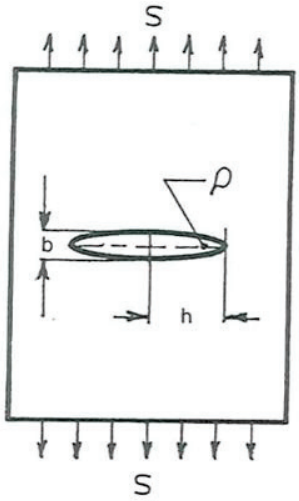

Fig. 2.2: Notation for elliptical hole (Shukla 2005)

By substituting *ρ* in Equ. (2.1) an alternative form of Inglis equation can be obtained, leading to Equ. (2.3).

$$S_{max} = S[1 + 2(^{h}/_{b})]. \qquad \text{Equ. (2.3)}$$

2.1.2.2. Griffith's criterion

Griffith (Griffith 1920) used the first law of thermodynamics which states, when a system goes from a non-equilibrium to an equilibrium state there is a net decrease in energy. Griffith applied this law to describe crack formation. A cracked body differentiates from an un-cracked body, because an additional surface is attached with the crack. The creation of a new surface consumes energy, because the surface carries higher energy then the body. Griffith's idea can be understood by considering a plate with a crack length of *2a* under a constant stress σ. By assuming the width of the plate significantly higher than *2a* as shown in Fig. 2.3, an increase in the crack size can be achieved when there is sufficient potential energy available to overcome the surface energy of the material. In Equ. (2.4) the Griffith energy balance for an increase of crack area *dA* under the equilibrium condition is shown (Anderson 2005).

$$\frac{dE}{dA} = \frac{d\Pi}{dA} + \frac{dW_S}{dA} = 0 \qquad \text{Equ. (2.4)}$$

Or,

$$-\frac{d\Pi}{dA} = \frac{dW_S}{dA} \qquad \text{Equ. (2.5)}$$

Where *E* is the total energy, *Π* the potential energy due to the internal strain energy and external force, and W_s the work required to create a new surface.

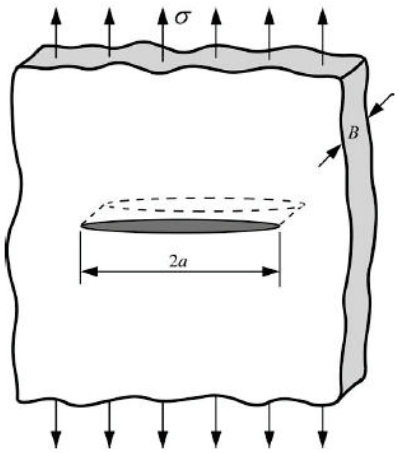

Fig. 2.3: A through thickness crack in an infinite wide plate under tensile stress (Anderson 2005)

Further Griffith used stress analysis of Ingles (Inglis 1913) for the plate with elliptic hole shown in Fig. 2.3. The potential energy can be written according to Equ. (2.6):

$$\Pi = \Pi_O - \frac{\pi\sigma^2 a^2 B}{E} \qquad \text{Equ. (2.6)}$$

Where *Πo* denote for the potential energy of un-cracked plate and *B* is the plate thickness. When a crack is formed, it creates two new surfaces and work W_s is required which is given by

$$W_s = 4aB\gamma_S \qquad \text{Equ. (2.7)}$$

γ_s represents the surface energy of the material. Thus, the change in potential energy is deduced as:

$$-\frac{d\Pi}{dA} = \frac{\pi\sigma^2 a}{E} \qquad \text{Equ. (2.8)}$$

The required work per surface is given by:

$$\frac{dW_S}{dA} = 2\gamma_S \,. \qquad \text{Equ. (2.9)}$$

The fracture stress is finally solved by equating Equ. (2.8) and Equ. (2.9):

$$\frac{\pi\sigma^2 a}{E} = 2\gamma_S \qquad \text{Equ. (2.10)}$$

$$\sigma_{f=}\sqrt{\frac{2E\gamma_S}{\pi a}} \quad . \qquad \text{Equ. (2.11)}$$

Equ. (2.11) is strictly-speaking valid only for ideally brittle solids.

As shown in Fig. 2.3, a distinction between the projected area *2aB* of the crack and the surface area *2A* of two matching surfaces is important. Griffith approach is as well applicable for the fracture of a penny shaped flaw embedded in the material, showed in Fig. 2.4. Fracture stress for the embedded crack is given by Equ. (2.12).

$$\sigma_{f=}\sqrt{\frac{2E\gamma_S}{2(1-\nu^2)a}}, \qquad \text{Equ. (2.12)}$$

Where *a* represents the radius of a crack and *υ* is the Poison's ratio of the material.

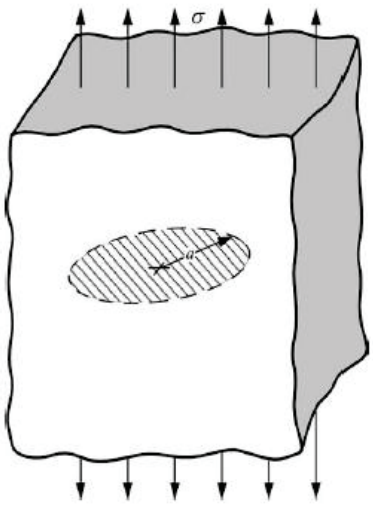

Fig. 2.4: A penny shaped embedded crack (Anderson 2005)

2.1.2.3. Modified Griffith equation

Griffith achieved good agreement between Equ. (2.11) and experimental fracture strength of glass, but this equation however underestimates the fracture strength of metals, since it is valid only for ideally brittle solids. A modification of Griffith expression for materials capable for plastic flow was done individually by Irwin (Irwin 1947) and Orowan (Orowan 1948) as given in Equ. (2.13)

$$\sigma_{f=}\sqrt{\frac{2E(\gamma_S+\gamma_p)}{\pi a}} \qquad \text{Equ. (2.13)}$$

Where γ_p represents plastic work per unit area of surface, which is significantly higher than γ_s.

The crack formation in an ideal brittle solid is achieved by breaking of atomic bonds (Anderson 2005). The total energy required for breaking of bonds per unit area can be represented with γ_s. Additional energy dissipation is caused in the vicinity of the crack through crack propagation in a ductile metal. Griffith model can be then generalized for any kind of energy dissipation.

$$\sigma_{f=}\sqrt{\frac{2Ew_f}{\pi a}} \qquad \text{Equ. (2.14)}$$

Where w_f is the fracture energy and could include material dependent viscoelastic, viscoplastic, or plastic effects (Orowan 1948). It can also be affected through crack meandering and branching effects (Anderson 2005).

2.1.2.4. The energy release rate

Irwin (Irwin 1956) proposed a more convenient energy approach for solving engineering problems that is more equivalent to the Griffith model (Irwin 1956). According to Irwin´s definition, energy release rate *G* is the measure of energy which is available for an increment of crack extension.

$$G = -\frac{d\Pi}{dA}. \qquad \text{Equ. (2.15)}$$

To avoid from confusion the term energy release rate is used for the rate of change in potential energy with respect to the crack area, not with respect to time. *G* is also called crack extension force or crack driving force. Refering to Equ. (2.8), the energy release rate for a wide plate under stress σ can be written as:

$$G = \frac{\pi\sigma^2 a}{E}. \qquad \text{Equ. (2.16)}$$

Crack extends when *G* reaches its critical value.

$$G_c = \frac{dW_s}{dA} = 2W_f \qquad \text{Equ. (2.17)}$$

Where G_c represents the fracture toughness of the material.

Equ. (2.18) defines the potential energy of an elastic body.

$$\Pi = U - F \qquad \text{Equ. (2.18)}$$

Where *U* represents the strain energy and *F* the work due to an external force. By considering a loaded plate with a constant mass force *P*, as shown in Fig. 2.5, the structure is called a loaded controlled structure when the loading force is fixed at a point.

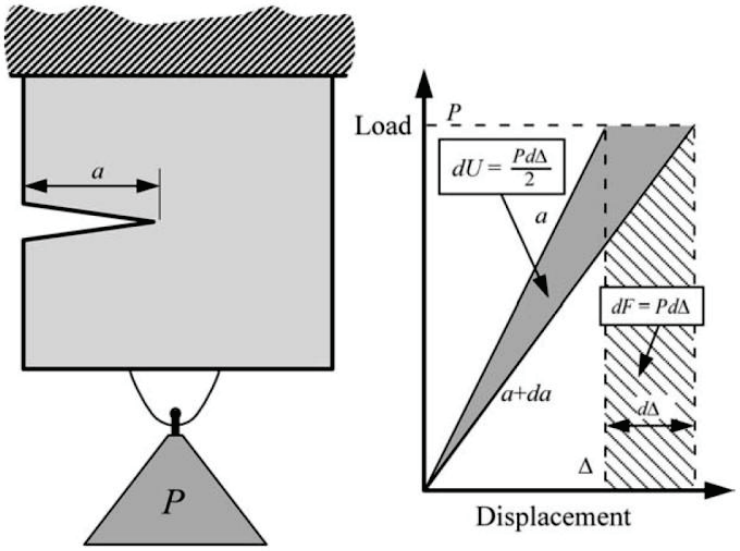

Fig. 2.5: Cracked plate at fixed load P (Anderson 2005)

The external applied work is written as in Equ. (2.19):

$$\mathrm{F} = \mathrm{P}\mathrm{d}\Delta \qquad \text{Equ. (2.19)}$$

The change in strain energy is the difference between the two triangles in Fig. 2.5 evaluating at the crack length a and a+da. It leads to Equ. (2.20):

$$\mathrm{U} = \frac{\mathrm{P}}{2}(\Delta + \mathrm{d}\Delta - \Delta) = \frac{\mathrm{P}\mathrm{d}\Delta}{2}. \qquad \text{Equ. (2.20)}$$

Which shows an increase in strain engery:

$$\Pi = -\mathrm{U} \qquad \text{Equ. (2.21)}$$

and the corresponding energy release rate is:

$$\mathrm{G} = \frac{1}{\mathrm{B}}\left(\frac{\mathrm{dU}}{\mathrm{da}}\right)_{\mathrm{p}} = \frac{\mathrm{P}}{2\mathrm{B}}\left(\frac{\mathrm{d}\Delta}{\mathrm{da}}\right)_{\mathrm{p}}. \qquad \text{Equ. (2.22)}$$

Now in the case of fixed displacement, the plate is said to be under displacement control, see Fig. 2.6 in this case *F=0* and *Π=0* , therefore, the change in strain energy is the difference between the two triangle under the crack length a and a+da.

$$\mathrm{U} = \frac{\Delta\mathrm{P}}{2}(\mathrm{P} - (\mathrm{P} - \Delta\mathrm{P})) = \frac{\Delta\mathrm{d}\mathrm{P}}{2} \qquad \text{Equ. (2.23)}$$

Which shows an decrease in strain energy.

$$G = -\frac{1}{B}\left(\frac{dU}{da}\right)_{\Delta} = -\frac{\Delta}{2B}\left(\frac{dp}{da}\right)_{\Delta}. \qquad \text{Equ. (2.24)}$$

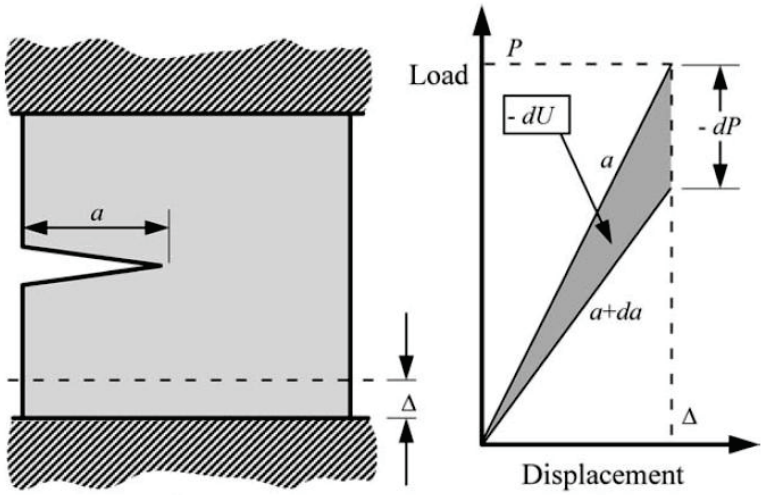

Fig. 2.6: Cracked plate at a fixed displacement (Anderson 2005)

Now compliance *C* is introduced as the inverse of the plate stiffness, the ratio of displacement and load value in Equ. (2.25):

$$C = \frac{\Delta}{P}. \qquad \text{Equ. (2.25)}$$

By substituting compliance *C* in Equ. (2.22) and Equ. (2.24) it can be shown that

$$G = \frac{P^2}{2B}\frac{dC}{da}. \qquad \text{Equ. (2.26)}$$

It shows that energy release rate for load control and displacement control is same as shown in Equ. (2.27):

$$-\left(\frac{dU}{da}\right)_{\Delta} = \left(\frac{dU}{da}\right)_{p}. \qquad \text{Equ. (2.27)}$$

In the case of load control by crack extension *da*, there will be an increase in strain energy, which is graphically demonstrated in Fig. 2.5.

$$(dU)_p = Pd\Delta - \frac{Pd\Delta}{2} = \frac{Pd\Delta}{2} \qquad \text{Equ. (2.28)}$$

In displacement control there is a decrease in the strain energy as depicted in Fig. 2.6:

$$(dU)_{\Delta} = \frac{\Delta dP}{2} \qquad \text{Equ. (2.29)}$$

2.1.2.5. Stress intensity factor

The stress intensity factor *K* is used to predict the stress intensity near the crack tip caused by a remote load or residual stress. Irwin (Irwin 1947) showed that the stress *σ(r, θ)* in the vicinity of an infinite sharp crack can be mathematically written as

$$\sigma_{xx}=\frac{K_I}{\sqrt{2\pi r}}\cos\frac{\theta}{2}\left(1-\sin\frac{\theta}{2}\sin\frac{3\theta}{2}\right) \quad , \qquad \text{Equ. (2.30)}$$

$$\sigma_{yy}\frac{K_I}{\sqrt{2\pi r}}\cos\frac{\theta}{2}\left(1+\sin\frac{\theta}{2}\sin\frac{3\theta}{2}\right) \quad , \qquad \text{Equ. (2.31)}$$

$$\tau_{yy}=\frac{K_I}{\sqrt{2\pi r}}\cos\frac{\theta}{2}\sin\frac{\theta}{2}\cos\frac{3\theta}{2} \quad , \qquad \text{Equ. (2.32)}$$

The term involving $K_I/\sqrt{2\pi r}$ in above equations describes the magnitude of the stress and the term involving θ describes its distribution. K_I is defined in Equ. (2.33) (Anderson 2005).

$$K_I = \sigma_a Y\sqrt{\pi c} \qquad \text{Equ. (2.33)}$$

Where K_I is the stress intensity factor, σ_a the externally applied stress, Y the geometry factor and C the crack half length. In Equ. (2.33), π and Y are constants that show that the value of stress intensity factor depends only on external applied stress σ_a and the square root of the crack length c, in the case of infinite plate with a centre crack. The value of the stress intensity factor increases by the applied stress σ and crack length c. Y is a function whose value depends on the geometry of the specimen and the applied stress σ_a. For an infinite plate with a centre crack the geometry function is $Y=1$ if the crack length is much smaller than the plate thickness.

$$Y = f\left(\frac{a}{W}\right) \qquad \text{Equ. (2.34)}$$

2.1.2.6. Plane stress and plane strain condition

- **Plane stress**

A plane stress condition occurs when a thin plate, as shown in Fig. 2.7, is loaded symmetrically with a force parallel to its plain surface. There are three nonzero and three zero stress components, in detail except σ_x, σy and τ_{xy}, all other components are zero (Wang 1996).

$$\sigma_z = \tau_{zx} = \tau_{zy} = 0$$

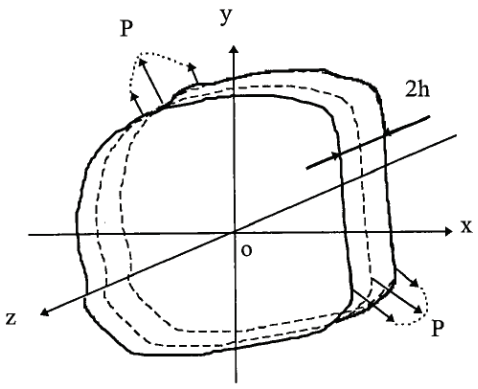

Fig. 2.7: Plane stress state (Wang 1996)

The stress and strain tensors can be expressed as

Stress tensor: $\begin{vmatrix} \sigma_{xx} & \tau_{xy} & 0 \\ \tau_{yx} & \sigma_{yy} & 0 \\ 0 & 0 & 0 \end{vmatrix}$,

Strain tensor: $\begin{vmatrix} \varepsilon_x & \gamma_{xy} & 0 \\ \gamma_{yx} & \varepsilon_y & 0 \\ 0 & 0 & \varepsilon_z \end{vmatrix}$,

Where the strain in thickness direction is:

$$\varepsilon_z = -\frac{\nu}{E}(\sigma_x + \sigma_y). \qquad \text{Equ. (2.35)}$$

According to Hooke´s law (Wang 1996):

$$\varepsilon_x = \frac{1}{E}(\sigma_x - \nu\sigma_y), \qquad \text{Equ. (2.36)}$$

$$\varepsilon_y = \frac{1}{E}(\sigma_y - \nu\sigma_x), \qquad \text{Equ. (2.37)}$$

$$\gamma_{xy} = \frac{1+\nu}{E}(\tau_{xy}). \qquad \text{Equ. (2.38)}$$

- **Plane strain**

To understand a plane strain condition, consider a long, cylindrical body subjected to a non-varying force normal to its axis along the whole length, compare to Fig. 2.8.

Again, there are three none-zero (ε_x ,ε_y γ_{xy},) and three (ε_Z $\gamma_{XZ,}$ γ_{YZ}) zero strain components (Wang 1996).

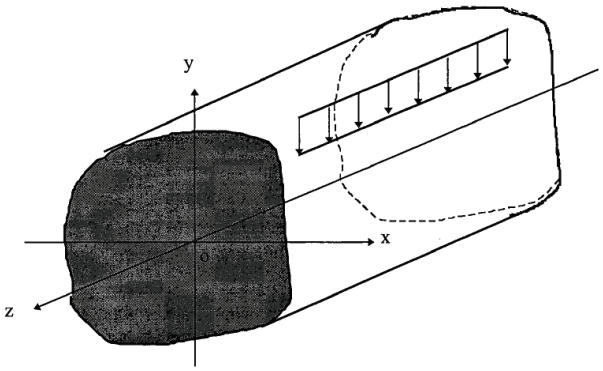

Fig. 2.8: Plane strain state (Wang 1996)

Stress tensor: $\begin{vmatrix} \sigma_x & \tau_{xy} & 0 \\ \tau_{yx} & \sigma_y & 0 \\ 0 & 0 & \sigma_z \end{vmatrix}$,

Strain tensor: $\begin{vmatrix} \varepsilon_x & \gamma_{xy} & 0 \\ \gamma_{yx} & \varepsilon_y & 0 \\ 0 & 0 & 0 \end{vmatrix}$,

Where the stress in thickness direction is:

$$\sigma_z = \nu\,(\sigma_x + \sigma_y), \qquad \text{Equ. (2.39)}$$

The above mentioned Hooke´s law for plane stress condition is also applicable for plain strain condition with the following formal changes

$$\nu \text{ by } \nu' = \frac{\nu}{1-\nu}\ , \qquad \text{Equ. (2.40)}$$

and

$$E \text{ by } E' = \frac{E}{1-\nu^2}\ . \qquad \text{Equ. (2.41)}$$

2.1.3. Elastoplastic fracture mechanics (EPFM)

The validity of linear elastic fracture mechanics (LEFM) and of elasto-plastic fracture mechanics (EPFM) around the near crack tip region depends on the deformation behaviour of the material. As explained before, LEFM is only applicable if the

material deformation behaviour is non-linear. Fracture behaviour characterization for ductile materials is not possible using LEFM. For that purpose, EPFM is an alternative mechanical approach for non linear material behaviour. EPFM uses two important parameters: crack-tip opening displacement (CTOD) and *J* contour integral. Both methods are used as fracture criterion, and crack tip conditions in elastic-plastic material (Anderson 2005).

2.1.3.1. Crack-tip-opening displacement (CTOD)

Wells (Wells 1961) found that though and ductile materials, such as common structural steel, cannot be characterized properly using LEFM. He became to this conclusion after performing K_{IC} measurement experiments. He examined his test specimens and noticed that plastic deformation had blunted an initially sharp crack and that the crack face had moved apart prior to fracture. Fig. 2.9 shows that an initially sharp crack blunt with small plastic deformation results a finite displacement δ at the crack tip.

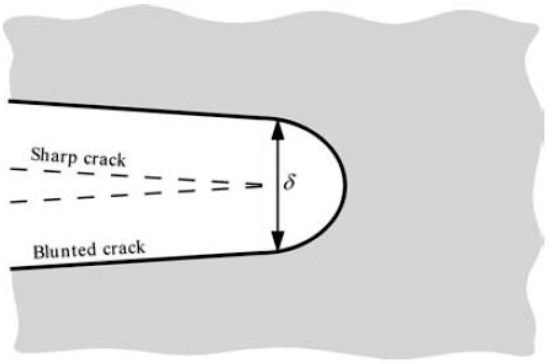

Fig. 2.9: Crack tip opening displacement as an initial sharp crack blunts with plastic deformation (Anderson 2005)

There is a proportional relationship between toughness of the material and the degree of blunting that led him to the idea to determine the toughness of the material by crack tip opening. The idea became to an important parameter in modern engineering known as crack-tip-opening displacement (CTOD).

Wells (Wells 1961) did an approximation analysis, that relates CTOD and stress intensity factor for small scale yielding. Now, consider a small crack as illustrated in Fig. 2.10. Irwin assumed (Irwin 1961) that due to crack tip plasticity crack behaves as cracks that were slightly long.

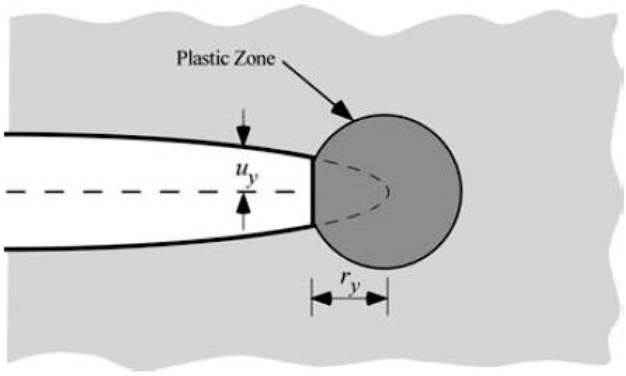

Fig. 2.10: Estimation of CTOD from the displacement of the effective crack in accordance to Irwin's plastic zone correction (Anderson 2005)

By solving the displacement at the crack tip gives an estimation of CTOD-value. By assuming an effective crack length of $a+r_y$, where r_y is the displacement behind the effective crack tip, the crack tip opening is given by:

$$u_y == \frac{\kappa+1}{2} K_I \sqrt{\frac{r_y}{2\pi}} = \frac{4}{E'} K_I \sqrt{\frac{r_y}{2\pi}} \ , \qquad \text{Equ. (2.42)}$$

Where E' is the effective Young's modulus. Irwin determined the plastic zone correction for plane stress condition as:

$$r_y = \frac{1}{2\pi} \left(\frac{K_I}{\sigma_{YS}} \right)^2 . \qquad \text{Equ. (2.43)}$$

Substituting Equ. (2.43) in Equ. (2.42) gives the value of δ:

$$\delta = 2u_y = \frac{4{K_I}^2}{\pi \sigma_{YS} E} \ . \qquad \text{Equ. (2.44)}$$

An alternative relationship of CTOD with energy release rate is given by Equ. (2.45)

$$G = \frac{{K_I}^2}{E} . \qquad \text{Equ. (2.45)}$$

$$\delta = \frac{4G}{\pi \sigma_{YS}} \qquad \text{Equ. (2.46)}$$

Thus, CTOD plays a big role for characterization of material when LEFM is not any more valid. CTOD is related to G and K_I in the limit of small scale yielding as an appropriate crack tip characterization parameter.

An alternative method to analyze CTOD is the strip-yield model (Burdekin et al. 1966) proposed by Dugdale (Dugdale 1960) and Barenblatt (Barenblatt 1962). Burdekin proposed the strip-yield model by assuming a long slender plastic zone at the crack tip for non-hardening material in plane stress. In this model, a crack length of $2a+2\rho$ is considered, where ρ represents the length of plastic zone with a closure stress equal to σ_{YS} at crack tip. Thus, strip-yield model is a classical application that approximates elastic-plastic behaviour by superimposing through crack under remote tension and through crack under closure stress (Anderson 2005).

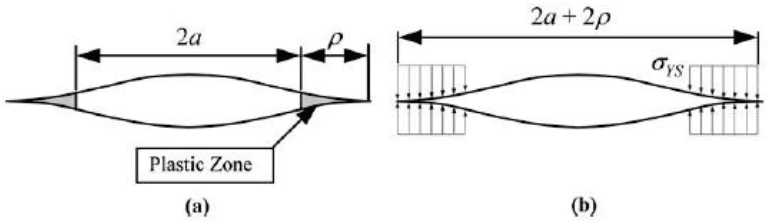

Fig. 2.11: The strip yield model (Anderson 2005)

Using this strip-yield model, CTOD is defined as the crack-opening-displacement at the end of strip-yield zone, as illustrated in the Fig. 2.12. CTOD of a through crack in an infinite plate under remote tensile stress is given by (Burdekin et al. 1966) as the formulae in Equ. (2.47):

$$\delta = \frac{8\sigma_{YS}a}{\pi E}\ln\sec\left(\frac{\pi\sigma}{2\sigma_{YS}}\right). \qquad \text{Equ. (2.47)}$$

A more general formation of the relationship between CTOD, K_I and G can be expressed by Equ. (2.48), (Anderson 2005):

$$\delta = \frac{K_I{}^2}{m\sigma_{YS}E'} = \frac{G}{m\sigma_{YS}}. \qquad \text{Equ. (2.48)}$$

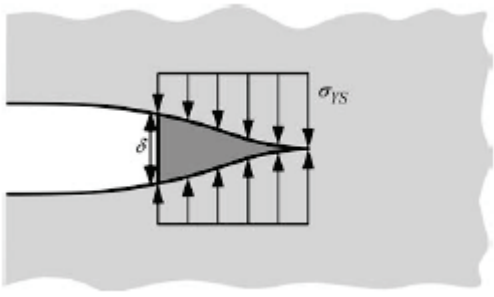

Fig. 2.12: CTOD in strip -yield model (Anderson 2005)

2.1.3.2. The *J* integral

The *J* counter integral is a fracture mechanical characterization parameter for non-linear materials. Rice (Rice 1968) investigated the elastic-plastic behaviour of ductile materials and introduced a methodology for beyond the validity limits of LEFM.
Loading and unloading behaviour of elastic-plastic and non-linear elastic materials is illustrated in the *σ, ε* diagram shown in Fig. 2.13. The stress-strain relationship shows an identical loading behaviour but a different unloading behaviour for elastic-plastic and non-linear elastic materials. For non-linear-elastic material, the path for loading and unloading is the same. In case of elastic-plastic material, the σ, *ε* diagram shows a linear unloading path with a certain slope which is equal to Young's modulus. Mechanical behaviour of elastic-plastic and non-linear elastic materials is identical in the case of monotonically increase in stress, but when generalising the problem to three dimensions, the material loading behaviour may not be identical. Rice made an analysis of a crack in non-linear material by applying a plastic deformation and showed that the non-linear energy release rate *J* could be written as a path independent line integral.

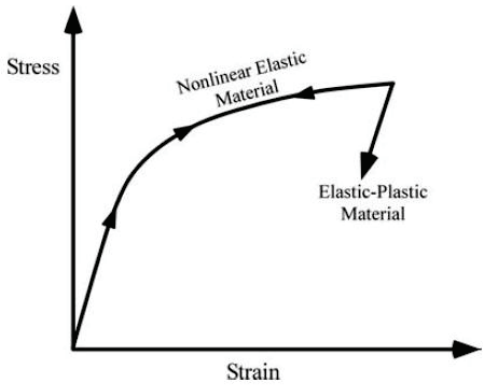

Fig. 2.13: Stress-strain diagram for schematic comparison of elastic-plastic and non-linear elastic materials (Anderson 2005)

Considering a non-linear material, energy release rate *J* characterizes the stress and strain at crack tip and can be seen as a energy release rate or stress intensity parameter, (Hutchinson 1968), (Rice et al. 1967).

2.1.3.3. Non-linear energy release rate

According to Rice (Rice et al. 1967) the path independent contour integral *J* equals to the energy release rate, by considering non-linear materials. Equ. (2.49) shows the energy release rate for linear materials:

$$\mathrm{G} = -\frac{\mathrm{d}\Pi}{\mathrm{dA}} . \qquad \text{Equ. (2.49)}$$

Now *J* is replaced by *G*, which is the same definition for non-linear elastic materials.

$$\mathrm{J} = -\frac{\mathrm{d}\Pi}{\mathrm{dA}} \qquad \text{Equ. (2.50)}$$

Where *A* is the crack area and *Π* the potential energy in Equ. (2.51):

$$\Pi = \mathrm{U} - \mathrm{F} \qquad \text{Equ. (2.51)}$$

U is the strain energy and *F* the work done by an external force. A load controlled cracked plate with unit thickness leads to crack area equal crack length, *A*=*a*, and exhibits a non-linear load-displacement curve, as shown in Fig. 2.14. The strain energy can be written as:

$$\Pi = \mathrm{U} - \mathrm{P}\Delta = \mathrm{U}^* \qquad \text{Equ. (2.52)}$$

Where *U** is the complimentary strain energy:

$$\mathrm{U}^* = \int_0^{\mathrm{p}} \Delta \mathrm{dP} \qquad \text{Equ. (2.53)}$$

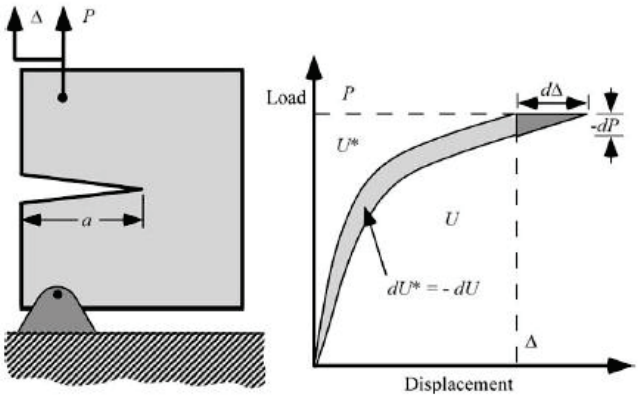

Fig. 2.14: Non-linear energy release rate (Anderson 2005)

Under the condition of a load-controlled plate, *J* can be written as in Equ. (2.54):

$$\mathrm{J} = \left(\frac{\mathrm{dU}^*}{\mathrm{da}}\right)_{\mathrm{p}} . \qquad \text{Equ. (2.54)}$$

If the crack propagates in the condition of fixed displacement, the value of *F* is zero and *J* can be written as:

$$J = \left(\frac{dU}{da}\right)_{\Delta} . \qquad \text{Equ. (2.55)}$$

Under the condition of load control, *dU** differs from (*–dU)* and under the condition of displacement control, *dU** differs from *(½)ΔdP.* But the value of - *dU* and *(½)ΔdP* is comparatively very small and can be in most cases neglected therefore, hence *J* for load control is set equal to *J* for displacement control. This leads to the significant values for the energy release rate and stress intensity.

$$J = G , \qquad \text{Equ. (2.56)}$$

$$J = \frac{K_I{}^2}{E'} . \qquad \text{Equ. (2.57)}$$

2.1.3.4. *J* as a stress intensity parameter

To show that *J* characterizes crack tip condition for non-linear elastic materials, Hutchinson (Hutchinson 1968), Rice and Rosengren (Rice et al. 1967) independently assumed a power law relationship between plastic stress and strain for uniaxial deformation if plastic stains are included. This relation can be written as

$$\frac{\varepsilon}{\varepsilon_0} = \frac{\sigma}{\sigma_0} + \alpha\left(\frac{\sigma}{\sigma_0}\right)^n , \qquad \text{Equ. (2.58)}$$

Where $\varepsilon_o = \sigma_o / E$, σ_o is a reference stress value equal to σ_{YS}, α is a dimensionless constant and *n* is strain-hardening exponent. Near the crack tip, stress and strain should correlate to the inverse of the radius in order to remain path independent. In the plastic zone near the crack tip, elastic strains are significantly small compared to the total strain, which reduces the stress-strain behaviour to a simple power law. By applying the above mentioned conditions, ahead the crack tip following variations occur to the stress and strain path:

$$\sigma_{ij=} K_1 \left(\frac{J}{r}\right)^{\frac{1}{n+1}} \qquad \text{Equ. (2.59)}$$

$$\varepsilon_{ij=} K_2 \left(\frac{J}{r}\right)^{\frac{n}{n+1}} \qquad \text{Equ. (2.60)}$$

Where K_1 and K_2 are constants of proportionality. By setting the value of *n=1 in* Equ. (2.59) and in Equ. (2.60) the equations give a 1/r singularity (Anderson 2005). This means, that the equations are consistent with linear elastic materials. By setting appropriate boundary conditions, the actual stress and strain conditions can be obtained in Equ. (2.61) and Equ. (2.62):

$$\sigma_{ij}=\sigma_0\left(\frac{EJ}{\alpha\sigma_0{}^2 l_n r}\right)^{\frac{1}{n+1}}\tilde{\sigma}_{ij}(n,\theta) \qquad \text{Equ. (2.61)}$$

$$\varepsilon_{ij}=\frac{\alpha\sigma_0}{E}\left(\frac{EJ}{\alpha\sigma_0{}^2 l_n r}\right)^{\frac{1}{n+1}}\tilde{\varepsilon}_{ij}(n,\theta). \qquad \text{Equ. (2.62)}$$

The above equations are called HRR (Hutcinson, Rice, and Rosengren) singularity whose magnitude is defined by the *J* Intigral. Thus the *J* Intigral describes the condition within plastic zone, where I_n is *n*-dependent Integration constant and $\acute{\varepsilon}_{ij}$, $\acute{\alpha}_{ij}$ are dimensionless functions of n and ϑ. There are two singularity dominated zones in small scale yielding for the elastic and plastic region with *1/r* and $r^{-1/n+1}$ stresses respectively.

2.1.4. Numerical analysis

Mathematical models are used in most of engineering analyses, which leads to differential equations. As engineering problems are often too complex to be analysed with analytical methods, numerical techniques can be used to solve such kind of problems. Numerical analyses are the study of algorithms that uses numerical approximations for solving problems of mathematical analysis.

Some of the numerical methods used in fracture mechanics analyses are,

- Finite element method (FEM)
- Extended Finite element method (X-FEM)
- Boundary element method (BEM)

2.1.4.1. Finite element method (FEM)

Finite element method (FEM) is a numerical procedure of analysis widely used for solving differential or integral equations. The method essentially consists of assuming a piecewise continuous function as the solution and obtaining the parameters of functions in a manner that reduces the error in the solution.

Engineers developed the FE-method using physical insight to apply it to problems for stress analysis, later on used to calculate a field quantity such as displacement or stress field, temperature or heat flux, stream or velocity function. The FE-method results in peak value of field quantity or its gradient can be obtained. The FEM method cuts a structure into several elements which describes the behaviour of each element in a simple way. These elements are rejoined at nodes, which hold elements as they are pined or glued together, see Fig. 2.15. By this way, a number of simultaneous algebraic equations are obtained, that represents equilibrium equations in the case of stress analysis and requires computer implementation.

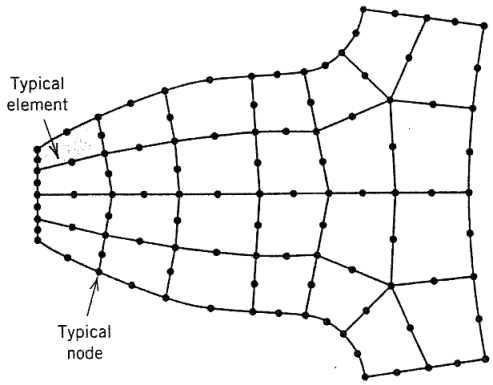

Fig. 2.15: A two dimensional model of a gear tooth (Cook 1995)

According to another description of FEM, FEM is piecewise polynomial interpolation of a complex part. The field quantity of a node is interpolated over the element and then further interpolated over the entire structure by connecting all of its elements. Values of field quantity that minimize the value of some function at nodes are the most accurate values. This minimizing process causes number of simultaneous algebraic equations that can be written in a matrix symbolism such as. (Cook 1995)

$$\mathrm{K\,D} = \mathrm{R} \qquad \text{Equ.(2.63)}$$

Where *D* is vector of unknown value of field quantity at nodes such as displacement, *R* is a known vector of load, and *K* is the stiffness matrix of the simulated mechanical system. FE is a versatile method because it can analyze structures with arbitrary shape, support and loads in comparison with classical analytical methods. For example classical methods handle temperature dependent stress analysis with much difficulty but FE-method supports it as easily as load dependent stress analysis.

2.1.4.2. Extended Finite element method (X-FEM)

The extended finite element method (X-FEM) is a numerical method that extends the FEM technique. It deals with differential equations of discrete functions and enriches the solution space. Problems unsolvable through the mesh refinement with localized features method can easily be handled with X-FEM (Singh et al. 2012). X-FEM enriches the degree of freedom of an element with displacement functions in the case of the presence of discontinuities. Normally, the approximation done by X-FEM consists of standard finite elements. The X-FEM approximation captures singularities and discontinuities by using in the major part of the domain and enriched elements in enriched sub domain. By using enriched elements in standard, X-FEM expands the approximation space function of the standard FEM. A simulation of crack initiation and crack growth can thus be effectively done through the X-FEM in contrast to finite elements which needs continuous re-meshing at the growing crack tip.

- **Interpolation scheme in XFEM**

The approximated scalar variable *u(x)* can be extended to a vector field. The shape function and the correspondent nodal displacement of the dependent variable can be denoted at node *i* by $N_i(x)$ and u_i respectively.

According to Skumar, the approximation of the standard X-FEM consists of a standard finite element part, i.e., the approximation of the FEM and the enrichment based on the idea of the partition of unity approach (Sukumar et al. 2003).The crack tip singularity and Heavyside functions as discontinuities can be captured by approximation of enriched term in the domain *(k)*.

$$u(x) = \sum_{i\epsilon k} N_i(X) u_{i+} \sum_{i\epsilon k^*} N_i^*(X) b_i(X)\, a_i \qquad \text{Equ. (2.64)}$$

Where *k** represents the enriched nodes and *k**$\text{is a member of } k$, u_i the unknown of the standard FEM at node *i,* a_i the unknown enrichment at the node *i* and $b_i(x)$ the local enrichment function of node *i.* The discontinuities are captured in the function $b_i(x)$ within the evaluated domain.

$$\sum_{i\epsilon k} N_i(X) \mathrm{b}_i(\mathrm{X}) = \mathrm{b}_i(\mathrm{X})\ . \qquad \text{Equ. (2.65)}$$

- **Crack enrichment functions**

Jiang and Ying (Jiang et al. 2010) gave Heaviside enrichment function that simplifies the crack representation away from the crack tip. The X-FEM displacement approximation is done by incorporating two enrichment functions into the X-FEM as a

common practice. A Heaviside step function represents the crack away from the tip. To represent the crack tip asymptotic displacement field, an extended set of complex functions is used (Soheil 2007). The Heaviside step function is given as (Bordas et al. 2006):

$$H(x) = \begin{cases} 1, above\ crack \\ -1, below\ crack \end{cases} \quad \text{Equ. (2.66)}$$

The enrichment that introduces a discontinuity in displacement across the crack is written as:

$$a_i(r,\theta) = \left\{ \begin{matrix} \sqrt{r}sin\left(\frac{\theta}{2}\right); \sqrt{r}cos\left(\frac{\theta}{2}\right); \\ \sqrt{r}sin\left(\frac{\theta}{2}\right)sin\theta; \sqrt{r}cos\left(\frac{\theta}{2}\right)sin\theta \end{matrix} \right\} \quad \text{Equ. (2.67)}$$

Where *r* and *θ* stand for the components of a polar coordinate system local to the crack tip . Sukumar (Sukumar. et al. 2009) described that the origin is at the crack tip and *θ=0* is parallel to the crack. Equ. (2.67) (Giner et al. 2009) gives four enrichment functions for a linear-elastic crack tip. These equations are used to incorporate a displacement field into elements containing the crack tip.

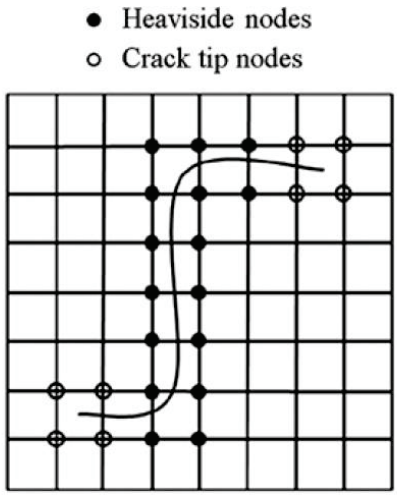

Fig. 2.16: Representation of Heaviside and crack tip enrichment features

The first enrichment function in Equ. (2.67) acts as a Heaviside enrichment and is discontinuous across the crack behind the tip in the element containing crack tip. Fig. 2.16 shows the nodes to be enriched by Equ. (2.68) and Equ. (2.67).

2.1.4.3. Boundary element method (BEM)

Boundary element method (BEM) is an alternative to the finite element method with the advantage of reduced number of nodes for the same degree of accuracy. Using BEM, the object is discretised into elements only along the boundary. Discretisation into elements for a 2D body is the line contour Fig. 2.17. In a 3D body case a surface is enclosing as shown in Fig. 2.18 (Gupta 1999).

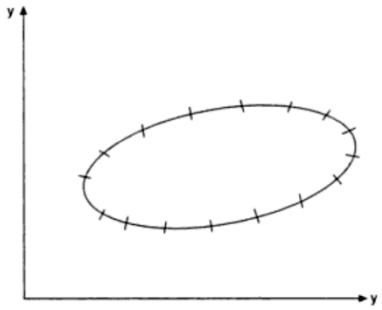

Fig. 2.17: 2D Boundary discretisation (Gupta 1999)

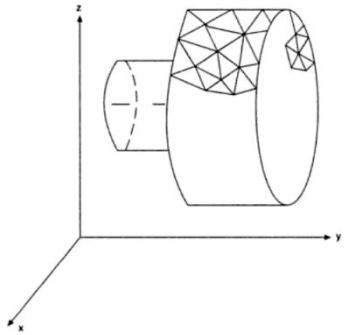

Fig. 2.18: 3D Boundary discretisation (Gupta 1999)

Using BEM, the basic governing equation of the problem is solved for the whole solution domain. The equation is solved in such manner that the unknowns involved in equation are only parameters at the nodes on the boundary. These unknown values can be for example displacements or temperature. No nodes exist in the interior of the object. This leads the problem to be reduced about an order of the magnitude. Once the nodal parameters are determined at the boundary, the governing equation is used again to derive simple algebraic relations. These algebraic relations give interior point values with reference to a parameter along the boundary nodes.

- **BEM in fracture mechanics**

Advances in BEM give the possibility to deal with critical problems such as life expectancy of flawed or cracked structures. A dual boundary element method is

developed by Portela (Portela et al. 1992) for two dimensional and by Mi and Aliabadi (Mi et al. 1992) for three dimensional crack problems involving embedded cracks, edged cracks, and kinked cracks.

- **The dual boundary element method**

The displacement and the traction integral equations are the dual boundary integration equations on which the dual boundary element method (DBEM) is based. These equations are related to the boundary displacement components u_i and the traction components t_i and can be written as (Cruse 1977):

$$c_{ij}(x',x)u_j(x') + \oint_\Gamma T_{ij}(x',x)u_j(x)d\Gamma(x) = \int_\Gamma U_{ij}(x',x)t_j(x)d\Gamma(x) \qquad \text{Equ. (2.69)}$$

Where *i, j* are cartesian components $T_{ij}(x',x)$ *and* $U_{ij}(x',x)$ that represent Kelvin traction and the displacement fundamental solution, $\oint$ stands for the Cauchy principle value integral. The stress components σ_{ij} in the case of body force absence, and assuming continuity of both strain and traction, can be given by Equ. (2.70):

$$\frac{1}{2}\sigma_{ij}(x') + \oint\!\!\!\!\!\!- _\Gamma T_{kij}(x',x)u_k(x)d\Gamma(x) = \oint_\Gamma T_{kij}(x',x)t_k(x)d\Gamma(x) \qquad \text{Equ. (2.70)}$$

Where $\oint\!\!\!\!\!\!-$ stands for the Hadamard principal value integral, $T_{kij}(x',x)$ *and* $U_{kij}(x',x)$ contains the derivatives of $T_{ij}(x',x)$ *and* $U_{ij}(x',x)$ respectively. The traction components t_j on a smooth boundary are given by Equ. (2.70). $n_i(x')$ is the component of outward unit normal to the boundary at x' (Mi et al. 1994)

$$\frac{1}{2}t_j(x') + n_i(x')\oint\!\!\!\!\!\!- _\Gamma T_{kij}(x',x)u_k(x)d\Gamma(x) = n_i(x')\oint_\Gamma U_{kij}(x',x)t_k(x)d\Gamma(x) \qquad \text{Equ. (2.71)}$$

The dual boundary element method is a promising numerical tool to calculate the stress intensity of complex three-dimensional structures with acceptable numerical effort.

2.2. Fatigue of welded joints

Welded joints are used as integral part in most of the complex load carrying structures including offshore and nuclear installations. Welded joints are the weakest areas of the structures and their quality affects structural integrity. Geometrical discontinuities of welded joints such as incomplete penetration or lack of fusion determines the fatigue strength of a structural weld detail. Weld imperfection during fabrication process are partially considered in the conventional design rules (Nykänen et al. 2005). Conventional design rules are primarily based on Wöhler S-N curves found through experimental results.
The existence of imperfections in welded joints is considered at the crack initiation stage of fatigue life, which should be minimized to produce high-quality welds with suitable strength and reasonable manufacturing costs. Characterization of subcritical crack-growth of welds using stress intensity factor gives the possibility for prediction of crack growth rate under cyclic loading. Weld root and weld toe are mostly considered as potential sites for critical crack initiation (Nykänen et al. 2005). A calculation of local geometry dependent stress intensity factor is the basis for fatigue life estimation of welded joints, as described further on in this chapter.

There are different types of approaches to fatigue strength and service life assessment. If the approach precedes directly from the acting forces and moments or under the assumption of a constant or linearised stress distribution nominal stresses, then strength assessments are termed as global approaches. In the global approach, limit values of load or nominal stress are used. These limit values are related to a global phenomenon, as plastic yielding or final fracture of the specimen.

If the approach bases on local stress and strain parameters, then strength assessments are termed as local approaches. Cyclic crack initiation, cyclic crack propagation, and final fracture are considered as the local process of damaging by fatigue. A notch root approach is related to crack initiation, which is based on notch root stress and strain values. A fracture mechanical approach describes the crack propagation until final rupture (Radaj 1996). Fig. 2.19 shows the different types of global and local approaches.

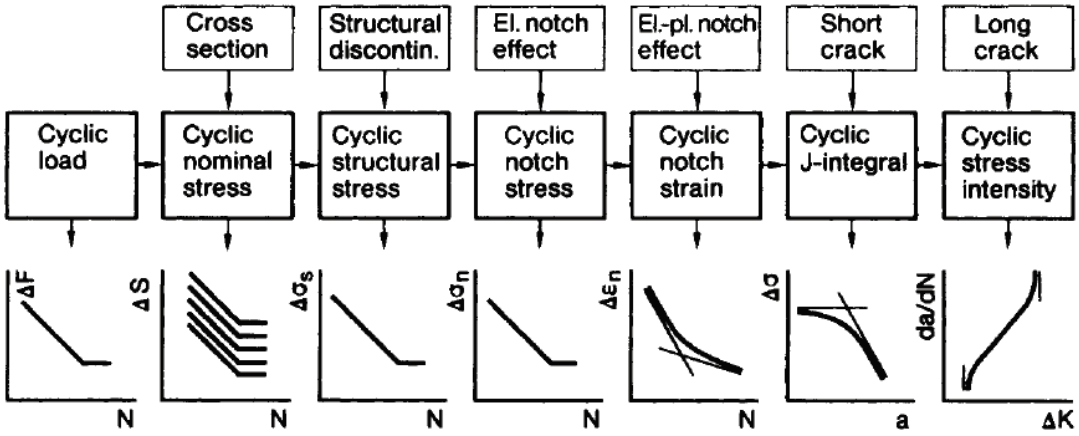

Fig. 2.19: Global and local approaches for describing the fatigue strength (Radaj 1996)

2.2.1. Nominal stress approach

Nominal stress is the average stress in a welded joint. The nominal stress approach proceeds with the nominal stress amplitude in a component and then compared with a nominal S-N curve as shown in Fig. 2.20

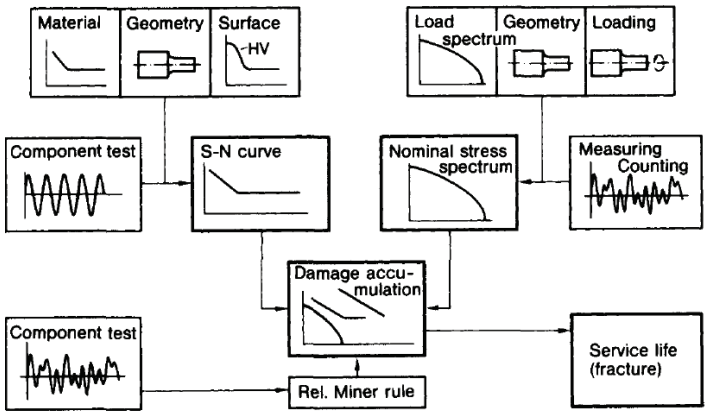

Fig. 2.20: Nominal stress approach for assessing the fatigue strength and service life (Kloos 1989)

The stress S-N curve comprises all influences due to material, shape, and surface. In cases where nominal stresses are not clearly defined, acting forces and moments can also be directly used. A simple hypothesis damage accumulation according to relative Miner rule gives from stress S-N curve and nominal stress spectrum the final service life results, see Fig. 2.20.

Nominal stress spectrum is obtained considering load spectrum, geometry and type of loading. The calculations of service life are performed with respect to a final fracture but they can also be performed with respect to an initial crack (Radaj 1996).

2.2.2. Structural stress approach

In the structural stress approach, structural stress amplitudes are compared with stress-based Wöhler S-N curve for assessing fatigue strength and service life. This approach is particularly developed for welded structures. An incomplete 'hot-spot' version of the approach is the finite element analysis with the aim to optimize macro-geometrical influence parameters. Because the quantitative statements for fatigue strength and service life are possible for the un-notched areas of structure only, that is why actual notches are not considered.

From this approach indications for quantitative statements for the notched area can be obtained by using specific hot-spot extrapolation formulae (Radaj 1996).

2.2.3. Notch root approach

The notch root approach assesses fatigue strength and service life up to the crack initiation stage. It proceeds with elastic-plastic strain amplitudes at the notch root and compare with a strain S-N curve of the un-notched specimen.

The notch root approach idea is based on, that the mechanical behaviour of the material of notch root in respect to local deformation, local damage and crack initiation is similar to the un-notched or mildly notched axially loaded specimen in respect of global deformation, global damage and complete fracture, see Fig. 2.21 (Radaj 1996).

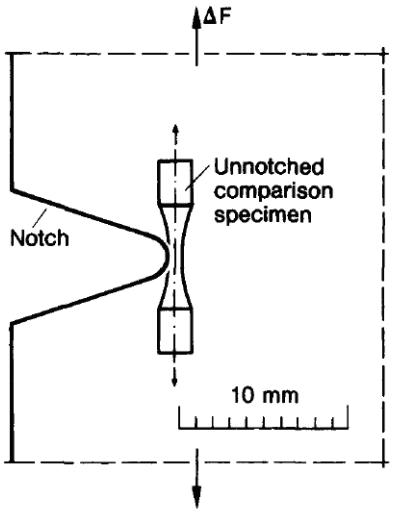

Fig. 2.21: Comparison specimen for simulating the cyclic stress-strain and crack initiation behaviour at the notch root (Radaj 1996)

2.2.4. Notch stress approach

The notch stress approach supports the fatigue strength assessment of welded joints independent from the macroscopic structural detail. It is based on the stress concentration at the evaluated notch, for example weld root or weld toe, and takes microstructural support hypothesis into account for sharp notches.
This means that the linear-elastically derived notch stress K_t is not directly decisive for crack initiation but instead a comparably reduced fatigue strength factor K_f. The fictitious notch stress approach according to Radaj incorporates Neuber's microstructural support theory leads to a fictitious radius of one millimetre for welded joints with sharp notches.

2.2.5. Fracture mechanical approach

The fracture mechanical approach supplements the notch root approach to determine the fatigue strength and service life of the structure in the presence of an incipient crack. Paris and Erdogan proposed a simple formula to analyse cyclic stress intensity factor ΔK for crack propagation rate of an incipient crack. The crack propagation occurs when the threshold value of the stress intensity factor exceeds and ends with critical stress intensity of remaining cross-section (Radaj 1996).

2.2.6. Stress intensity factor determination

Stress intensity range ΔK is an important parameter that describes the fatigue action at crack tip. The stress intensity can be defined by considering an infinite plate with centre crack as shown in Fig. 2.22 (Hobbacher 2013) and can be mathematically written as:

$$\mathrm{K} = \sigma\sqrt{\pi \mathrm{a}} \qquad \text{Equ. (2.72)}$$

Where σ is the tensile stress applied to the plate and a the half distance between two crack tips in a centre crack.

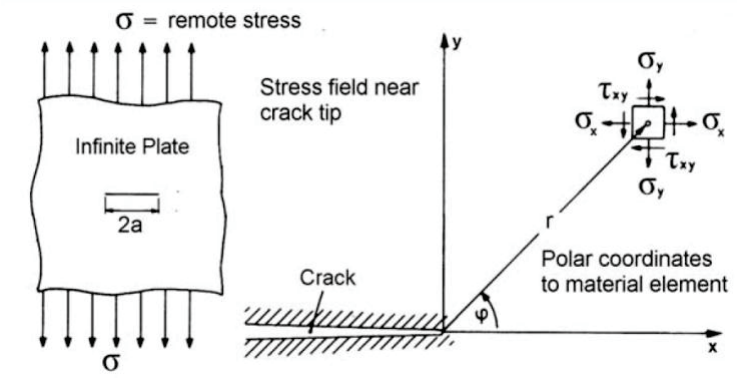

Fig. 2.22: A centre crack infinite plate under tensile stress (Hobbacher 2013)

2.2.6.1. Standard configuration

Correction should be done due to deviation of crack configurations and geometrical shapes from a centre cracked infinite plate considering following parameters and crack locations:

1. Edge distance,
2. Crack shape most of condition an elliptic form,
3. Geometry with limitation of width or wall thickness,
4. Embedded crack, and
5. Free surface of crack.

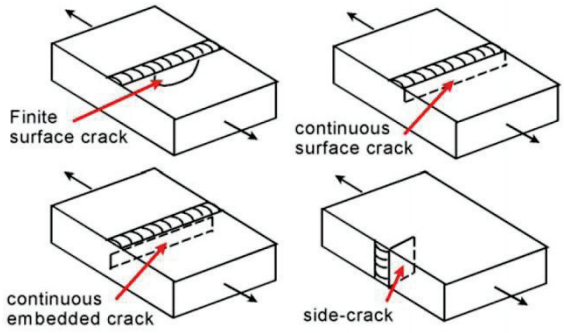

Fig. 2.23: Different types of cracks to a weld toes (Hobbacher 2013)

A correction function $Y_u(a)$ is introduced to the basic formula of stress intensity factor of a centre cracked infinite plate.

$$K = \sigma\sqrt{\pi a}Y_u(a) \ . \qquad \text{Equ. (2.73)}$$

The correction function depends on the type of crack and load condition, sees Equ. (2.73). This correction function is based on the type of evaluated stress, for example membrane or bending stresses in structural stress evaluation (Newman et al. 1983).

2.2.6.2. Stress intensity factor for welded joints

In the case of full-penetrated welded joints, calculations are generally based on the stress state at the weld toe taking the notch effect into account. For this purpose, the universal correction function $Y_u(a)$ is split into $Y(a)$ and $M_k(a)$.

$Y(a)$ and $M_k(a)$ are the correction of a standard configuration and the correction for the local notch of weld toe respectively. $Y(a)$ and $M_k(a)$ are further separated for membrane and shell bending stress:

$$K = \sigma\sqrt{\pi a}(\sigma_m Y_m(a) M_{k,m}(a) + \sigma_b Y_b(a) M_{k,m}(a)) \quad \text{Equ. (2.74)}$$

Where K is the stress intensity factor, σ_m is the membrane stress, σ_b shell bending stress, $Y_m(a)$ is the correction function for membrane stress intensity factor, $Y_m(b)$ is the correction function for shell bending stress intensity factor, $M_{k,m}(a)$ is the correction for non-linear stress peak in term of membrane action, and $M_{k,b}(a)$ is the correction for non-linear stress peak in term of shell bending (Hobbacher 2013).

2.2.6.3. Weight function technique

Requirements of most numerical methods are a separate calculation of the stress intensity factor for each stress distribution and the crack length. Bückner (Bueckner 1970) developed the weight function procedure that simplifies the method for the determination of stress intensity factor.

The stress intensity factor can be determined simply by multiplying known weight function by stress distribution and integrating it along the crack length. The weight function is dependent on the geometry of component. This enables the incorporation of non-linear stress distributions into the crack propagation analysis. Equ. (2.75) shows basic formulation of stress intensity factor using the weight function method:

$$K = \int_{x=0}^{x=a} \sigma(x) h(x, a) dx \,. \quad \text{Equ. (2.75)}$$

The weight function for a plate with a centre crack can be simplified to a split force formulation see Equ. (2.76):

$$h(x,a) = \frac{2}{\sqrt{\pi}} \cdot \sqrt{\frac{a}{a^2 - x^2}}. \qquad \text{Equ. (2.76)}$$

By using the stress concentration factors:

$$K_t(x) = \sigma(x)/\sigma_{ref}, \qquad \text{Equ. (2.77)}$$

$$\sigma(x) = \sigma_{ref} K_t(x). \qquad \text{Equ. (2.78)}$$

The stress intensity gets:

$$K = \frac{2}{\sqrt{\pi}} \int_{x=0}^{x=a} \sigma(x) \sqrt{\frac{a}{a^2 - x^2}}\, dx$$

$$K = \sigma_{ref} \sqrt{\pi a}\, \frac{2}{\sqrt{\pi}} \int_{x=0}^{x=a} \frac{K_t(x)}{\sqrt{a^2 - x^2}}\, dx \qquad \text{Equ. (2.79)}$$

By applying the correction formula *Y(a)* to Equ. (2.79), the equation can also be used for standard solutions, see Equ. (2.80):

$$K = \sigma_{ref} \sqrt{\pi a} Y(a)\, \frac{2}{\sqrt{\pi}} \int_{x=0}^{x=a} \frac{K_t(x)}{\sqrt{a^2 - x^2}}\, dx. \qquad \text{Equ. (2.80)}$$

By use of Equ. (2.80), an accurate fatigue estimation and crack propagation calculation is done into the depth of a plate in direction *a* as shown in Fig. 2.24. The formula cannot be used for the calculation of stress intensity factor to calculate crack propagation on the surface in the *c* direction because this formula originates from a two- dimensional solution.

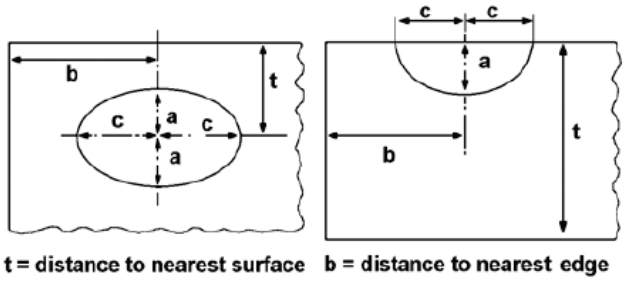

Fig. 2.24: Dimensions of elliptical cracks (Hobbacher 2013)

The total stress in a welded joint, as shown in Fig. 2.25, is a sum of membrane stress, shell bending stress, and non linear peak stress.

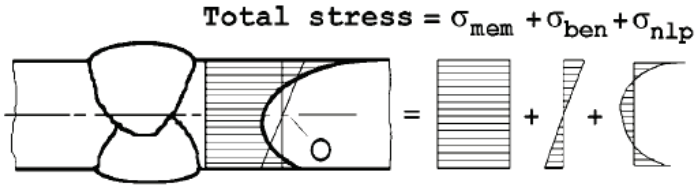

Fig. 2.25: Stress parts considered in fracture mechanics (Hobbacher 2013)

The formula is also applicable for considering non-linear peak stress. $K_{t,nlp}$ denote for the remaining non-linear peak stress concentration factor distribution. Standard solution of stress intensity factor is found in the literature considering shell and membrane stress. Correction for the local notch of weld toe $K_{t,nlp.}$ is determined using the $M_k(a)$ value.

2.2.6.4. Aspect ratio

The consideration of an aspect ratio of a/c or of a/2c is very important in fracture mechanics and a significant parameter for the stress intensity factor (Hobbacher 2013). There are different ways to consider aspect ratio as stated below:

- For a conservative approach the aspect ratio of a:c=0.1 is taken constant (Bowness et al. 1996)
- Three dimensional $M_K(a)$ formulae (Bowness et al. 1996) or weight function (Niu et al. 1989) gives stress intensity factor at the surface governing crack propagation in *c* direction.
- Formulae for elliptical surface crack at the weld toe of a fillet weld by Engesvik (Engesvik et al. 1983).
- In case of a butt weld formulae it is conservative to use the following a/c ratio:

$$2.\mathrm{c} = -0.27 + 6.34.\mathrm{a} \qquad \text{if } \mathrm{a} < 3\ mm$$

$$\frac{\mathrm{a}}{2\mathrm{c}} = 0 \qquad \text{if } \mathrm{a} > 3\ mm$$

- To calculate the stress intensity factor for crack propagation in the *c* direction in the case of two dimensional M_k formulae with a singularity at the surface, a *0.15mm* distance from the surface may be used (BS-7910 2005).

2.3. Fatigue crack growth testing procedure

The American Society for Testing and Materials (ASTM) has published the Standard ASTM E647), which describes a test method for fatigue crack growth measurements. According to this method, pre-cracked notched specimens are cyclically loaded and then the size of crack is measured by different techniques. This method is used to determine *da/dN* as a function of *ΔK*. The Value of K_{min}, K_{max} and the crack length are monitored throughout an experiment. According to ASTM E647, compact specimens and middle tension panel specimens are used in experiments. The behaviour of the specimen should be predominately elastic during the test for the procedure to be valid. The specimen geometry is well documented in ASTM E647. The requirement for un-cracked compact specimen according to ASTM E647 is given by the following Equ. (2.81):

$$W - a \geq \frac{4}{\pi}(K_{max}/\sigma_{YS})^2 \qquad \text{Equ. (2.81)}$$

There are no requirements on specimen thickness. In the pre-cracking process, the value of K_{min} should not exceed an initial value of K_{max} otherwise retardation effects influence growth rates ASTM E647. According to this standard there are two types of fatigue tests listed below

2.3.1. K-decreasing procedure (Load reduction test)

This procedure is valid for a crack growth rate of $da/dN<10^{-8}$ *m/cycle*. In this process *ΔK and* K_{max} values for pre-cracking should be equal or greater than the terminal pre-cracking value referring to ASTM E647. To achieve the lowest *ΔK* or crack growth rate of interest, force is continuously reduced at a rate of *C=-0.08/mm* and then the test data is recorded. For crack growth rate above 10^{-8} m/cycle, the K-decreasing method is not recommended since prior loading history at such associated *ΔK* level influence the near threshold fatigue crack growth rate behaviour (Newman et al. 2010). By achieving a target of 10^{-10}*m/cycle* test control can be changed to constant-amplitude loading at higher *ΔK* for mid and upper regions of crack growth rate as depicted in Fig. 2.26.

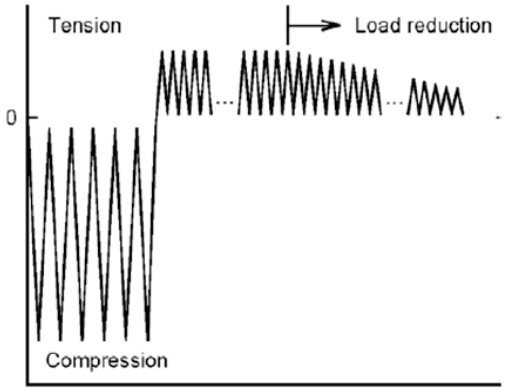

Fig. 2.26: CPLR loading (Newman et al. 2010)

2.3.2. K-increasing procedure (constant force amplitude test procedure)

This testing procedure is well applicable for fatigue crack growth above 10^{-8} *m/cycle.* K-increasing procedure cannot be used below 10^{-8} *m/cycle* because of pre-cracking consideration. Using this method, constant ΔP and a fixed set of loading stress ratio and frequency are preferred. Changed loading variables tend to raise potential problems due to several types of transient phenomena (ASTM E647).

2.3.3. Compression pre-cracking constant amplitude

By compression pre-cracking constant amplitude (CPCA) loading method, specimens are pre-cracked under compression-compression loading. A back-face-strain-gage compliance procedure will be followed to monitor the crack length according to the standard ASTM E647.To transmit cyclic compressive loads from clevises to the specimen, metallic block are attached on both side of the compact specimen. With compression-compression loading cycles, a small fatigue crack is produced at the tip of crack starter notch, which stops growing after specific crack length. A tensile residual-stress field instead of the typical compressive residual stresses from tension-tension loading envelops the resulting crack tip. At the time when the crack no longer grows and the crack surfaces are fully opened, it means that the crack has reached its threshold value (Newman et al. 2010). The calculation of compressive load levels to make a fatigue crack grow can be done with Equ. (2.82):

$$\left|K_{cp}\right|/E=0.00032\sqrt{m} \qquad \text{Equ. (2.82)}$$

Where K_{CP} is the maximum compressive stress intensity factor during compression pre-cracking and E is the elastic Young modulus. When compression pre-cracking is completed, loading with constant amplitude at same or less than anticipated threshold stress intensity factor is performed to get a steady crack growth. After reaching one million cycles, if there is no crack growth recorded, the load can be increased to 5-10% until once again a crack begins to grow slowly. Then, the load can be held constant. The testing procedure is shown in Fig. 2.27.

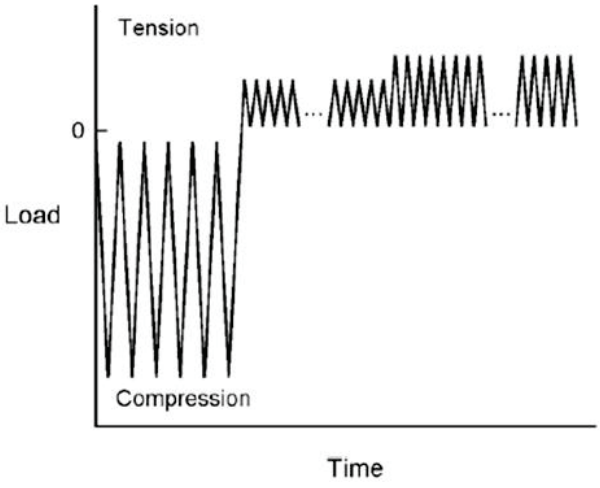

Fig. 2.27: CPCA loading (Newman et al. 2010)

Fig. 2.28 shows three typical-fatigue-crack growth data for different test procedures. The threshold is only determined properly by means of the compressive pre-cracking method.

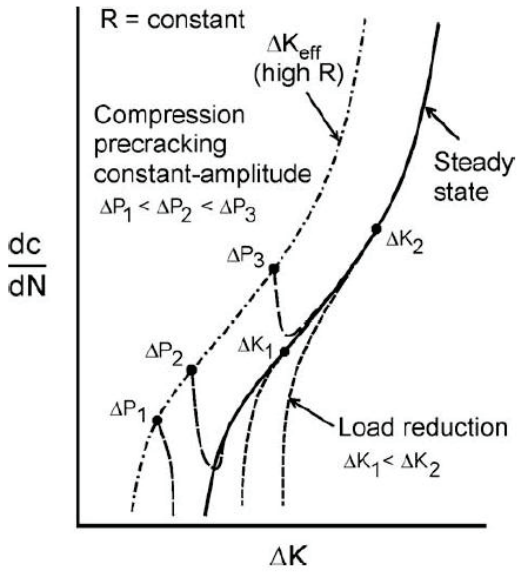

Fig. 2.28: Typical-fatigue-crack growth data under constant-amplitude, load-reduction and CPCA loadings (Newman et al. 2010)

2.3.4. Crack length measurement

2.3.4.1. Compliance method

The crack length of a structure can be measured by the compliance of the structure. The compliance method is a simple and accurate method to find crack closure response. Compliance is closely related to parameter of crack tip fracture mechanics. When a cracked structure is under a load *P* and loading point have a specific distance to structure, then crack dependent compliance of the structure can be expressed as given in Equ. (2.83) (Marsh et al. 1991).

$$C = \frac{P}{v} \qquad \text{Equ. (2.83)}$$

The relation between strain energy release rate *G* and change in compliance with crack length is given in Equ. (2.84).

$$G = \frac{1}{2} P^2 \frac{dC}{da} \qquad \text{Equ. (2.84)}$$

To understand and measure the extra compliance due to the presence of a crack, consider a linear elastic infinite plate with a centre crack of length of *2a* under a remote tensile stress *σ* shown in Fig. 2.29.

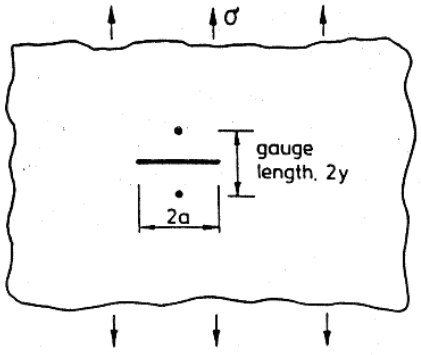

Fig. 2.29: Location of displacement gauge on centre cracked panel under remote tensile stress σ (Marsh et al. 1991)

A displacement gauge straddles the crack with gauge length *2y*. If there is no crack in plate, then total measured displacement is $2v_o = -2y/E$. Using methods to determine extra displacement in presence of a crack for *y/a >>1,* the following expression in Equ. (2.85) can be used.

$$\frac{\Delta v}{v_0} = \frac{3+V}{2} \left(\frac{a}{y}\right)^2 \qquad \text{Equ. (2.85)}$$

For an accurate measurement of crack length, the placement of the displacement gauge should be as close as possible to the crack tip. By increasing displacement gauge distance to the crack, causes the extra displacement falls off rapidly. Fig. 2.30 shows common compliance techniques for measuring crack closure.

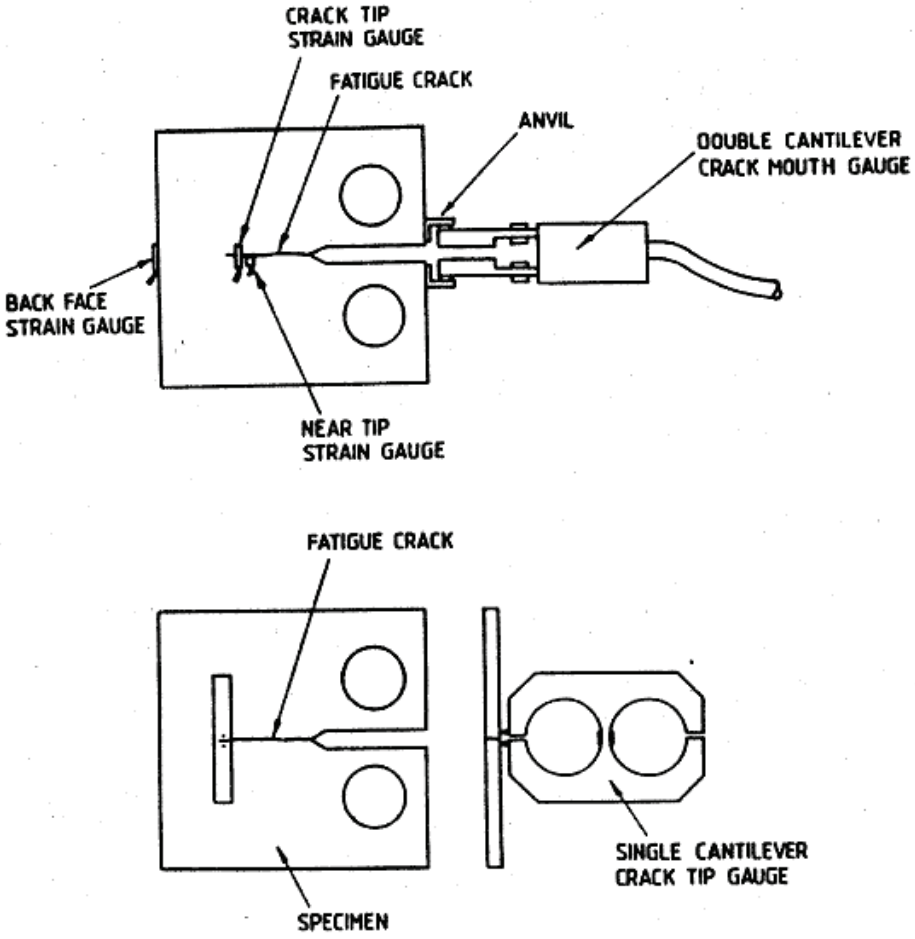

Fig. 2.30: Common compliance techniques for measuring crack closure (Marsh et al. 1991)

2.3.4.2. Classification of compliance gauges

Compliance gauges are classified into remote gauges and near tip gauges. Remote gauges are used to measure the crack length and the bulk crack closure response. They are classified into crack mouth gauge, back face strain gauge and near-tip gauges. Only near-tip gauges are applicable to measure the compliance near the crack tip, which can be grouped into displacement, strain and push rod gauges.

- **Crack mouth gauge**

Crack mouth gauge clips are mounted across the notch mouth of a CT-specimen or at the mid of a centre cracked plate. These gauges can be a single or double cantilever and have a strain gauge on the arm to measure the displacement, see Fig.

2.30. A single cantilever gauge is difficult and sensitive to mount, but it is more sensitive. Sullivan and Crooker(Sullivan et al. 1977) had measured crack opening displacement in a (CT) compact specimen as function of crack length. They give a calibration function for the geometry of such a specimen, which is given in Equ. (2.86) (Marsh et al. 1991). This equation is valid for crack lengths of thirty to sixty percent of total wall thickness. *E, B, w* and *P* are Young's modulus, the thickness, the width of specimen and the load, respectively.

$$\frac{vEB}{P} = 65.351 - 298.06\left(\frac{a}{w}\right) + 630.11\left(\frac{a}{w}\right)^2 \qquad \text{Equ. (2.86)}$$

- **Back face strain gauge**

Back face strain gauges are used for four point bending specimens and compact tension specimens. Compared with crack mouth gauge, these gauges show less hysteresis, are more sensitive, and are less influenced by mechanical noise of loading pin. These gauges can also be effectively used for centre crack panels. A relationship between back face strain and aspect ratio *a/w* was experimentally investigated by Richards and Deans (Richards et al.). They give a quadratic regression analysis to express their results in a closed form, shown in Equ. (2.87). It is also only valid within a limited crack growth ratio.

$$\frac{\varepsilon EBw}{P} = 13.841 - 72.506\left(\frac{a}{w}\right) + 138.45\left(\frac{a}{w}\right)^2 \qquad \text{Equ. (2.87)}$$

- **Displacement gauge**

Displacement gauges are single or double cantilever beams and could be fastened on a side of a specimen just behind the crack tip. The arms of gauge straddle the crack. Fastening a gauge on specimen is a sensitive issue. Gauge with needle tips needs the placement of small Vickers indents to assist location of the gauge. On the other hand, anvils are glued to the specimen to mount gauge on its side. Universal ball joints are used to locate gauge clips on anvils (Marsh et al. 1991).

- **Strain gauge**

A strain gauge can be positioned adjacently to one flank of the crack or it straddles the crack to detect compressive strain when crack closes, see Fig. 2.31. A strain gauge, which straddles a crack, is of *6-mm* length and 1-mm width. It is glued to the specimen one millimetre behind the crack tip. To ensure that only the end of the gauge is fastened to the specimen, *4-mm* width cellulose tape is used between

gauge and specimen. This tape also prevents any adhesive to enter the fatigue crack. After a few millimetres of crack, strain of a strain gauge is sufficiently large to fulfil its application.

On the other hand, one millimetre long and wide strain gauge can be applied behind the crack tip. The top edge of the gauge should be aligned to lower flank of the crack. This gauge experiences a compressive strain near to crack tip during crack closing. The necessary interruption of the fatigue test for fastening the strain gauge to the specimen counts as a severe disadvantage of this application method (Marsh et al. 1991).

- **Push rod gauge**

A push rod gauge is used to monitor the crack tip opening displacement (CTOD) behind the crack tip. To use the push rod gauge, the fatigue crack test is stopped to drill two holes of *1mm* and *0.5mm* diameter. These holes should be drilled *1mm* below and above the crack front respectively. A pushrod assembly is attached to specimen to measure the relative displacement between holes. Relative displacement can be measured by a twin cantilever displacement gauge, see Fig. 2.31 (Marsh et al. 1991).

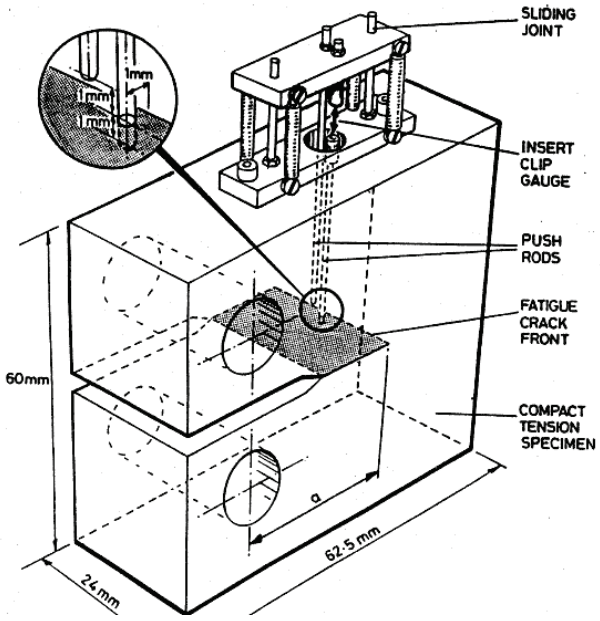

Fig. 2.31: The push rod closure gauge (Marsh et al. 1991)

2.3.4.3. Eddy current testing method

A varying magnetic field is produced by applying an alternating current (AC) to a coil. This causes an induced circulating current called eddy current in a conductive

material by countering the coil's primary magnetic field from a metal specimen. The eddy current loops are perpendicular to the direction of magnetic field. See Fig. 2.32.

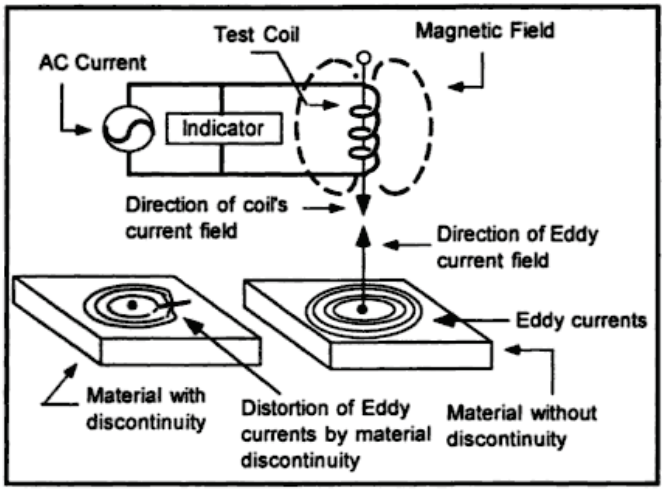

Fig. 2.32: Presence of flaws causes disruption in flow of eddy current (Farahmand 2001)

Eddy current loops and their normal direction are parallel to the conductive material surface and coil winding. A secondary magnetic field is produced due to eddy currents, opposes primary magnetic field, which then causes change in impedance of test coil. Any crack or discontinuity causes distortion of the secondary magnetic field, during scanning conductive material. Distortion of the secondary magnetic field can be recognized as a load change in the test coil. A change in load affects the coil impedance, which is monitored continuously during the whole test. Eddy current is influenced by heterogeneity in material such as flaws or cracks, which can easily be detected through this method (Diaz et al. 2007).

2.3.4.4. Potential drop method

The potential drop method is being used for thirty-five years as a non-destructive method to monitor crack propagation (Diaz et al. 2007). This method is often used to inspect walls of corded structures, petroleum fields, and atomic plants. The test is done by passing electric current to a specimen and then measuring a potential drop between electrodes placed on specimen. An increase in crack size reduces the cross-section area for the current flow. Reduced cross-section area causes a higher resistance to the current path, which leads to a potential drop. The size and shape of a crack can be estimated from potential drop data information.

The potential drop technique is further divided into the direct current potential drop (DCPD) and the alternating current potential drop (ACPD) methods.

- **Direct current potential drop (DCPD)**

Direct current potential drop is the most accurate, efficient and fully automated technique to monitor crack initiation and crack propagation. This method provides a total crack measurement including crack front curvature. DCPD technique uses two probes for the input current, which are fixed on the front end of the specimen, and two output probes to measure potential drop close to the crack, see Fig. 2.33 (Claudio et al. 2004).

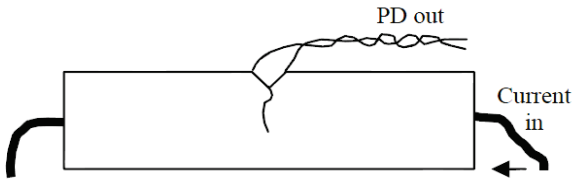

Fig. 2.33: Specimen with applied probes (Claudio et al. 2004)

Between five to fifty amperes of constant current passed through the probe. As the crack propagates, the un-cracked area of the test specimen decreases, which subsequently causes an increase in resistance and potential drop. Excessive heating due to large currents in the specimen can be avoided with a pulsated direct current.
Another pair of probes is attached to the specimen or a reference specimen is used to improve accuracy and resolution. To avoid the effect of the crack size on the reference voltage, reference probes should be located far away from the crack. With normalized potential measurement V across the crack, due to reference signal V_O all possible disturbances, such as a change in temperature, lack of stability, or instrumentation change, can be compensated.
A calibrating curve can be determined both experimentally and theoretically to calculate crack length. Analytical or numerical (FEM) methods are used to determine potential response for simple geometries. Experimental determination is the most frequently used method to determine calibration curve with the assistance of either visual crack growth inspection, for example by fracture surface analysis, or by change in compliance change.

- **Alternating current potential drop (ACPD)**

Alternating current potential drop technique is based on skin effect phenomena. It is used as non-destructive method for surface flaws in metal (Saguy et al. 2005). Skin effect means that the alternating-current flow through a conductor is restricted to the

skin of the metal with a specific thickness *δ,* as shown in Fig. 2.34.This thickness depends on the frequency *f* of current and physical properties of conductor (Saguy et al. 2007).

$$\delta = \frac{1}{(\pi \mu_r \mu_o \sigma f)^{\frac{1}{2}}} \qquad \text{Equ. (2.88)}$$

Where μ_r is relative magnetic permeability, $\mu_o$magnetic permeability and σ electrical conductivity. Specimens used for this technique have an input probe to inject current and output probe to collect current. Injected current concentrates into thin skin of thickness *δ*, flows through the specimen diverted down and up along the crack boundary and collected up from output probe as shown in Fig. 2.34.

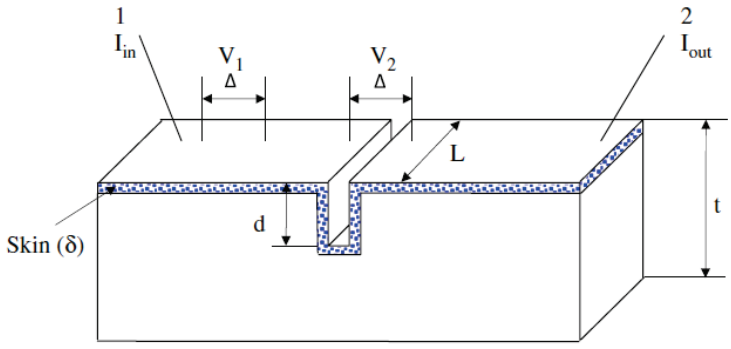

Fig. 2.34: A schematic description of the ACPD technique (Saguy et al. 2007)

A potential drop between electrodes is measured: V_1 as a reference voltage far away from the crack and a voltage V_2 near the crack is measured. The voltage ratio V_2/V_1 is translated into flaw depth using a theoretical or calibration procedure.

There are two different current flow modes called as thick and thin current flow modes. These current flow modes depend on flaw dimension (*d,L)*, current frequency *f* and probe material. The crack depth approximation with thin-skin is a well established and experimentally supported method. The thin skin approximation is done by following relationship shown in Equ. (2.89).

$$d = \frac{\Delta}{2}\left(\frac{V_2}{V_1} - 1\right). \qquad \text{Equ. (2.89)}$$

Equ. (2.89) is best suited for one dimensional approximation of crack depth, when all the thin-skin conditions are fulfilled. An approximation of crack depth for a thick-skin is given by the following relation shown in Equ. (2.90),

$$d = \frac{\Delta}{2}\left(\frac{V_1}{V_2}\right)^{1/2}\left(\frac{V_2}{V_1} - 1\right). \qquad \text{Equ. (2.90)}$$

2.3.4.5. Digital Image Correlation (DIC)

Many engineering applications have used versatile technique of digital image correlation (DIC) in fracture mechanics problems with satisfactory results. As a reference, an application of DIC in fracture problems is well documented in (Vanlanduit et al. 2009). Using DIC, the crack opening displacement (COD) is measured. COD is an important parameter to estimate the crack length and the stress intensity. COD method was first explained by Wells (Wells 1963), which defines COD as a function of crack length which can be expressed in Equ. (2.91).

$$COD = \frac{4\sigma}{E}\sqrt{a^2 - x^2}, \qquad \text{Equ. (2.91)}$$

Where σ is the applied tension, x the position on the crack and E the Young´s modulus of the material. Equ. (2.91) can be reduced to Equ. (2.92) by setting the value of x equal to zero at the crack centre resulting in:

$$COD_{max} = \frac{4\sigma}{E}a \qquad \text{Equ. (2.92)}$$

Sutton (Sutton et al. 1983) proposed DIC as an optical method to estimate displacement field of a deformed specimen. In this method, an image of an un-deformed specimen as a reference image and an image of deformed specimen as target image are used. The determination of displacement field is done by correlating these two images.

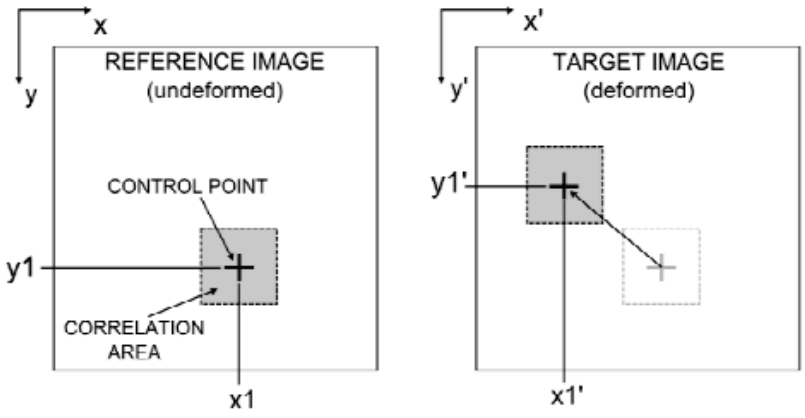

Fig. 2.35: Correlation area around the control point and displacement of the control point (Ozelo et al. 2009)

Fig. 2.35 shows the control points and the control area around the control point as small squares, which are then used to correlate these two images. A grid is created on the specimen with this control point where displacement should be measured. The bounded area around these points is a function used in image correlation. The function $I_O(x,y)$ is the corresponded correlation area function in the reference image. $I_n(x´,y´)$ is the corresponded correlation area function in the target image. It can be assumed that the correlation area function of the reference image is related to the correlation area function of the target image, whereby a displacement vector is applied to the target image.

$$I_0(x,y)=I_n(x+u,y+v) \qquad \text{Equ. (2.93)}$$

The value of the displacement x and y can be determined if the cross-correlation coefficients exhibits its maximum value. This parameter can be calculated through cross-correlation of the functions $I_O(x,y)$ and $I_n(x´,y´)$ given in Equ. (2.94) (Vendroux et al. 1994).

$$C(u,v) = \frac{\sum_{x,y} I_0(x,y) I_n(x+u,y+v)}{[\sum_{x,y} I_0(x,y)^2 \sum_{x,y} I_n(x+u,y+v)^2)]^{1/2}} \qquad \text{Equ. (2.94)}$$

3. Numerical analysis

The numerical crack propagation analysis is at first verified against the results of the IIW-Round Robin study on fracture mechanics. A short survey of this test is given in the next section.

3.1. IIW Round Robin calculation

The International Institute of Welding published a final report for calculating fatigue assessment of welded joints by Fracture Mechanics, see IIW Doc.XIII-1273r5-11 (Hobbacher 2013). According to this document, fracture mechanics is used as a common method for the assessment of fatigue properties of weld imperfection in welded joints. For the estimation of the fatigue life of joints, only the crack propagation period is considered, because the microscopic crack initiation period is comparatively very short to the total fatigue life. Engineers and analysts used different codes, recommendations in assessment of fatigue life and observed a quite huge variation of results. This variation cannot be attributed to the variation of the ingoing geometrical and material parameters. Major sources of variation of results are the determination of the stress intensity factor and applied numerical procedures. This document explains numerical procedures which cause variation in results and thus gives recommendation for a standardized procedure. (Hobbacher 2013)

To unify recommendations on fracture mechanical crack growth, it was decided at a meeting held in Oslo in March 2010 to calculate the fatigue assessment of welded joints by fracture mechanics with following aims as a Round-Robin study. Two milestones are especially important in regard to own fracture mechanical calculation:

- Paris-Erdogan power law integration scheme using different software and their numerical comparison and accuracy for small cracks and crack increments.
- The comparison of correction function $\mathrm{Y(a)}$ used in fracture mechanics and $\mathrm{M_k(a)}$ formula for two and three dimensional based problems.

3.1.1. Parameters

Calculations in the Round-Robin tests are done with following parameters.

Constant C_0	Exponent m	Initial crack a_i	Final crack a_f	Wall thickness	Stress
5.21e-13[N;mm]	*3.0*	*0.1 mm*	*10 mm*	*25 mm*	*100 MPa*

Tab. 3.1: Material and initial crack parameters (Hobbacher 2013)

3.1.2. Description of tasks

There are five different problem statements given in the IIW-document and the results are obtained from different participants. The three problems relevant to this master thesis are explained here. The three-dimensional task as well as the non-linear load stress distribution is discarded within this work.

1. Integration algorithm of software should be checked for a one-sided through going crack in a *100mm* wide flat bar.

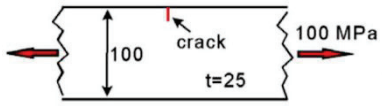

Fig. 3.1: Problem 1: one sided crack in flat plate (Hobbacher 2013)

2. A tensile bar is welded with a two-sided fillet weld to a *16mm* thick transverse attachment. Fillet weld throat *a* is *7mm* and weld toe angle *45°* with a leg length of *10mm* to tensile bar. Weld toe angle varies by *30°, 45°,60°* at same toe position. A through going crack edge to edge for two-dimensional problems is assumed for the 2D-crack growth calculation.

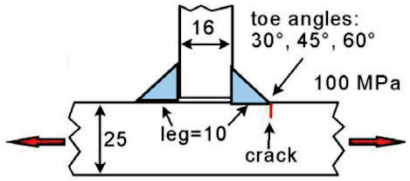

Fig. 3.2: Problem 2: weld toe crack of thick transverse attachment (Hobbacher 2013)

3. Root crack in cruciform joint with fillet welds. As shown in Fig. 3.3 a through going crack from edge to edge should be investigated for a cruciform joint with fillet welds in a partial penetration. Weld has a throat of *a= 7mm* and a root gape of *10mm* with weld angle *45°.*

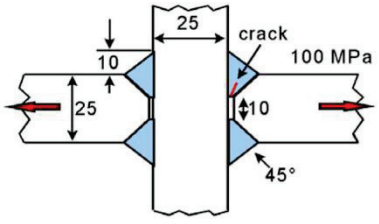

Fig. 3.3: Problem 4 : Root crack in cruciform joint with fillet welds (Hobbacher 2013)

3.2. Analysis using Franc2D

In this master thesis, the applicability of Franc2D is studied and verified against the results of the three selected tasks of the fracture mechanical IIW Round-Robin study.

3.2.1. Introduction

Franc2D is originally developed by Paul Wawrznek at Cornell University. This software has a modular design and works with topological data structures. Franc2D is a interactive program for simulating crack growth by representing layered structures as lap joints or bonded repairs (Lesulauro).

3.2.1.1. Finite elements

- **Continuum elements**

For elastic analyses, standard six or eight nodded elements with quadratic shape functions are used in Franc2D. The advantage of using such elements is that the stress singularity at crack tip can be combined in the solution by moving the side nodes to quarter point locations (Henshell et al. 1975).

- **Interface elements**

The main purpose of using interface elements is to represent the contact between surfaces. Using these elements, a relation between relative displacement and surface traction can be user-specified to get equivalent nodal loads through integration of surface traction. These equivalent nodal loads are included during the dynamic relaxation solution.

3.2.1.2. Fracture mechanical calculations

A two dimensional LEFM concept is used to incorporate fracture calculation in Franc2D. It uses all the three stress components of the tensor to determine the crack growth direction (Erdogan et al. 1963). This leads to varying crack paths dependent on the currently active load mode.

3.2.1.3. Remeshing

A modified mesh is required during crack analysis at each step near a crack tip to get information about the current crack configuration. For that purpose, Franc2D uses an automatic remeshing strategy, which deletes elements in the crack tip vicinity, moves the crack tip, and connects the new crack by inserting a trial mesh to the existing

mesh. A modification is done to Suhara-Fukuda (Shaw et al. 1978) algorithm to generate a trial mesh of triangulated elements.

3.2.1.4. Initial geometry and meshing

First step in all numerical analysis methods is to develop a finite element (FE) model which includes geometry, set of boundary and loading conditions used to define the real physical problem. For simulation using Franc2D, a mesh generating program CASCA is distributed with Franc2D which is used to create the initial geometry and the mesh the model. Instead of CASCA other programs can also be used with the help of a translator to convert the mesh description for Franc2D *.inp format.

3.2.2. Simulation process of task 1 using Franc2D

To check the integration algorithm of the Franc2D software for a one-sided through going crack in wide flat bar, as described in IIW document (Hobbacher 2013), an initial geometry and mesh for the model is prepared using CASCA shown in Fig. 3.4. A bilinear four-side meshing algorithm is selected to mesh the flat bar. This algorithm requires equal number of nodes on opposite sides of rectangular region.

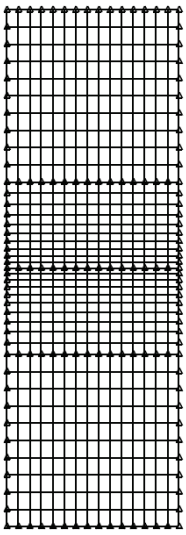

Fig. 3.4: Initial geometry and mesh using CASCA

- **Material properties**

The material used for the present study was steel. The fatigue simulation was done by applying a maximum stress *100* at stress ratios of $R=0$. The value of Poisson's ratio υ was chosen *0.25* and the modulus of elasticity E=210,000*MPa* respectively.

- **Loading and boundary conditions**

The boundary and loading conditions for the plat are shown in the figure Fig. 3.5. The nodes of the lower and upper left and right side of the model are fixed in *x*-direction. Lower edge nodes of the model are supported in *y*-direction and upper end nodes are applied with a distributed load of *100MPa*.

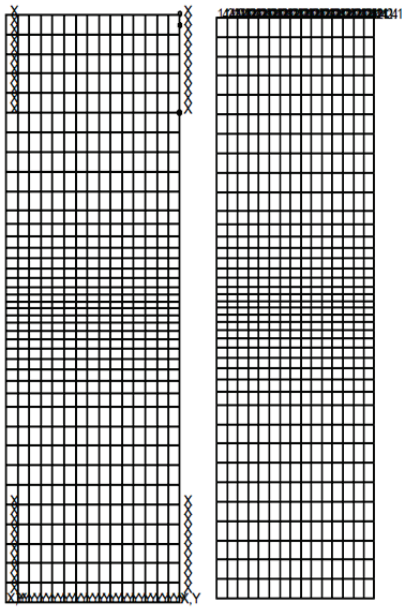

Fig. 3.5: Loading and boundary conditions for flat bar

- **Stress analysis and post processing**

A linear elastic stress analysis is performed. Fig. 3.6 shows a mesh of the model and the stress distribution in y-direction in flat bar.

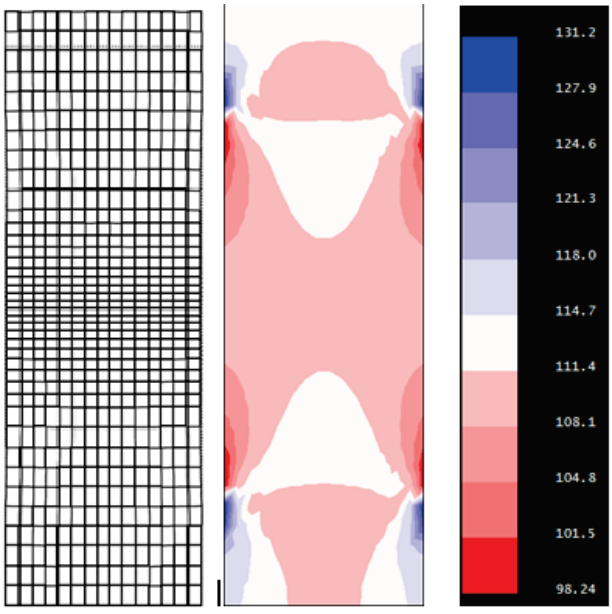

Fig. 3.6: linear elastic stress analysis for flat bar

- **Crack initiation**

A non-cohesive initial edge crack of *0.1mm* is placed in the mid of right edge of the flat bar. During this process the initial crack is manually inserted and program deletes a number of elements in the vicinity of the crack tip. It performs an automatic re-meshing which is shown in Fig. 3.7.

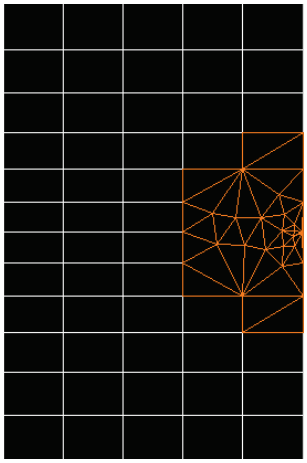

Fig. 3.7: An initial edge crack in flat bar with automatic re-meshing

The stress distribution results obtained from simulations after introducing an initial crack in flat bar shows that high critical tensile stresses occur at the crack tip. The maximum value of stress near crack tip is about *198 MPa* as shown in Fig. 3.8. This is only valid at the evaluated initial crack-length of *0.1mm*.

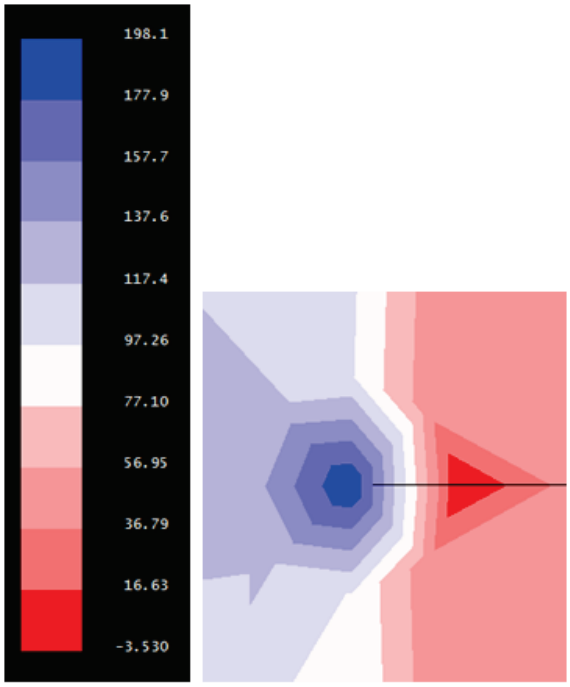

Fig. 3.8: Stress distribution results after introducing an initial crack in flat bar

- **Crack propagation**

Franc2D is well capable of predicting the direction in which the crack will propagate. Prior to performing numerical calculation of crack propagation it is necessary to specify the magnitude of the crack increment and also the number of steps over the crack should propagate. A crack increment of *0.66* and *15* steps were chosen without pre selection of crack path. Fig. 3.9 shows a deformed mesh of plate after automatic crack propagation.

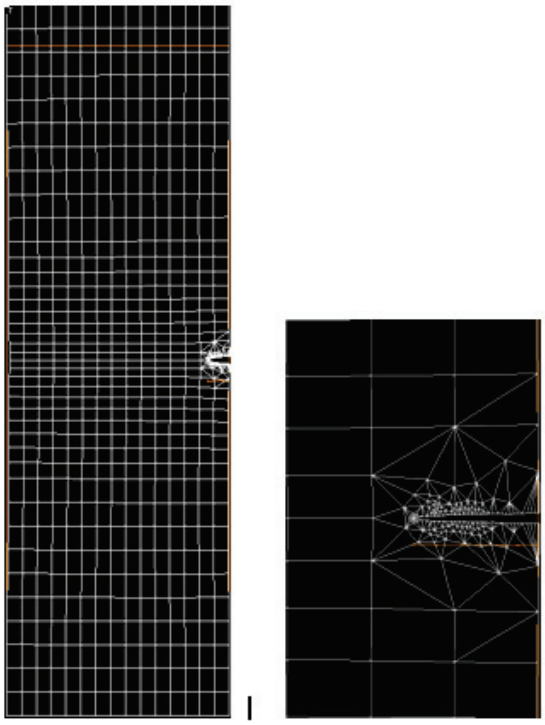

Fig. 3.9: Deformed mesh of plate after automatic crack propagation

- **Fatigue life analysis**

A simple fatigue life analysis is performed in Franc2D which is based on Paris-Erdogan law (Paris et al. 1961) The Paris law states that the crack growth rate is an exponential function of the stress intensity range ΔK.

$$\frac{da}{dN} = C(\Delta K)^m \ , \qquad \text{Equ. (3.1)}$$

Where $C=5.21e^{-13}$ and $m=3$ are the material specific input parameters. The fatigue life analysis results show that it takes approximately *1.6e6* cycles to reach a crack length of *10 mm* as shown in Fig. 3.10. The results of fatigue analysis depends highly on material parameters *C* and *m*. A small variation in the values leads to significant change in fatigue life.

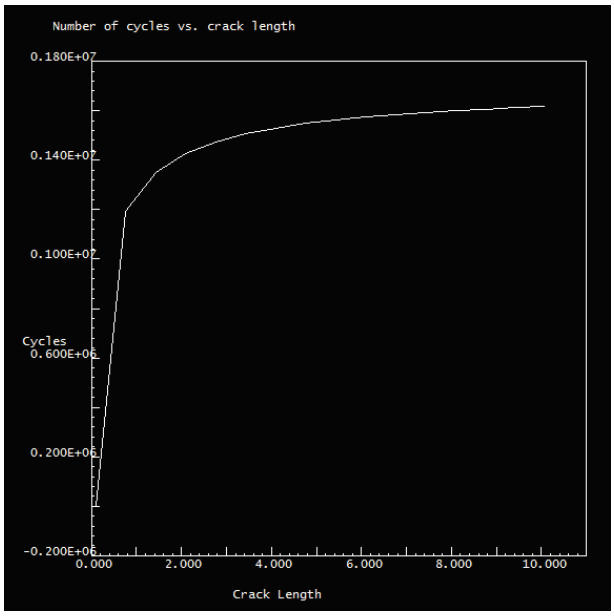

Fig. 3.10: Number of cycle's vs. crack length *a*

- **Results of Stress intensity factor K_I**

A set of K_I values is obtained for different crack lengths and finally the K_I values are plotted as a function of crack length in order to understand the crack propagation behaviour. The variation of K_I with respect to crack length is shown in Fig. 3.11. The stress intensity rate increases within the first millimetre and is subsequently nearly constant in the long-crack growth region.

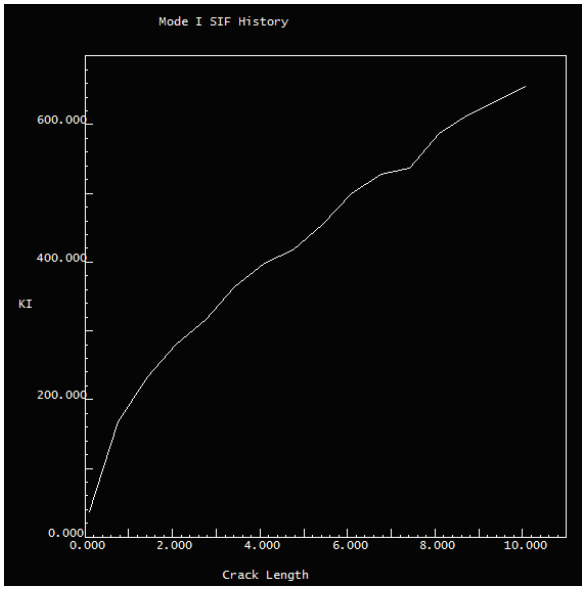

Fig. 3.11: Stress intensity factor K_I vs. crack length *a*

- **Comparison of own Franc2D results with IIW Round-Robin study**

Tab. 3.2 shows the simulation results using Franc2D. A comparison of the results to the results given in IIW document shows a 14% variation to the results from participant 2, 25% variation to participant 6 and 5% variation to participant 8, Which shows that the results are in quite good range compare to participant 8 and variation with other participants are due to user defined internal software settings. Tab. 3.3 shows the results of ten participants taken from IIW Round-Robin test.

Simulation results	1600000	Franc2D

Tab. 3.2: Simulation results from Franc2D for Round-Robin task1

Participants	cycles	remarks
1	1416000	ASTM E699-81
	1187099	3D weight function made 2D by ci=100
2	1385137	Franc2D
	1319753	Tada
3	1378900	Tada
4	----	----
5	1372300	AFGROW
6	1200000	Franc2D
7	1376000	weight function
8	1520000	Franc2D
9	1411100	Weight function by Fett and Munz
10	1400616	FEA BEASY (Boundary element analysis)

Tab. 3.3: Results from IIW document (Hobbacher 2013)

3.2.3. Simulation process of task 2 using Franc2D

The next problem stated in IIW Doc.XIII-1273r5-11 (Hobbacher 2013) is to check $M_k(a)$-function of a tensile bar which is welded with a two side fillet weld to a thick transverse attachment as shown in Fig. 3.2. $M_k(a)$-function should be evaluated performing three different simulations for the toe angle *30°, 45°, 60°* at the same weld toe position. Similar to task 1 an initial geometry and mesh with CASCA for a *45°*

weld toe angle is prepared to simulate in Franc2D. The same material is applied as in task 1. Initial meshed geometry in Franc2D is shown in the Fig. 3.12.

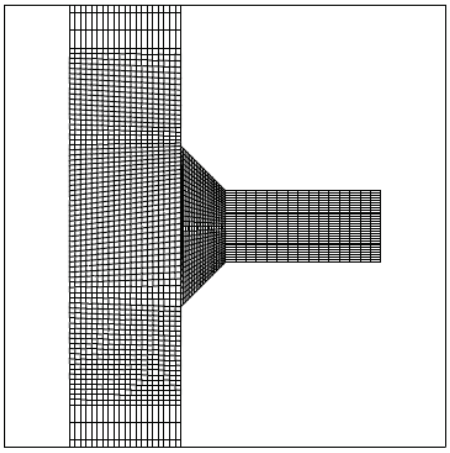

Fig. 3.12: Initial mesh of transverse attachment with 45° fillet weld

- **Loading and boundary conditions**

Left vertical edge of tensile bar is fixed in *x*-direction to avoid deflection and bending for this problem. Lower end nodes of the model are supported in *y*-direction and upper end nodes is applied with distributed load.

- **Stress analysis and post processing**

A linear elastic stress analysis is performed with given load condition and plane strain state to check the stress concentrations at the weld toe. The results shown in Fig. 3.13 gives a good agreement with above mentioned statement and shows high stress concentration at weld toe compared to the rest cross section of tensile bar. A deformed mesh of the model and stress distribution contour in y-direction shows the maximum stress at weld toes of approximately 228 *MPa*.

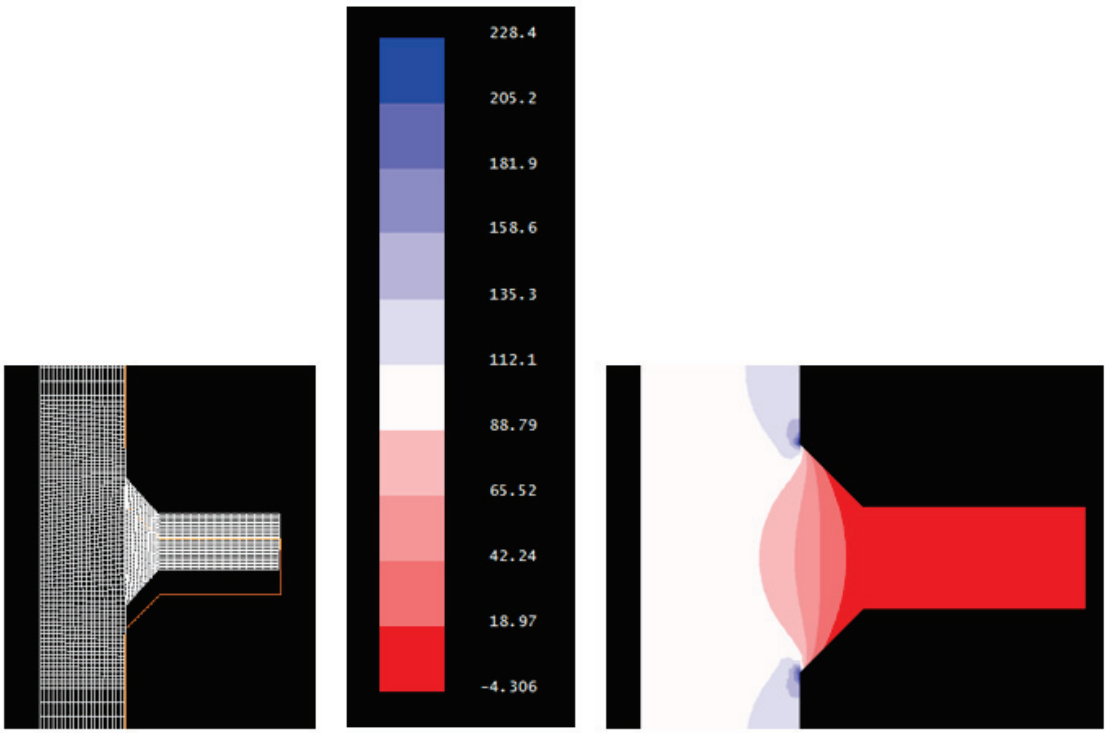

Fig. 3.13: Deformed mesh of model and stress distribution contour in y-direction

- **Crack initiation**

A non-cohesive initial crack of *0.1mm* is placed at the weld toe. During this process program inserts a crack by deleting a number of elements by performing automatic re-meshing. Stress distribution results obtained from simulations performed in Franc2D after introducing an initial crack in weld toe shows a high critical tensile stress at crack tip. The maximum value of stress near crack tip is about *2.4e4 MPa* as shown in Fig. 3.14.

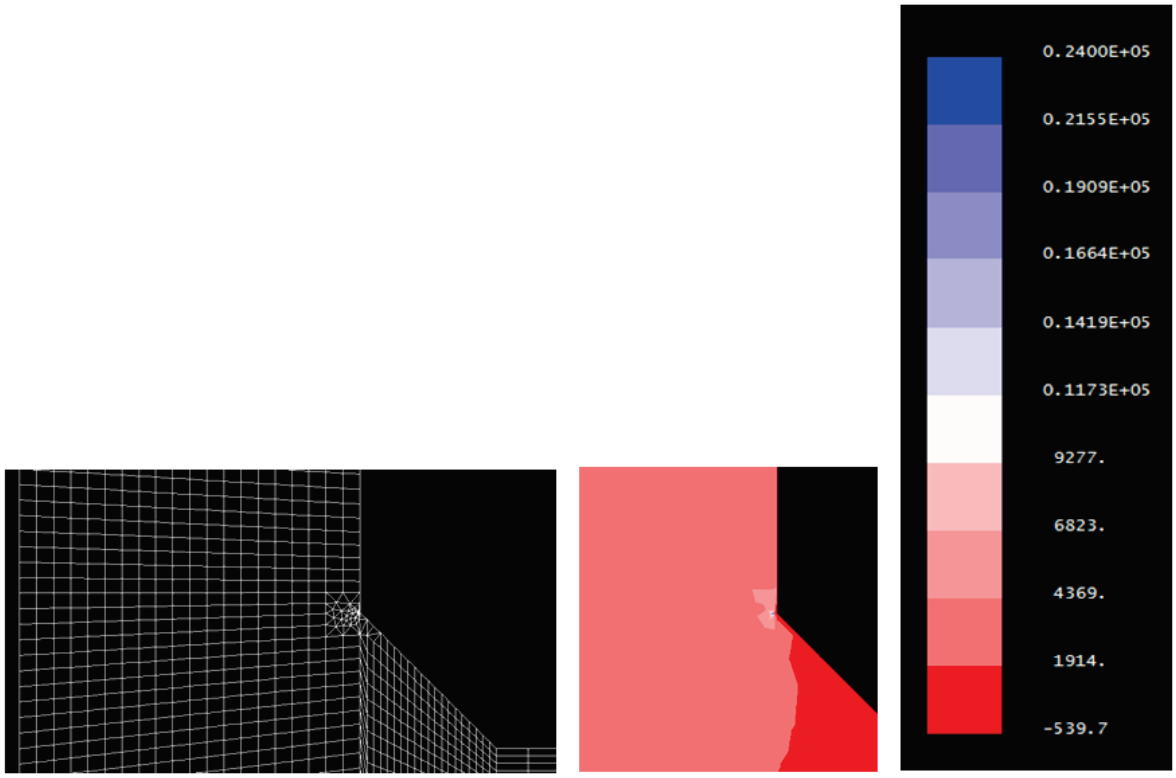

Fig. 3.14: An initial crack with high critical tensile stress at crack tip

- **Crack propagation**

The crack propagation settings in Franc2D in this case are the same as in task 1, only the geometry, loading and boundary conditions differs.

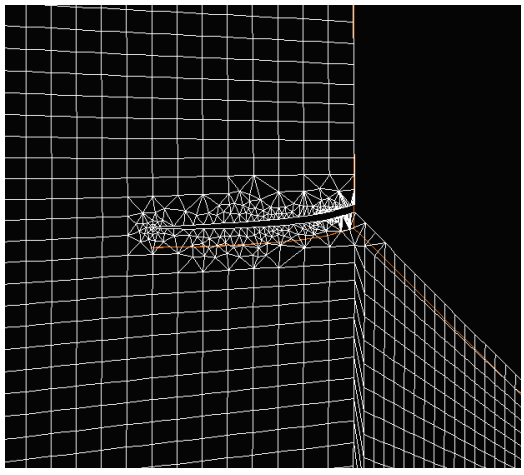

Fig. 3.15: Deformed mesh of the model after crack propagation

- **Fatigue life analysis**

Material input parameters $C=5.21e^{-13}$ and $m=3$ for the fatigue life analysis shows that it takes approximately *3.1e5* cycles to reach a crack length of *10 mm*.

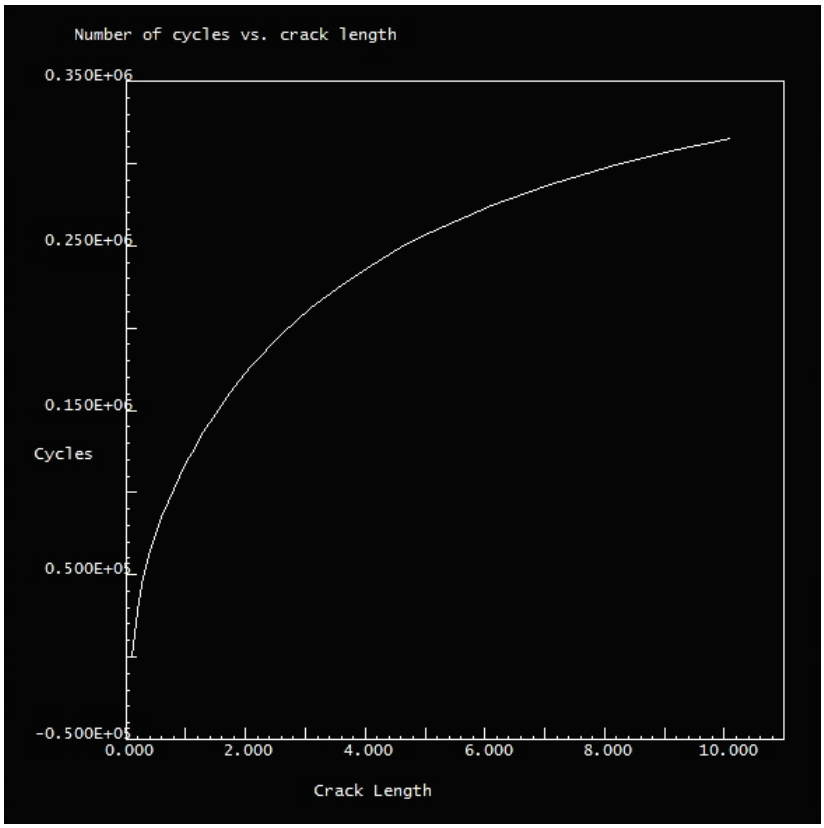

Fig. 3.16: Number of cycle's vs. crack length a for 45° fillet weld

Furthermore simulation of fillet weld joint with toe angle *30°* and *60°* is performed and results are summarized in Tab. 3.4. The comparison of fatigue life between weld toe angles is shown in Fig. 3.17.

It also shows that toe angle *30°* has a significant higher fatigue life compared to *45°* and *60°* weld toe angle.

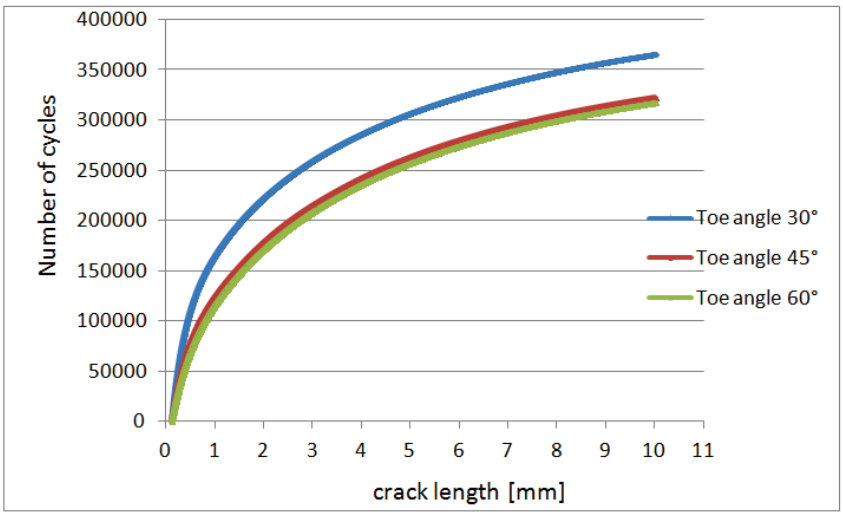

Fig. 3.17: Comparison of simulation results of fillet weld joint for 30°, 45° and 60° toe angle

- **Stress intensity**

The effect of different toe angles on stress intensity range *ΔKI* is shown in Fig. 3.18 and Fig. 3.19. A variation of stress intensity factor can be seen at crack propagation stage from *0.1 mm* to *1.2 mm* crack length. Simulation results show that different toe angles have a significant effect on stress intensity factor. After reaching a specific crack length in crack propagation stage, the values of stress intensity factor have the same values till final rupture. The observations of Fig. 3.19 show that a toe angle of *60°* have higher stress intensity values compared to toe angle of *30°* and *45°*.

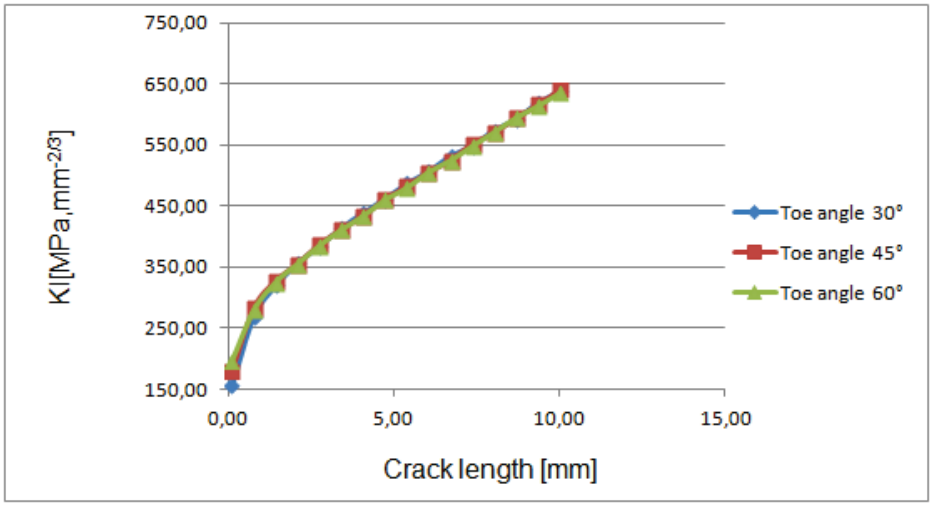

Fig. 3.18: Stress intensity factor of weld toe angle for 30°, 45°, and 60°

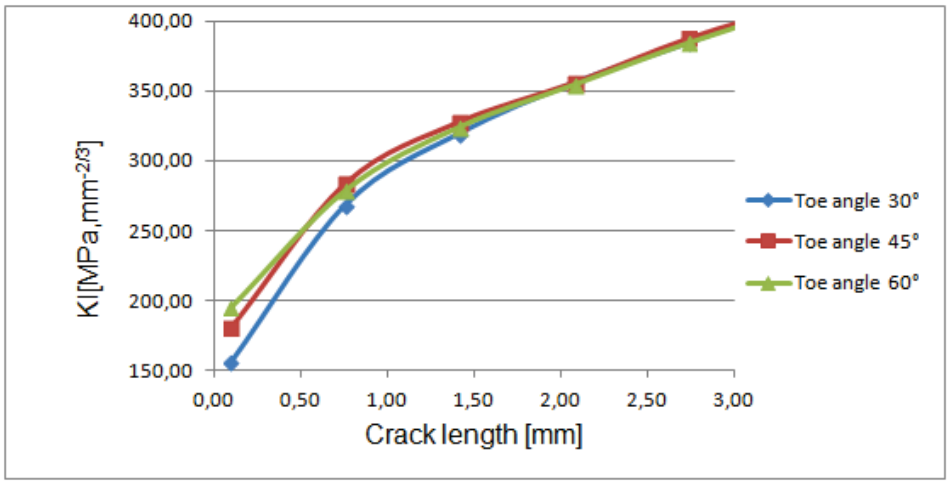

Fig. 3.19: Stress intensity factor of weld toe angle for 30°, 45°, and 60°

- **Comparison of results with IIW Round-Robin results**

Tab. 3.4 shows simulation results of fillet weld joint for *30°, 45° and 60°* weld toe angle. A comparison of this own results to the results given in IIW document shows a

1% variation for *30°* toe angle to the results from participant 2, 12*%* variation to participant 6 for *45°* toe angle and 14*%* variation to participant 3 for *60°* toe angle. Which shows that, the results are again in good range compare to participant 2 and variation with other participants are due to user defined internal software settings. Tab. 3.5 shows results of ten participant from IIW document.

	cycles	Remarks
Simulation results	385000	30°, Franc2D + Casca
	310000	45°, Franc2D + Casca
	290000	60°, Franc2D + Casca

Tab. 3.4: Simulation results of fillet weld joint for 30°, 45° and 60°

Participants	cycles	Remarks
1	208979	45°, Mk by Maddox
	265770	30°, Mk by Hobbacher
	192110	45°, Mk by Hobbacher
	140926	60°, Mk by Hobbacher
	267942	45°, weight function
2	410350	30°, FRANC2D
	360172	45°, FRANC2D
	353607	60°, FRANC2D
3	383735	30°, FRANC2D
	338434	45°, FRANC2D
	332330	60°, FRANC2D
4	----	----
5	277460	30°, AFGROW
	238220	45°,AFGROW
	194560	60°, AFGROW
6	355000	30°, Franc2D + Casca
	310000	45°, Franc2D + Casca
	255000	60°, Franc2D + Casca
7	442300	30° weight function
	261100	45° weight function
	162400	60° weight function
8	402831	30°, Franc2D
	363983	45°, Franc2D
	346036	60°, Franc2D
9	1411100	Program did not support Mk-corrections
10	411940	30° BEASY Boundary element program
	367131	45°
	361505	60°

Tab. 3.5: Results from IIW document (Hobbacher 2013)

3.2.4. Simulation process of task 4 using Franc2D

For the root crack problem as stated in the IIW document (Hobbacher 2013), the cruciform are symmetrical about both x and y-axes. In case of an initial crack at weld toe it makes the model unsymmetrical. Quarter symmetry is used for this problem. Material used in the present problem is same as for task 1 and 2.

- **Loading and boundary conditions**

Boundary conditions are shown in Fig. 3.20 for the quarter model. Left edge of the model was supported in the *x*-direction and a uniform distribution load was applied at the other end. Lower edge is supported in *y*-direction. One node of the model is locked in x and y-direction at left lower edge to prevent model from performing rigid body motions.

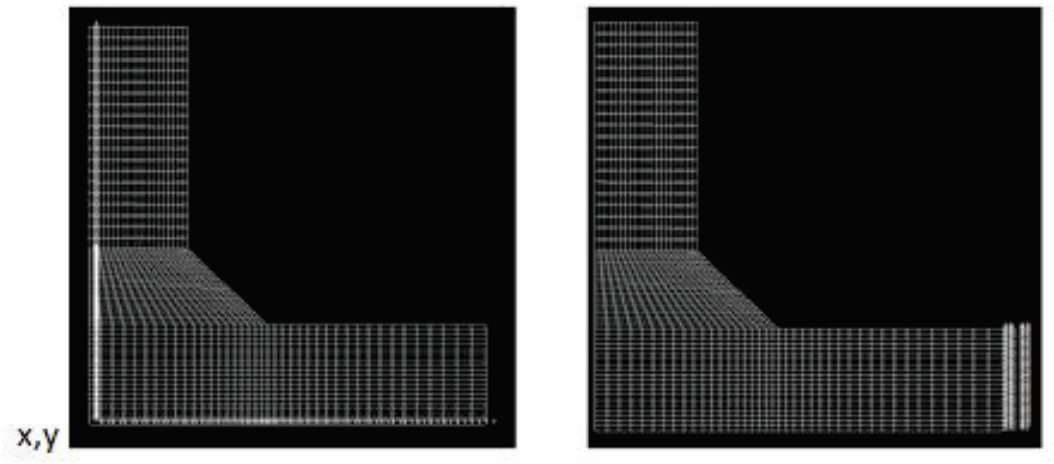

Fig. 3.20: Load and boundary condition for cruciform weld joint

- **Crack initiation and propagation**

A non-cohesive initial crack of *5.1 mm* is placed at the weld root. Stress distribution results obtained from simulations performed in FRANC2D after introducing an initial crack in weld root shows a high critical tensile stress at the crack tip. The maximum value of stress in x-direction near crack tip is about *495.5 MPa* shown in Fig. 3.21.

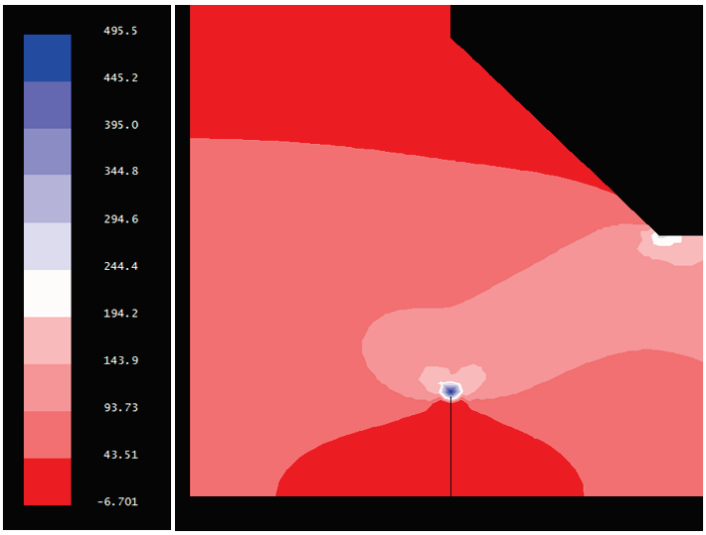

Fig. 3.21: Stress analysis after initial root crack

In crack propagation stage a crack increment of *0.66* and *15* steps were chosen without preselecting of crack path. Fig. 3.22 shows a deformed mesh of the model after automatic crack propagation.

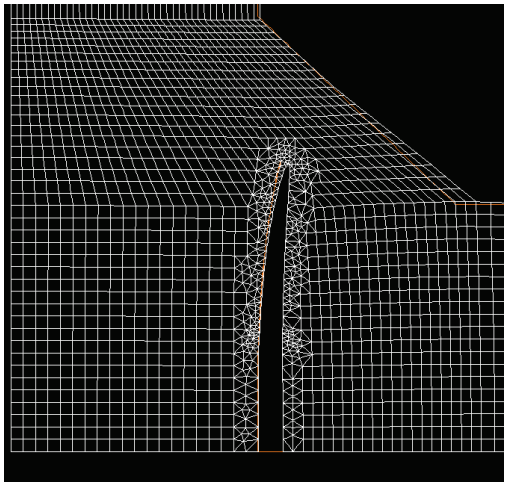

Fig. 3.22: A deformed mesh of the model after a final root crack

- **Fatigue life analysis**

  Fatigue life analysis results are obtained with same material specific input parameters $C=5.21e^{-13}$ and $m=3$ as in previous problems. The fatigue life analysis results show that it takes approximately *1.6e5* cycles to reach a crack length of *10mm*.

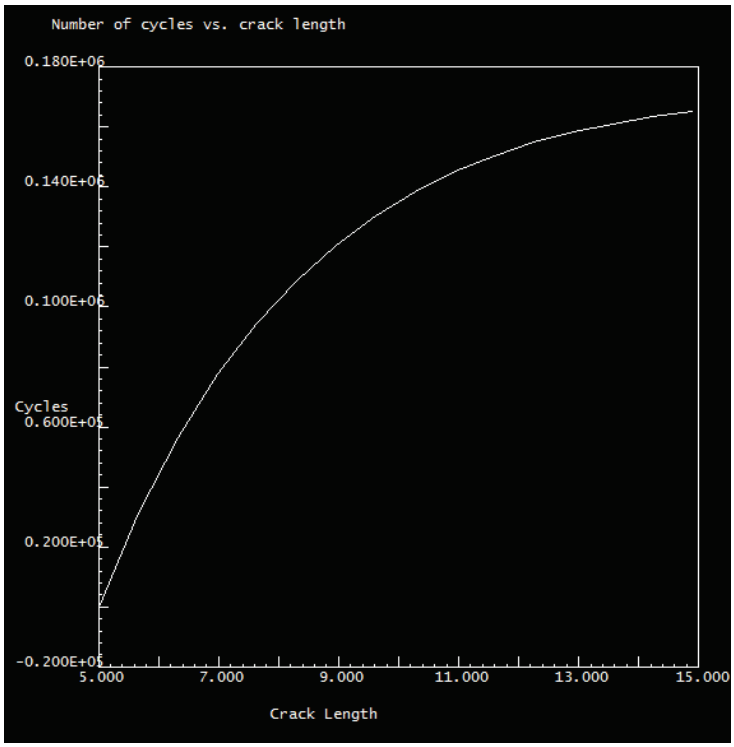

Fig. 3.23: Number of cycles vs. crack length *a*

The results of the fatigue life estimation are show in Tab. 3.6. A comparison of the results to the results given in IIW document shows a 70% variation to the results from participant 2, 15% to 38% variation to participant 3, 15% to 32% variation to participant 6 and 42% variation to participant 8. The results of ten participants from IIW document are shows in Tab. 3.7.

	cycles	Remarkes
Simulation results	160000	45° toe angle, Franc2D + Casca

Tab. 3.6: Simulation results from Franc2D

Participants	cycles	Remarks
1	298779	Frank+Fisher
2	273089	Franc2D
3	135760	Franc2D automatic model
	221205	Franc2D standard model
4	-----	-----
5	112650	AFGROW, beta set equal to MK,MK by BS7910
	189450	AFGROW beta set equal to MK,MK by Frank+Fisher
6	136000	Franc2D+Casca,two-sided crack, max principle stress
	212000	Franc2D+Casca,one-sided crack, max principle stress
7	375600	Readymade formula
8	228000	Franc2D
9	255330	API Recommended practice579, API 2000
10	166082	Boundary element program

Tab. 3.7: Results from IIW document (Hobbacher 2013)

- **Stress intensity**

A set of K_I values is obtained for different crack lengths. Tab. 3.8 shows K_I-values for different crack lengths.

a[mm]	K_I [MPa mm$^{-2/3}$]
0.1	334.9
0.2	341.5
0.5	352.7
1	367
2	407
5	542.3
10	962.7

Tab. 3.8: Stress intensity versus crack length

4. Analytical analysis

Beside the fracture mechanical calculation using Franc2D as numerical tool, an analytical based integration of fatigue life based on analytical stress intensity formulae is done in this section using the tool nCode.

4.1. Introduction

nCode consists of a set of commercial tools and is used for fatigue and crack growth analysis. The analysis is defined through a flow chart in the primary interface called Glyphs. Different glyphs provide sets of input data which are processed in a dedicated analysis glyph to give results, as shown in Fig. 4.1.

Fig. 4.1: Synopsis of nCode architecture (Michel 2012)

An input Glyph can be a signal, tabulate data, or can be even a Finite Element (FE) model. An analysis glyph can contain be a strain-based, stress-based, multiaxial criteria as Dang Van, crack growth or signal processing tool. Output glyphs show histograms, 2D curves or FE output (Michel 2012).

4.1.1. Fatigue analysis by crack calculation

Fatigue analysis by use of fracture mechanical calcualtion is done using nCode Glyphworks, which is a data processing system for engineering test data. Analysis work flow can be created by dragging and dropping of analysis building blocks shown in Fig. 4.2. Glyphworks performs a fatigue analysis from measured data in addition to general signal processings (Michel 2012). A Glyphworks environment consist of,

1. Input signal
2. Crack growth Glyph
3. Visualisation Glyph
4. Glyphs menu
5. Files menu
6. Rainflow and FE visualisation

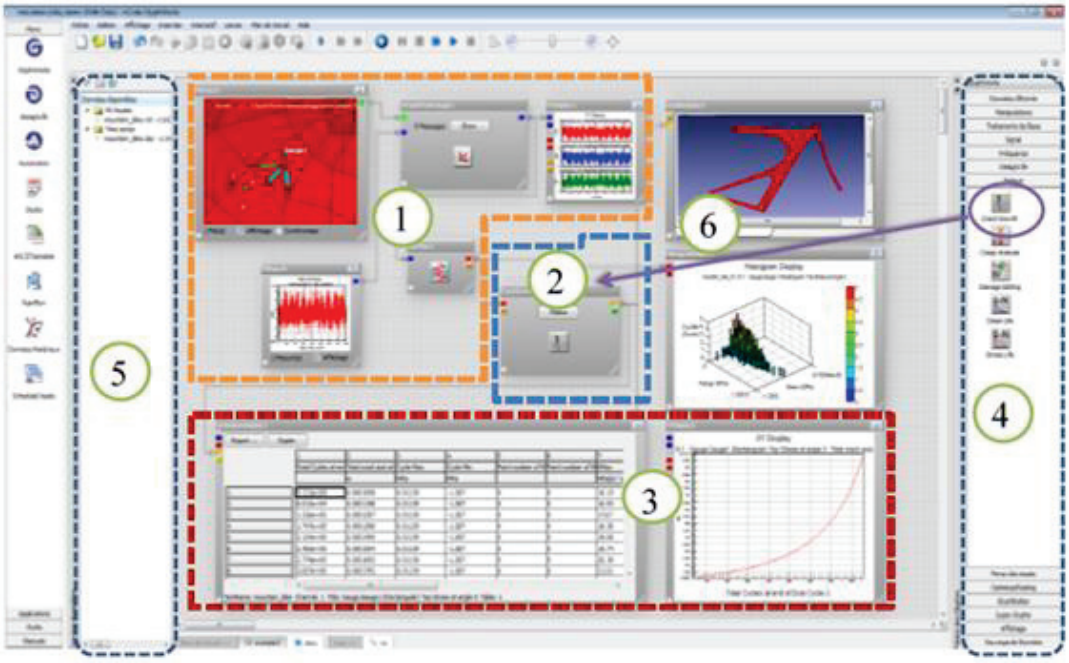

Fig. 4.2: Glyphworks environment (Michel 2012)

The crack growth glyph will be used in the following analysis to verify the IIW Round-Robin test results.

4.1.2. Fatigue analysis by stress or strain-based approaches

Fatigue life estimation from finite element results can be done using nCode DesignLife. Such a finite element based design analysis is sketched in Fig. 4.3.

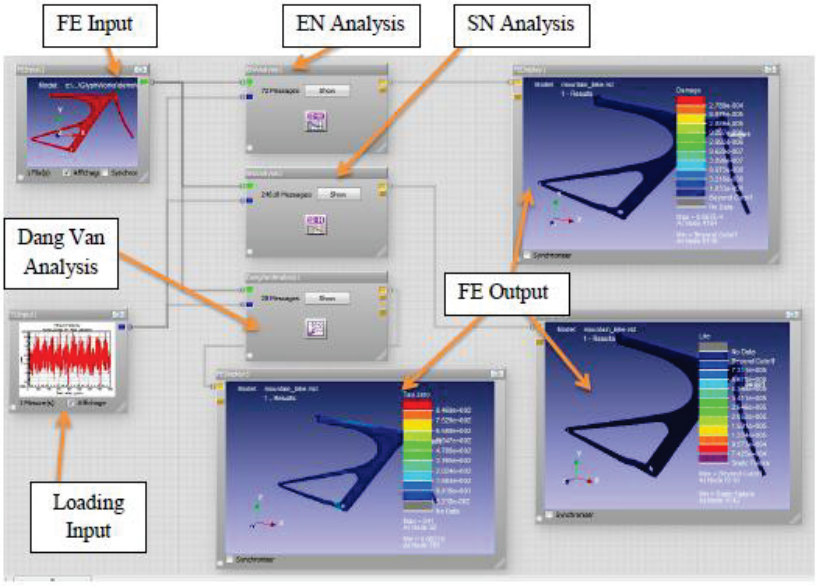

Fig. 4.3: DesignLife fatigue analysis (Michel 2012)

4.2. Analytical IIW Round-Robin cases analysis

There are three different possibilities to investigate the crack propagation behaviour using nCode in regard to the definition of the stress intensity factor of a welded joint:

- Integrated library solution
- Standard SIF equation
- Using Ksn file

4.2.1. Simulation process of task 1 using nCode

The single-edge crack specimen is investigated using three different types of stress-intensity-factor SIF definition procedures.

4.2.1.1. Integrate library solution

The nCode glyph flow shown in Fig. 4.4 is build-up to investigate task1. Calculations are performed selecting a single-edge crack specimen in tension from the integrate library as shown in Fig. 4.5

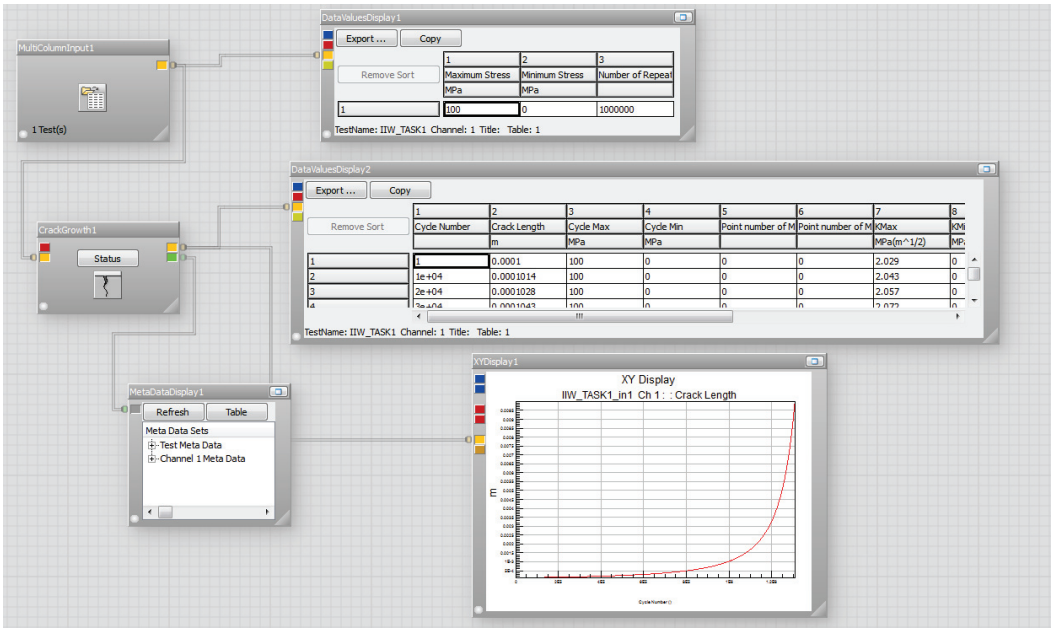

Fig. 4.4: Glyph definition for round robin calculation

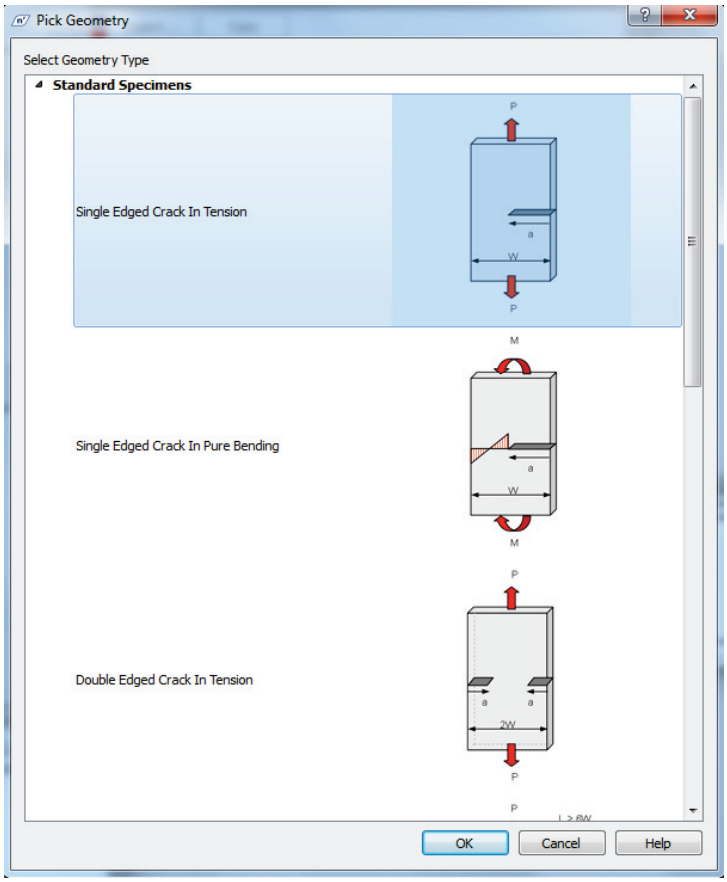

Fig. 4.5: Standard geometry for single edge crack in tension

The results of task 1 with integrated solution are shown in Fig. 4.6. The results obtained through integrated solution method are too conservative compared to the ones provided in IIW-document. It takes approximately *7.622e5* number of cycles to reach the crack length of *10mm*.

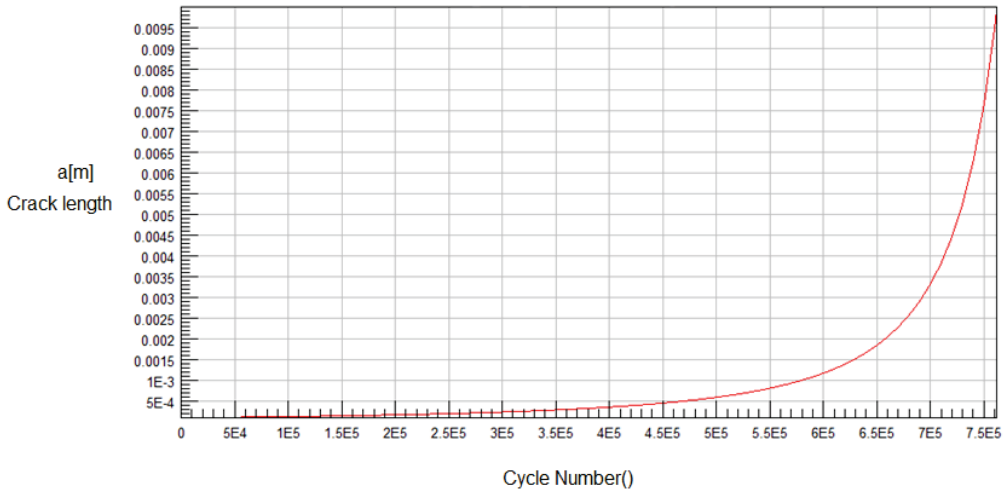

Fig. 4.6: nCode integrated solution result

4.2.1.2. Standard SIF equation

SIF solution from Rooke and Cartwright (ROOKE et al. 1976) as given in Equ. (4.1) is used to check the results in nCode. SIF parameters are applied using standard SIF equation option as shown in Fig. 4.7.

$$\mathrm{SIF} = 1.112 - 0.231\left(\frac{a}{w}\right) + 10.55\left(\frac{a}{w}\right)^2 - 21.7\left(\frac{a}{w}\right)^3 + 30.39\left(\frac{a}{w}\right)^4 \qquad \text{Equ. (4.1)}$$

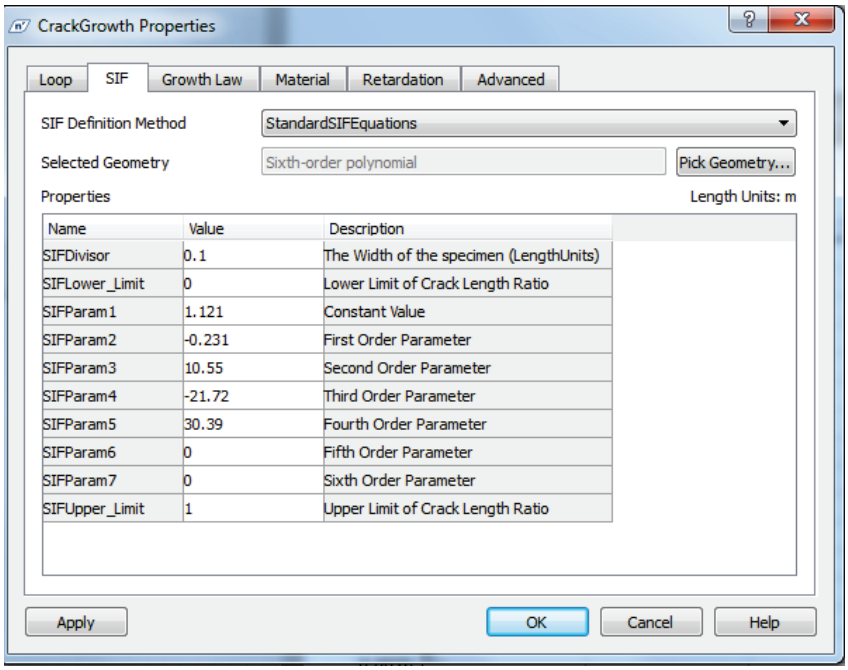

Fig. 4.7: Polynomial definition of SIF

Results obtained using SIF equation according to Rooke and Cartwright (ROOKE et al. 1976) are dominantly high as compared to the results obtained by integrate library solution shown in Fig. 4.8. It takes *1.389e6* cycles to reach the crack length of *10mm.*

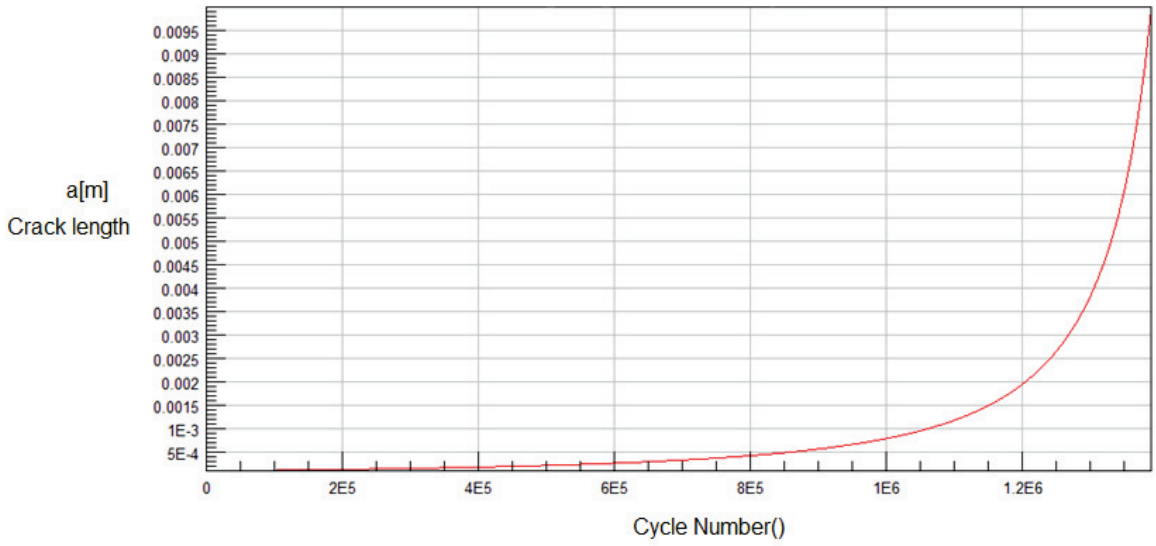

Fig. 4.8: Results using standard SIF equation

A comparison between integrate library solution and standard SIF equation is shown inFig. 4.9. The stress intensity at small crack lengths is significantly higher than the analytically SIF-formulae for this type of welded jont.

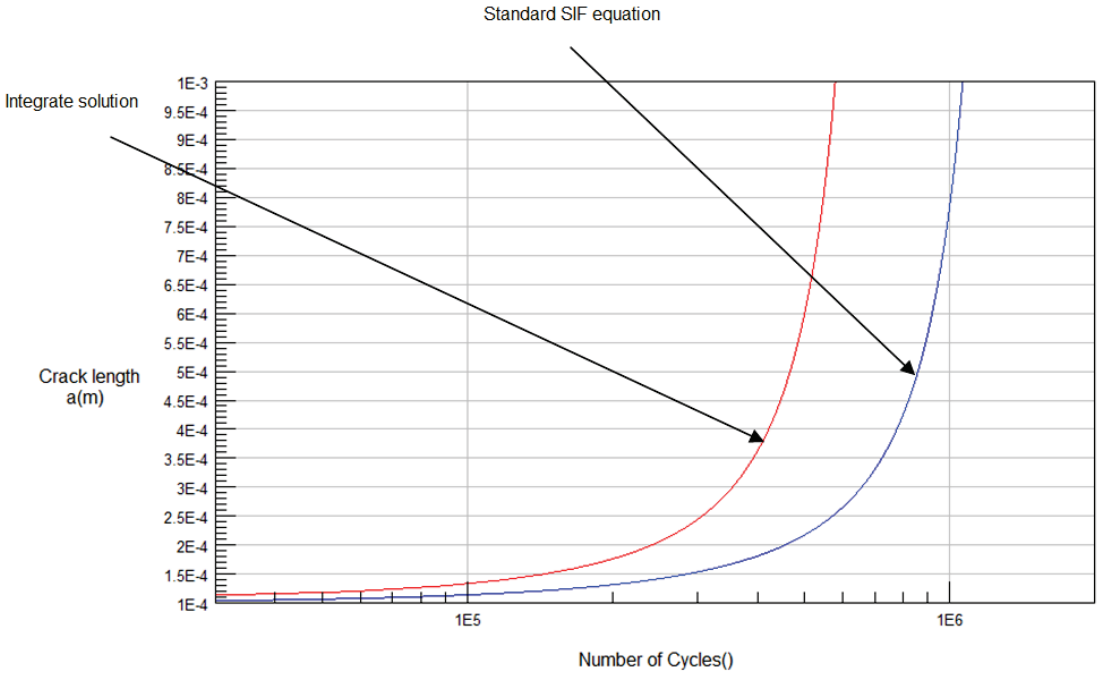

Fig. 4.9: Integrated library solution vs. standard SIF equation

4.2.1.3. Solution using ksn file

SIF equation from Rooke and Cartwright (ROOKE et al. 1976) shown in Equ. (4.1) is solved using MathCAD, for a crack ratio between 0.2 and 0.8. These limits were

chosen because of the fact that the integrated library solution limits the SIF-values in a range between twenty and eighty percent relative wall thickness. SIF values are then imported to a comma-separated spreadsheet, which can be used in nCode to generate a Ksn file. The derived SIF-course is shown in Fig. 4.10.

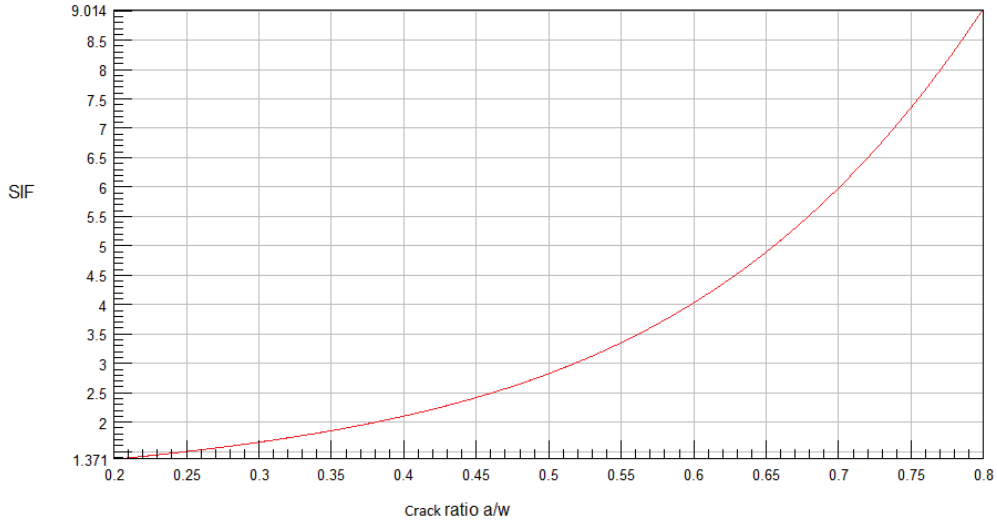

Fig. 4.10: SIF vs. crack ratio

The results obtained in nCode using ksn file in Fig. 4.11 are the same as standard library solution. The reason for the identical results in both options is the use of same SIF equation from Rooke and Cartwright (ROOKE et al. 1976) in nCode.

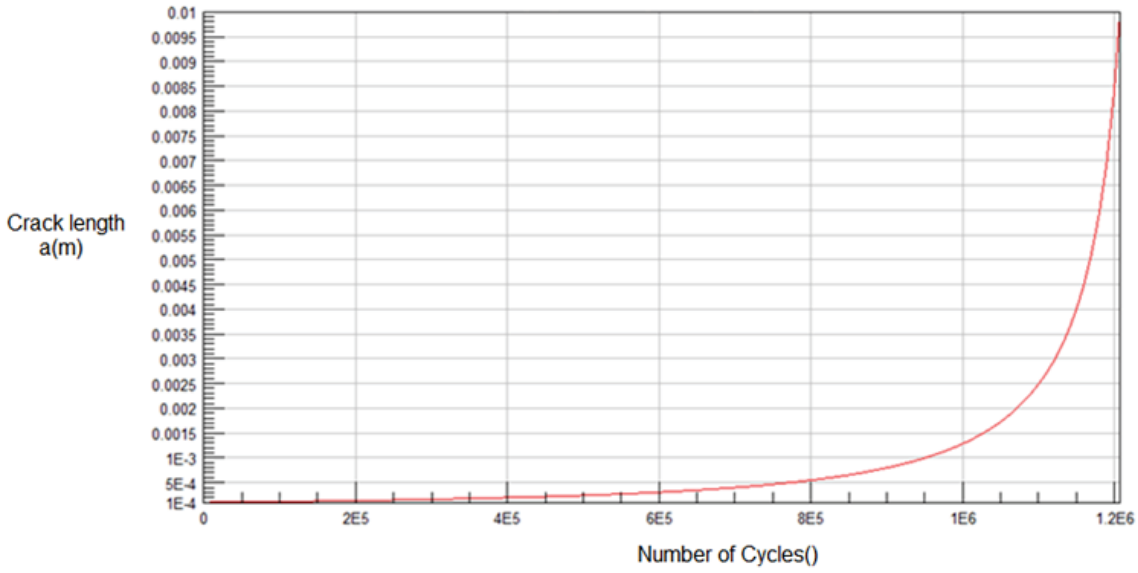

Fig. 4.11: results using ksn file

4.2.2. Simulation process of task 2 using nCode

Analytical investigation of tensile bar with a welded on transverse attachment using nCode is performed with the integrate library solution and by use of a ksn-file for two different stress intensity factor equations.

4.2.2.1. Integrate library solution

In case of welded joints the integrate library solution gives a very high number of cycles compared to that in the IIW document. It takes *1.022e6* cycles to reach the crack length of *10 mm* (Fig. 4.12).

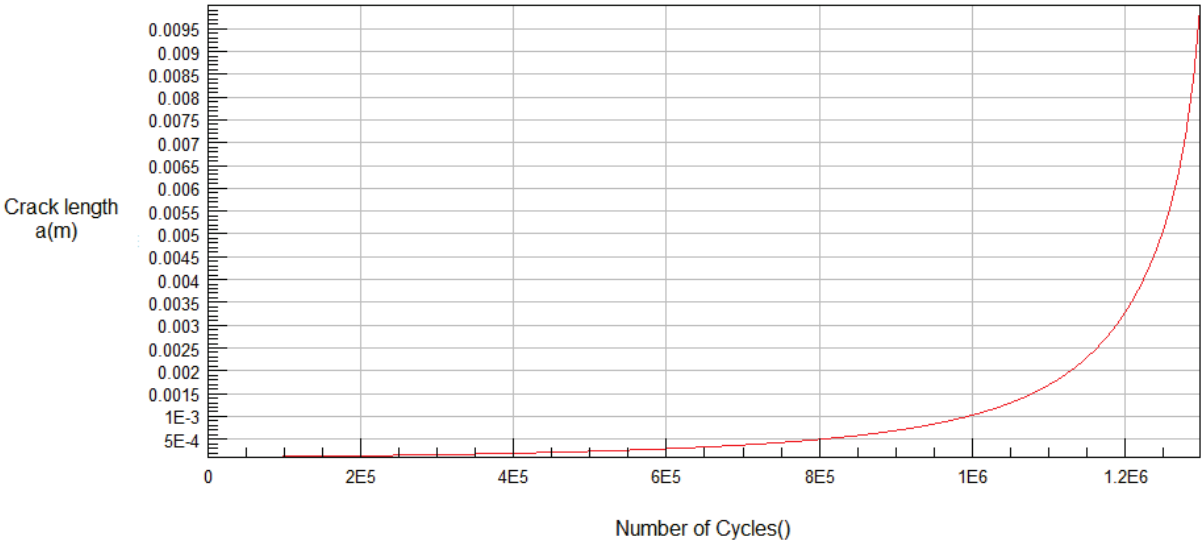

Fig. 4.12: Crack length vs. number of cycles

4.2.2.2. Solution using ksn file

Further investigations of welded joint are done using ksn file for the SIF-calculation. A single edge crack formula from Rice and Leavy is used with a correction function from Maddox (Maddox 1975). The effect of weld toe angle is captured by dividing the calculation SIF into a angle-dependent part SIF1 and an independent value SIF2 (Michel 2012).

$$\mathrm{At}(a,\theta) = 13.09610^{-3} + 28.11910^{-3}.\theta - 139.4510^{-6}.\theta^2 \quad \text{Equ. (4.2)}$$

$$\mathrm{ft}(a,\theta) = \left(10\frac{a}{w}\right)^{-5\log(\mathrm{At}(\theta)).0.4342945} \quad \text{Equ. (4.3)}$$

$$M(a) = 1.112 - 0.231\left(\frac{a}{w}\right) + 10.55\left(\frac{a}{w}\right)^2 - 21.7\left(\frac{a}{w}\right)^3 + 33.19\left(\frac{a}{w}\right)^4 \quad \text{Equ. 4.4)}$$

$$\mathrm{Mk(a)} = 0.83\left(\frac{\mathrm{a}}{\mathrm{w}}\right)^{-0.15\left(\frac{\mathrm{a}}{\mathrm{w}}\right)^{.46}} \qquad \text{Equ. (4.5)}$$

$$\mathrm{SIF1(a)} = \mathrm{M(a).Mk(a)}\frac{\mathrm{ft(a,\theta)}}{\mathrm{ft(a,45)}} \qquad \text{Equ. (4.6)}$$

$$\mathrm{ft2} = 1 \qquad \text{Equ. (4.7)}$$

$$\mathrm{SIF2(a)} = \mathrm{M(a).Mk(a)ft2} \qquad \text{Equ. (4.8)}$$

The SIF solution is prepared using MathCad and respective data is imported to an spreadsheet file. It is then used in nCode to generate a binary ksn file. Fig. 4.13 shows respective ksn file computed in nCode.

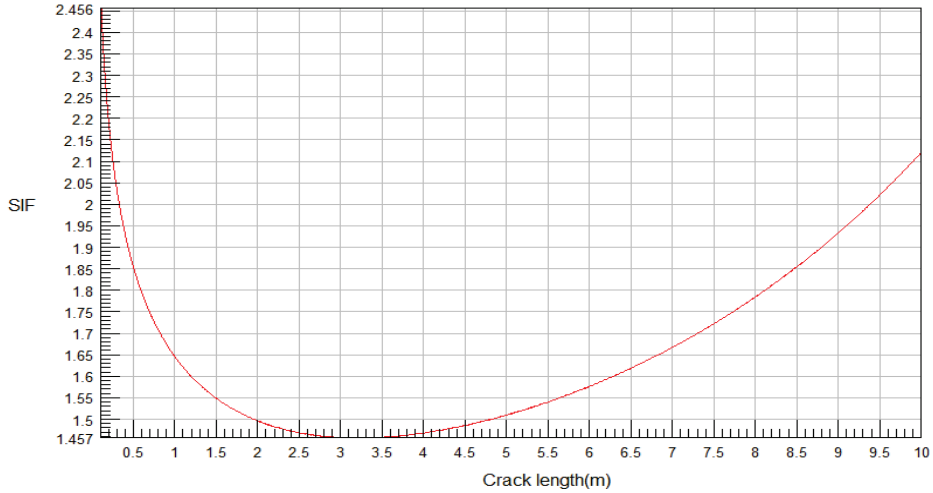

Fig. 4.13: Crack length vs. SIF

Results using this ksn file are in the range of the reported IIW-results of the Round-Robin study, shown in Fig. 4.14.

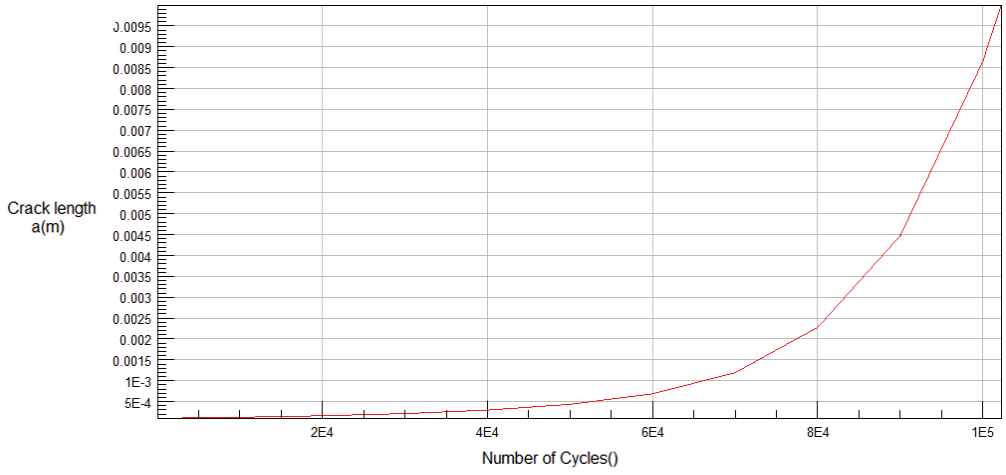

Fig. 4.14: Crack length vs. number of cycles

5. Experimental work

5.1. Specimen design

In the first phase of experimental work welded T-joints are manufactured. During the manufacturing process of welded joints, the steel plates are arranged, tacked and then welded. Specimen design is shown in Fig. 5.1.

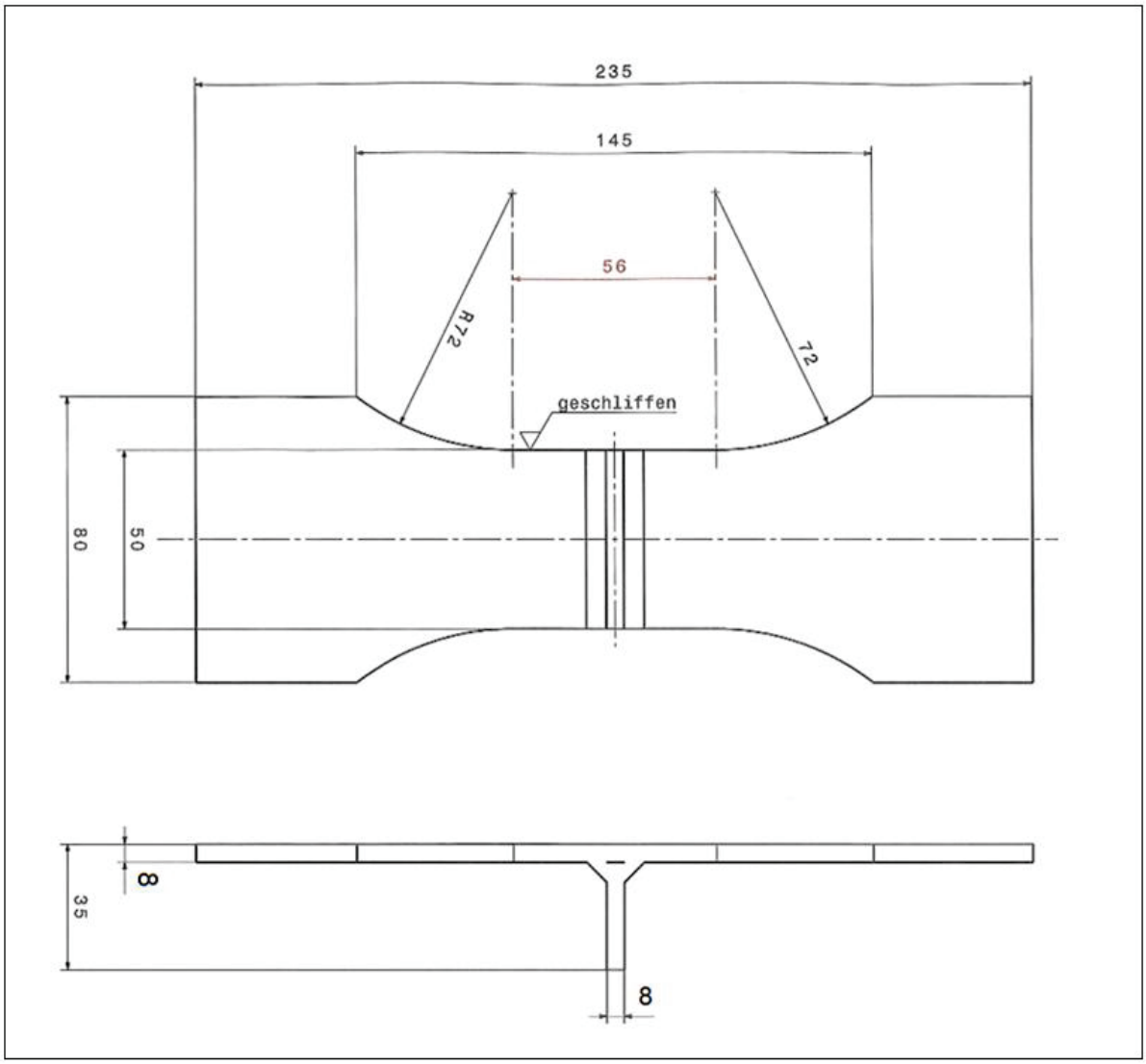

Fig. 5.1: Illustration of T-joint specimen

A number of T-joint welded specimens are manufactured at the same time to ensure similar stiffness and residual stress conditions for every single specimen (Stoschka et al. 2013). The manufacturing scheme is shown in Fig. 5.2.

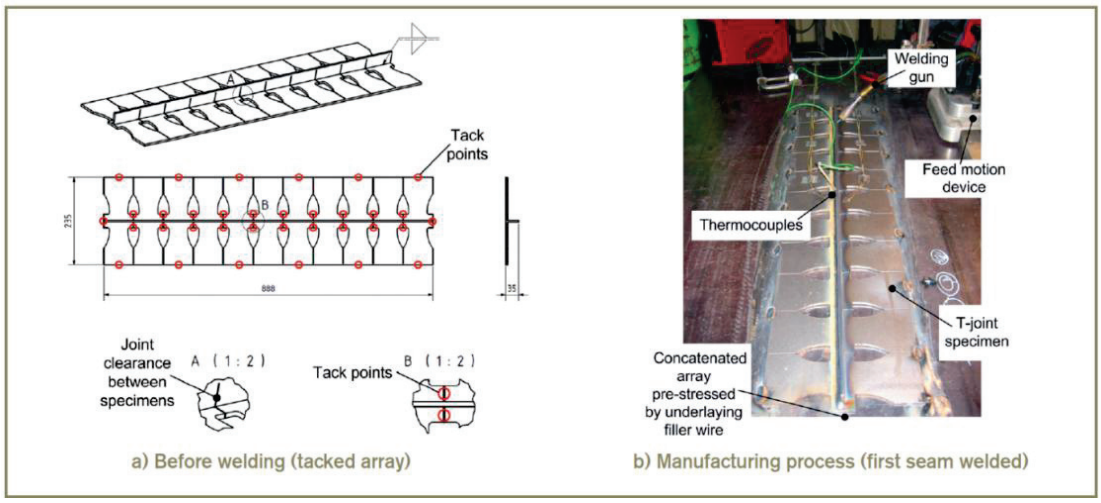

Fig. 5.2: Manufacturing process of T-joint specimen array (Stoschka et al. 2013)

5.2. Experimental investigations

These T-joints are investigated using universal resonance pulsation machine MOT600 shown in Fig. 5.3, which is suitable to apply axial, bending and tensional loads with the corresponding devices. Almost all strength-relevant components and assemblies can be tested due to the universality of such test systems. The specimens were clamped by hydraulic grips.

Fig. 5.3: MOT 600 (upper force limit 600kN)

The material used in the experimental investigation was a high-strength steel *S690* and common construction steel *S355*.

5.2.1. Testing with constant stress ratio to reflect single overload

The *S690* experiments are performed by single-block overloading to introduce macroscopic beachmarks. Probst (PROBST et al. 1974) recommended a typical overloading and fatigue cycling which make macroscopic beachmarks on the cracked surface as shown in Fig. 5.4.

The tests were performed for a stress range of $\Delta\sigma=400$ *MPa* with $R=0$ stress ratio. The experiment is performed till a reduction in frequency is detected. Reduction in frequency due to reduction in stiffness of the material indicates the presence of a macroscopic long crack in the specimen. The experiment is stopped and ten overload cycles with a stress range of $\Delta\sigma=600$ *MPa* were manually applied. After overloading, the baseline loading $\Delta\sigma=400$ was resumed till final rupture.

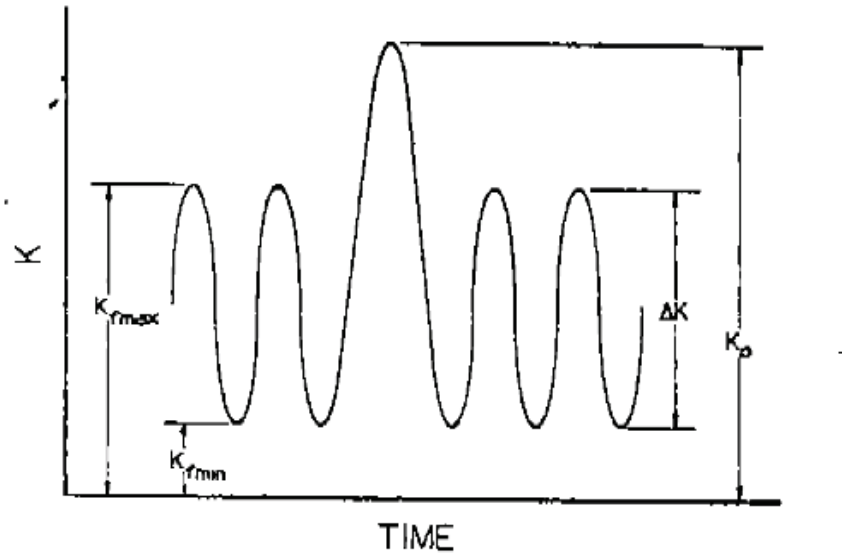

Fig. 5.4: Typical overloading and fatigue cycling used by Probst (PROBST et al. 1974)

The experimental results are documented in Tab. 5.1 depicting the block test program as well as the individual and aggregated number of cycles per load stage.

Steel S690_8mm						
Specimen No.	F_amp [kN]	F_mean [kN]	F_upper [kN]	Stress ratio R [-]	Number of cycles N	Stress range $\Delta\sigma$ [N/mm²]
Specimen1						
1_1	78,40	78,40	156,80	0.0	74,441	400,00
				Total	74,441	
Specimen2						
2_1	78,40	78,40	156,80	0.0	50,000	400,00
2_2	117,60	117,60	235,20	0.0	10	600,00
2_3	78,40	78,40	156,80	0.0	40,090	400,00
				Total	90,100	
Specimen3						
3_1	78,40	78,40	156,80	0.0	100,000	400,00
3_2	117,60	117,60	235,20	0.0	10	600,00
3_3	78,40	78,40	156,80	0.0	3,647	400,00
				Total	103.657	
Specimen4						
4_1	78,40	78,40	156,80	0.0	60,000	400,00
4_2	117,60	117,60	235,20	0.0	10	600,00
4_3	78,40	78,40	156,80	0.0	19,272	400,00
				Total	79,282	

Tab. 5.1: Experimental results of Steel S690

It can be seen that constant amplitude test result of specimen 1 exhibits a lower total burst life than the specimens objected to some overload cycles. This can be deduced to an increased crack closure effect by these single overload cycles. The fracture surface by light-optical microscopy is shown in Fig. 5.5. At about ten percent relative crack growth, a fine marker line is recognizable. This region is investigated further by use of scanning electron microscopy in Fig. 5.6. In these figures, the effect of overloading is recognizable by a characteristic change in crack tip leading to an increase in crack closure effects for the subsequent last stage of constant-amplitude-loading. The ten overload cycles change the crack tip front and the subsequent striation markers are visible in the direction of maximum shear loading.

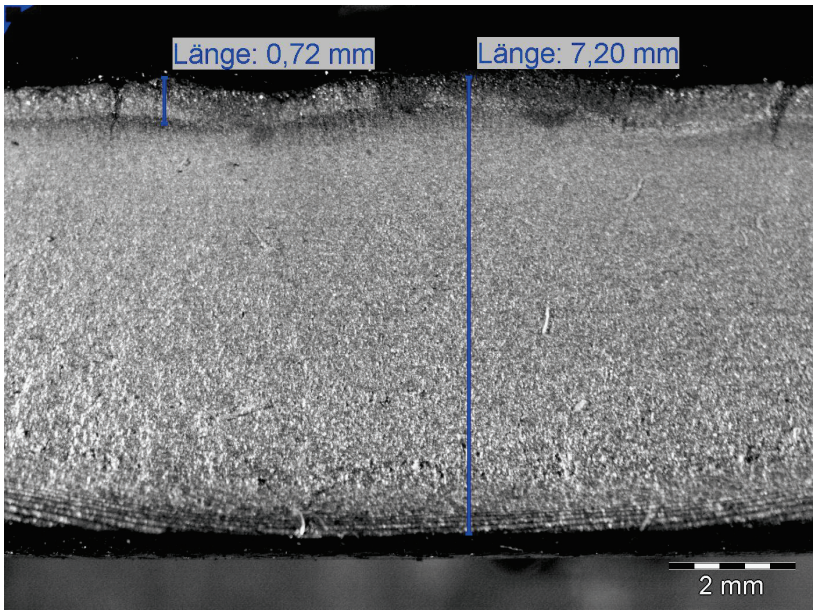

Fig. 5.5: Fracture surface of specimen number 2 of S690 tests

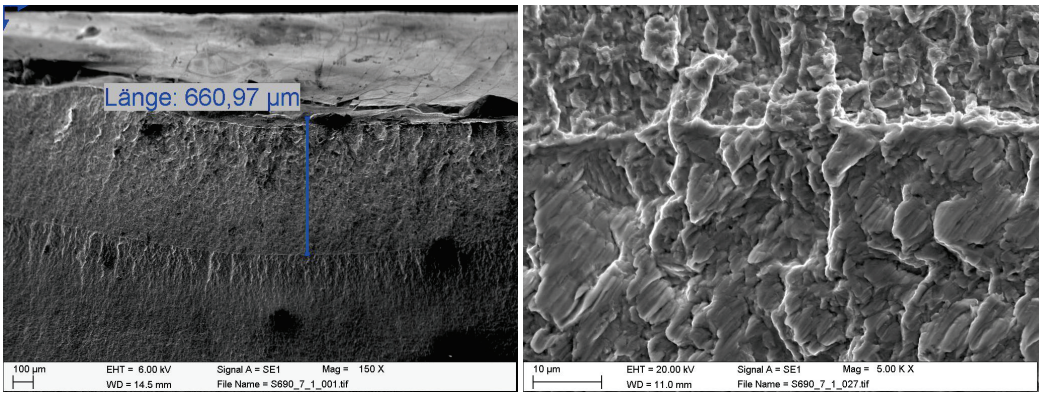

Fig. 5.6: Fracture surface of specimen number 2 using scanning electron microscopy

Summing up, the crack ratio *a/W* can be evaluated from the fracture surfaces and compared to the amount of cycles until burst failure for this type of specimens.

T-joint S690-8mm	Specimen #1	Specimen #1	Specimen #1
Crack ratio a/W	8%	22%	60%
Cyclic fraction until burst average failure	55%	66%	~100%

Tab. 5.2: Relative crack growth of S690 specimens

5.2.2. Testing with constant upper stress reflecting cyclic block loading

In case of *S355*, test program are performed according to Schijve (Schijve 2015) with large number of cycles between baseline cycles to create visible bands on the fatigue fracture surface as shown Fig. 5.7. Baseline loading was performed with tumescent

stress ratio and overloading with stress ratio of *R=0.5.* From experiments obtained result is shown in Tab. 5.3.

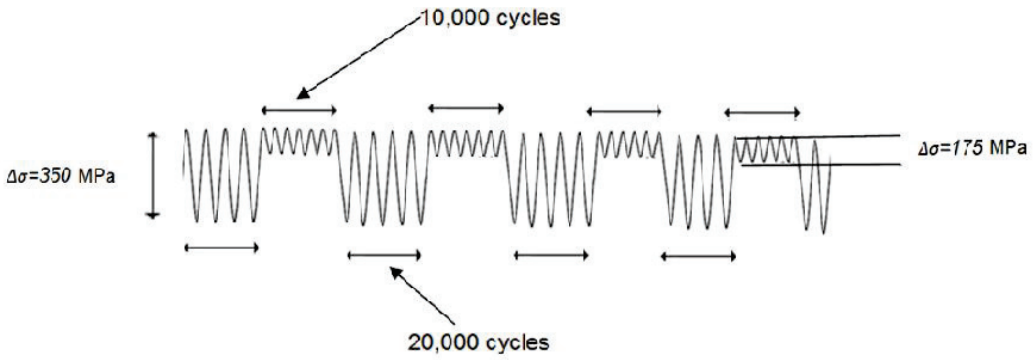

Fig. 5.7: Marker load cycles (Schijve 2015)

The one block-loaded specimen in Tab. 5.3 depicts no characteristic increase in lifetime compared to other constant amplitude test results of this joint. This can be reasoned due to the constant upper stress limit. Hence, no major additional crack close affects occur during this type of cyclic block loading.

Steel S355_8mm						
Specimen No.	F_amp [kN]	F_mean [kN]	F_upper [kN]	Stress ratio R [-]	Number of cycles N	Stress range Δσ [N/mm²]
Specimen1						
1_1	68,60	68,60	137,20	0.0	20,000	350,00
1_2	34,30	102,90	137,20	0.5	10,000	175,00
1_3	68,60	68,60	137,20	0.0	20,000	350,00
1_4	34,30	102,90	137,20	0.5	10,000	175,00
1_5	68,60	68,60	137,20	0.0	20,000	350,00
1_6	34,30	102,90	137,20	0.5	10,000	175,00
1_7	68,60	68,60	137,20	0.0	20,000	350,00
1_8	34,30	102,90	137,20	0.5	10,000	175,00
1_9	68,60	68,60	137,20	0.0	8,097	350,00
				Total	128,097	

Tab. 5.3: Experimental result block-loaded S355 steel specimen

The fracture surface focussing on the region of technical crack initiation is shown in Fig. 5.8. No characteristic plastic deformation zones are visible, instead the polycrystalline structure of the material makes it quite difficult o determine differences in crack growth. Nevertheless, the stepwise different stress ranges causes local changes in crack growth of the surface, for example by change of local crack plane angle or increased propagation along a different grain boundary at step-increased load sequence.

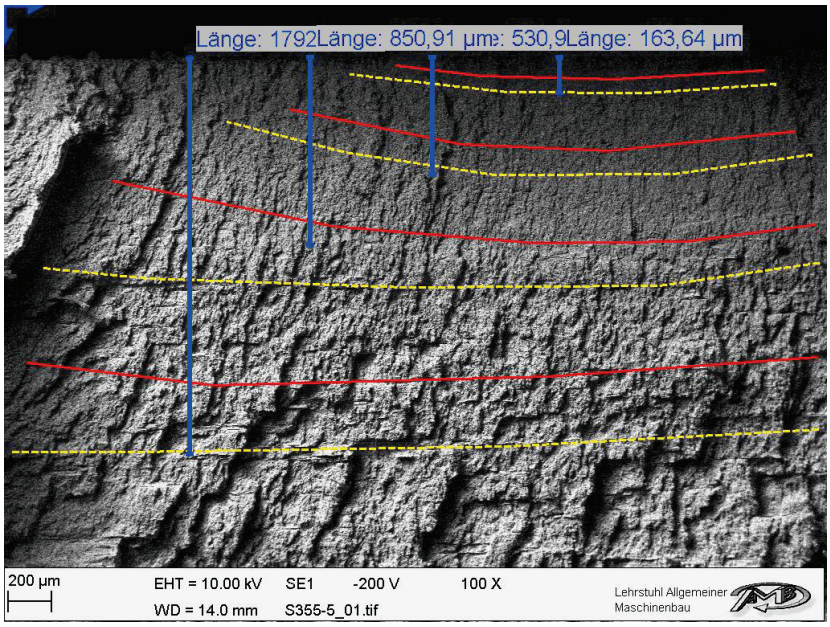

Fig. 5.8: Fracture surface of specimen number 1 of S355 block testing

The evaluation of the light-optical-microscopy depicted fracture surface was supported by scanning-electron-microscopy to detect local, for example grain-boundary influenced, striation markers during crack propagation of the mild steel specimen. The relation between aggregated block test cycles and corresponding crack growth length is shown in Fig. 5.9. The majority of lifetime is needed to propagate the crack within the first millimetre plate depth.

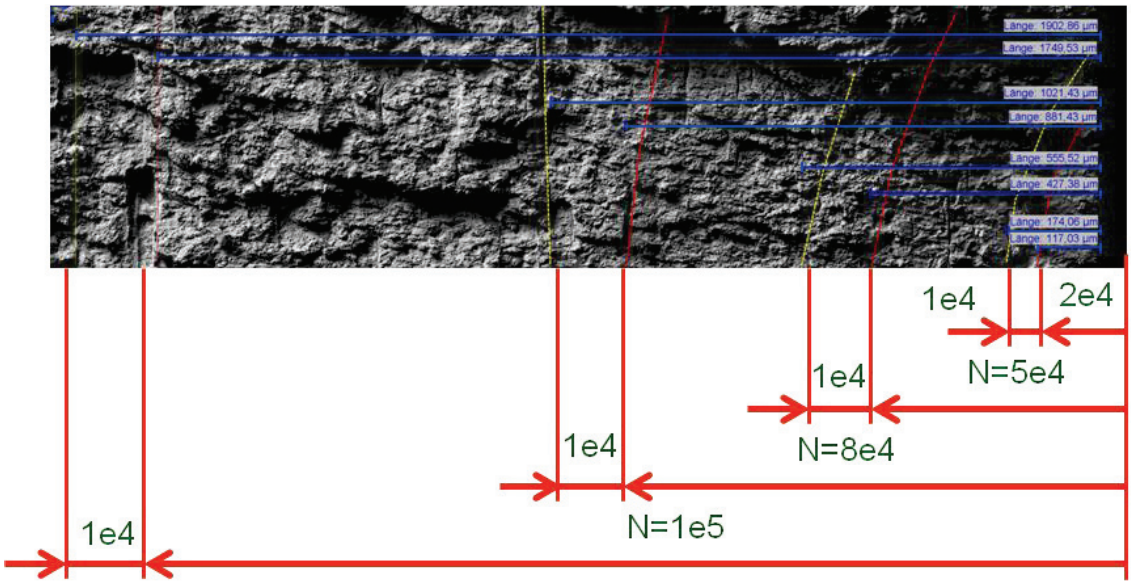

Fig. 5.9: Block test cycles compared to crack growth length

5.3. Calculated lifetime

Fracture mechanical calculations are done to simulate the lifetime of the experimentally used specimen geometry. An extensive set of numerical Franc2D calculations are performed using numerous different material parameters given in guidelines, recommendations and published literature. Beside the study of applicable material parameters for the investigated S690 high-strength steel non-load carrying transversal attachments, the influence of initial crack length was examined.

Recommendation *da/dN [mm/c]* $\Delta K[N.mm^{-2/3}]$	Material	m[-]	c	a_i[mm]	N at 0.76mm crack length	N at 1.53mm crack length	N at 4.93mm crack length	N at 8mm crack length
IIW(Hobbacher 2013)	Steel	3	$5.21e^{-13}$	0.01	17,100	19,000	19,500	19,900
				0.05	7,900	9,500	10,250	10,250
				0.1	5,600	7,300	7,800	7,900
				0.15	4,450	6,070	6,100	6,700
(Henkel 1985)	Structural steel	3.16	$6.351e^{-14}$	0.01	54,000	59,000	61,000	61,300
				0.05	23,100	27,800	29,600	29,600
				0.1	15,970	20,500	22,300	22,900
				0.15	13,100	17,500	19,000	19,000
FKM(Forschungskuratorium Maschinenbau 2001)	StE47 Rm =630[MPa]	2.26	$2.31e^{-11}$	0.01	33,900	41,000	44,500	44,900
				0.05	18,800	25,000	28,800	29,250
				0.1	14,400	20,400	24,100	24,600
				0.15	11,400	18,300	21,000	21,600
FKM(Forschungskuratorium Maschinenbau 2001)	26 NiCrMoV14 5 $R_{p0.2}$=690[MPa]	2.76	$9.56e^{-13}$	0.01	40,000	45,000	47,400	47,900
				0.05	19,000	23,800	26,400	26,500
				0.1	13,900	18,900	20,800	21,200
				0.15	10,700	16,200	18,200	18,200
Huth(Huth 1979)	Structural steel	2.7	$2.54e^{-11}$	0.01	2,190	2,450	2,590	2,610
				0.05	1,050	1,320	1,470	1,470
				0.1	760	1,040	1,100	1,180
				0.15	610	880	1,000	1,030
(ESCS-Report 2001)	S690QLI	3	$2.17e^{-13}$	0.01	41,000	45,700	47,200	47,700
				0.05	18,400	22,400	24,500	24,600
				0.1	13,500	17,500	19,000	19,000
				0.15	9,800	14,050	15,000	15,300
(Gurney 1979)	S690	2.17	$3.31e^{-11}$	0.01	39,900	49,500	55,500	56,000
				0.05	23,400	31,100	36,500	37,100
				0.1	17,700	26,100	31,400	31,900
				0.15	15,000	22,800	27,800	28,200
(Al Mukhta)	S690	2.25	$2.96e^{-11}$	0.01	38,200	32,800	37,200	37,700
				0.05	15,300	20,600	24,000	24,100
				0.1	13,500	17,500	19,000	19,000
				0.15	9600	15,000	18,100	18,400

Tab. 5.4: Simulation results using different material parameter and initial crack length

It is further on shown that the initial crack length is the most important factor for crack propagation and total life time. A detailed study of the initial crack length shows that a value of *0.01mm* is well applicable for the fatigue-tested high strength steel specimen under the assumption of a sharp-notched weld toe. The simulation results are condensed in Tab. 5.4.

The most conservative simulation results are obtained for structural steel using the material parameter *m= 2.7* and *C=2.54e-11* according to the FKM-guideline (Forschungskuratorium Maschinenbau 2001).
On the other hand, the results obtained by using material parameter from Gurney (Gurney 1979) shows a relative high number of cycles compared to FKM recommendations but are still in the safe range compared to the experimental results.

Calculation of relative cycle fraction is performed using results from Tab. 5.4 with material parameter according to gurney (Gurney 1979) and given in Tab. 5.5.

	a_i[m]	**N at 0.76mm crack length**	**N at 1.53mm crack length**	**N at 4.93mm crack length**	**N at 8mm crack length**
(Gurney 1979)	0.01	39,900/56,000 =71[%]	49,500/56,00 =88[%]	55,500/56,000 =99[%]	56,000
	0.05	23,400/37,100= 63[%]	31,100/37,100 =83[%]	36,500/37,100 =98[%]	37,100
	0.1	17,700/31,900 =55[%]	26,100/31,900 =81[%]	31,400/31,900 =98[%]	31,900
	0.15	15,000/28,200 =53[%]	22,800/28,200 =80[%]	27,800/28,200 =99[%]	28,200

Tab. 5.5: Relative cycle number from simulation results in [%]

A calculation of crack growth fraction in regard to sheet thickness is carried and shown in Tab. 5.6.

N at 0.76mm crack length	**N at 1.53mm crack length**	**N at 4.93mm crack length**	**N at 8mm crack length**
0.76/8 =9.5[%]	1.53/8 =19.1[%]	4.93/8 =61.6[%]	8/8 =100[%]

Tab. 5.6: Relative sheet thickness in [%]

Finally, a calculation of relative cycle numbers from experimental investigation are done by using the experimental results from Tab. 5.1 and presented in Tab. 5.7.

Specimen1 (With overload)	**Specimen2** (With overload)	**Specimen3** (With overload)	**Specimen4** (Without overload)
50,000/75,000 =67[%]	60,000/75,000 =80[%]	100,000/75,000 =95[%] assumed	75,000/75,000 =100[%]

Tab. 5.7: Relative cycle numbers from experiments in [%]

A graphical evaluation, using data from Tab. 5.5, Tab. 5.6 and Tab. 5.7 is performed to sketch the relationship between sheet thickness and fatigue life and presented in Fig. 5.10. By observing the diagram, it can be seen that during crack propagation fifty percent of fatigue life is spent in first ten percent of the sheet thickness. At twenty percent wall thickness the crack growth has spent about eighty percent of cycles until burst fracture. The results match the experimental and fracture surface investigations quite well.

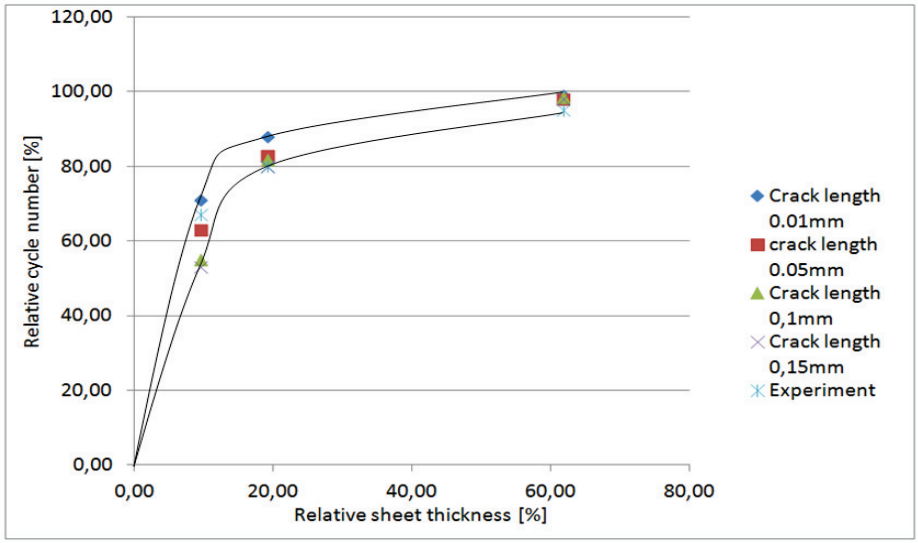

Fig. 5.10: Relation between relative sheet thickness and relative cycle numbers

The variation of fatigue life using different material parameters is shown in Fig. 5.11. From diagram it can be seen that material parameters used from the IIW-recommendations give relative conservative results. Most critical results with lower number of cycles is obtained with material parameter used from Huth (Huth 1979).

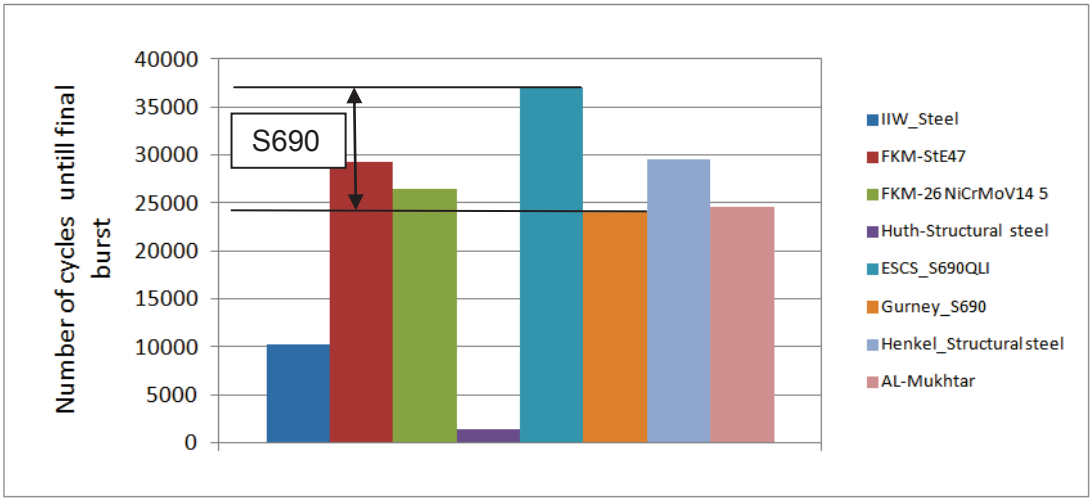

Fig. 5.11: Effect of different material parameter on fatigue life

The reason for these unexpected results is, that the material parameters which are used for crack propagation analysis, are only valid for a wide range of steels possessing also defected components (Fig. 5.12).

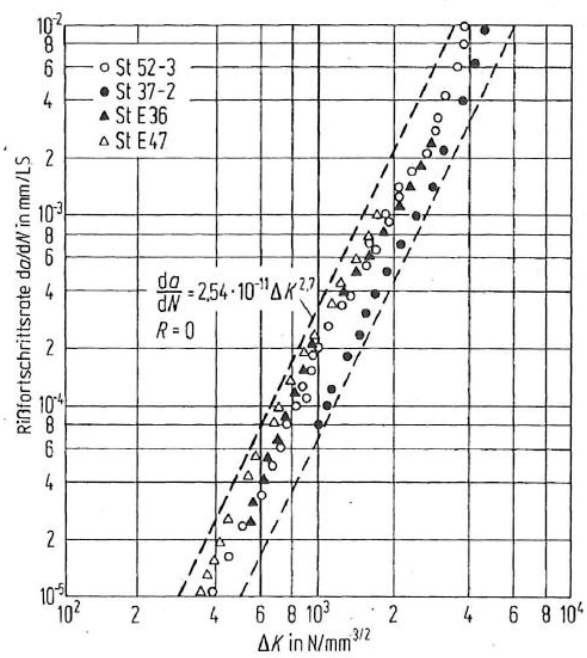

Fig. 5.12: Crack propagation behaviour with upper and lower limit curve for different structural steel (Berger et al. 2009)

Except Huth, all other results obtain from different literate are in safe scatter range for welded joints. This can be reasoned by the recommended stress scatter band of $1{:}T_S{=}1{:}1.5$ for welded joints. If a inverse slope of $k{=}3$ is applied, the subsequent

scatter range in term of load cycles is about *1:T_N=1:3.4*. This scatter band reflects the examined fracture mechanical analysis results quite well.

If only S690 high-strength steel results are compared, then the scatter band changes to about *1:1.5* in terms of life cycles. It can be concluded that the applicable set of fracture mechanical parameters has to be adjusted to the material parameters, but also the effective weld toe radius should be taken into account for comparison purposes to get correct stress intensities for weld toe failure.

6. Summary

The study of fatigue crack growth is important in fatigue strength of engineering components and their service life. The aim of this master-thesis is the numerical, analytical and experimental investigation of crack propagation in welded joints. A comparative study of crack propagation design tools such as Franc2D and nCode is done on different structural details. Special focus was laid on crack propagation for a standard single edge crack plate and welded joints ranging from non-load carrying transversal stiffener to partial penetrated load-carrying transversal stiffener. This enables a direct comparison to the results given by IIW-Round Robin document.

The material data for the Franc 2D crack propagation simulation was taken from the IIW-recommendations. The Franc2D-based numerical number of life cycles matches the recommended values. The obtained results are slightly conservative because of user-dependent internal Franc2D integration procedure settings. The analytical tool nCode offers several possibilities to define the stress intensity factor further used in crack-propagation analysis. The default weld joint SIF´s are only valid within twenty to eighty percent crack length related to the wall thickness. The more accurate analytical calculation of the SIF based on SIF-equations such as e.g Cartwright and Tada leads to the definition of an advanced SIF versus crack length table. In case of welded joints, the non-linear stress peak can be incorporated by e.g Maddox equation into an aggregated SIF relation. The comparative investigation based on the IIW-Round Robin document exhibits a quite strong conservative fatigue life based on the integration procedure used in nCode. Summing up the preliminary work based on the IIW-Round Robin procedure, about ninety percent of the total life time under cyclic loading is spent within the first twenty percent wall thickness.

The experimental work focuses on the creation and microscopic assessment of the blocked constant amplitude fatigue test with and without overloads. The investigated material range from common construction steel S355 to a high-strength steel S690. Single overload cause macroscopic beach marks which can be detected by light-optical-microscopy. But striation markers within the polycrystalline microstructure are only detected by scanning-electron-microscopy. The quite heterogeneous grain

distribution and grain orientation of the investigated steel fracture surface activates several slip planes. The crack growth is transgranular at low stress intensity factor values and gets further on intergranular. The crack growth of a fatigue block tested specimen is analysed by SEM. Characteristic striation markers are recognisable and basically match the numerically obtained crack propagation results.

Finally an extensive set of numerical Franc2D calculations was done using the material parameters based on the recently published IIW-document, FKM guideline and the article written by Gurney. Initial crack length is the most important factor in fatigue life assessment of welded joints. A study of initial crack length showed that a value of a_{init} =*0.01mm* is well applicable for the fatigue tested high strength steel specimens. A comparison between simulation and experimental results proved that all crack growth parameters leads to a safe design if the initial crack length is not lower than *0.01mm* gives a defined crack length, all evaluated material parameters lead to fatigue life which is below the recommended scatter range.
It has to be mentioned that this evaluated quite low initial crack length is only meaningful if the theoretically fillet weld cross section is applied, for example in this study a weld toe angle of forty-five degrees and a sharp transition without notch radius in the weld toe area.

Further work should focus on the effect of notch radius on initial crack length, for example by evaluating specimens weld toe radii. A shallower notch reduces the local stress intensity and may subsequently increase the applicable crack initiation length up to the IIW-recommended range of *0.1mm* to *0.15mm* for crack initiation. In addition, the effect of mean stresses can be incorporated by use of the effective stress intensity factor to study the influence of residual and mean stress effects on fatigue strength.

7. Literature

1 E647, 2000: Standard Test Method for Measurement of Fatigue Crack Growth Rates.

2 Anderson, Ted L. (2005): Fracture mechanics. 3rd ed. Boca Raton, FL: Taylor & Francis.

3 Barenblatt, G. (Hg.) (1962): Advances in Applied Mechanics Volume 7: Elsevier (Advances in Applied Mechanics).

4 Berger, Christina; Blauel, Johann Georg; Hodulak, Ludvik; Pyttel, Brita; Igor, Varfolomeyev (2009): FKM-Richtlinie_Bruchmechanischer Festigkeitsnachweis_2009.

5 Bordas, Stéphane; Brian, Moran (2006): Enriched finite elements and level sets for damage tolerance assessment of complex structures. In: *Engineering Fracture Mechanics* 73 (9), S. 1176–1201.

6 Bowness, D.; Lee, M.M.K (1996): Stress intensity factor solutions for semi-elliptical weld-toe cracks in T-butt geometries. In: *Fat Frac Eng Mat Struct* 19 (6), S. 787–797.

7 BS-7910 (2005): Guide to methods for assessing the acceptability of flaws in metallic structures.

8 Bueckner, H. F. (1970): Novel principle for the computation of stress intensity factors. Unter Mitarbeit von Akademie-Verlag GmbH (00032129).

9 Burdekin, F. M.; Stone, D. E. W. (1966): The crack opening displacement approach to fracture mechanics in yielding materials. In: *The Journal of Strain Analysis for Engineering Design* 1 (2), S. 145–153.

10 Claudio, R A; Maia, J; Dias, J M; Pereira,; Baptista,, R; Branco,, C M; Byrne, J (2004): Development of a DC potential drop system controlled by computer.

11 Cook, Robert Davis (1995): Finite element modeling for stress analysis. New York: Wiley.

12 Cruse, T A (1977): Mathemmatical formulation of the boundary integral equation methods in solid mechanics, Pratt and Whitney Aircraft Group.

13 Diaz, A A; Mathews:J. Hixon1, R A; Doctor, S R (2007): Assessment of Eddy Current Testing for the Detection of Cracks in Cast Stainless Steel Reactor Piping Components, Division of Fuel, Engineering, and Radiological Research, Division of Nuclear Regulatory Research, U.S. Nuclear Regulatory Commission.

14 Dugdale, D. S. (1960): Yielding of steel sheets containing slits. In: *Journal of the Mechanics and Physics of Solids* 8 (2), S. 100–104.

15 Engesvik, Knut M.; Moan, Torgeir (1983): Probabilistic analysis of the uncertainty in the fatigue capacity of welded joints. In: *Engineering Fracture Mechanics* 18 (4), S. 743–762.

16 Erdogan, F.; Sih, G. C. (1963): On the Crack Extension in Plates Under Plane Loading and Transverse Shear. In: *J. Basic Engineering* 85 (4), S. 519.

17 ESCS-Report (2001): High strength steel in welded state in lightweight construction under high and variable stress peak, final report European Commision ,Luxembourg.

18 Farahmand, Bahram (2001): Fracture mechanics of metals, composites, welds, and bolted joints. New York: Springer.

19 Fischer-Cripps, Anthony C. (2007): Introduction to contact mechanics. 2nd ed. New York: Springer (Mechanical engineering series).

20 Forschungskuratorium Maschinenbau (2001): Bruchmechanischer Festigkeitsnachweis für Maschinenbauteile. 1. Ausg. Frankfurt am Main (FKM-Richtlinie), zuletzt geprüft am 03.07.2013.

21 Giner, E; Sukumar, N (2009): An Abaqus implementation of the extended finite element method.

22 Griffith, A. A. (1920): The Phenomena of Rupture and Flow in Solids. In: *Philosophical Transactions, Series A* 221, S. 163–198.

23 Gupta, O. P. (1999): Finite and boundary element methods in engineering. Rotterdam, Netherlands, Brookfield, Vt.: A.A. Balkema.

24 Gurney, T. R. (1979): Fatigue of welded structures. 2d ed. Cambridge [England], New York: Cambridge University Press.

25 Henkel, C. (1985): Beitrag zur bruchmechanischen Bewertung des Risswachstumsverhaltens höherfester schweiß-bar Baustähle und deren Schweißverbindungen unter zyklisch mechanischer Beanspruchung.

26 Henshell, R. D.; Shaw, K. G. (1975): Crack tip finite elements are unnecessary. In: *Int. J. Numer. Meth. Engng.* 9 (3), S. 495–507.

27 Hobbacher, Adolf (2009): The new IIW recommendations for fatigue assessment of welded joints and components – A comprehensive code recently updated. In: *International Journal of Fatigue* 31 (1), S. 50–58.

28 Hobbacher, Adolf (2013): Final Report of IIW Round Robin Calculations on Fatigue Assessment of Welded Joints by Fracture Mechanics, International Institute of Welding (IIW-Doc., XIII-2476-13), zuletzt geprüft am 19.09.2013.

29 Hutchinson, J. W. (1968): Singular behaviour at the end of a tensile crack in a hardening material. In: *Journal of the Mechanics and Physics of Solids* 16 (1), S. 13–31.

30 Huth, H. (1979): Berechnungsunterlagen zur Rißfor tschritts- und Restfestigkeitsvorhersage rißbe-hafteter Großbauteile.

31 Inglis, C. E. (1913): Stresses in a plate due to the presence of cracks and sharp corners. In: *Trans. Inst. Nav. Archit*, S. 219–230.

32 Irwin, G. R. (1947): Fracture Dynamics. In: ASM (Hg.): Symposium Fracturing of Metals. Trans. ASM 40A. Cleveland, S. 147–166.

33 Irwin, G. R. (1956): Onset of fast crack propagation in high strength steel and aluminium alloys, AD0099305, Naval Research Lab Washington DC.

34 Irwin, G. R. (1961): Plastic Zone Near a Crack and Fracture Toughness. In: *Sagamore Research Conference Proceedings* (Vol. 4), S. 63–78.

35 Jiang, Shouyan; Ying, Zongquan; Du, Chengbin (2010): The optimal XFEM approximation for fracture analysis. In: *IOP Conf. Ser.: Mater. Sci. Eng.* 10, S. 012067.

36 Kloos, K. H. (1989): kerbwirkung und schwingfestigkeitseigenschaften, DVM-Berihte.

37 Lesulauro, Erin: A crack propagation simulator for plane layered structures.version 1.5 User guide.

38 Maddox, S. J. (1975): An analysis of fatigue cracks in fillet welded joints. In: *Int J Fract* 11 (2), S. 221–243.

39 Marsh, K. J.; Smith, R. A.; Ritchie, R. O. (1991): Fatigue crack measurement. Cradley Heath, Warley [England]: Engineering Materials Advisory Services.

40 Mi, Y.; Aliabadi, M. H. (1992): Dual boundary element method for three-dimensional fracture mechanics analysis. In: *Engineering Analysis with Boundary Elements* 10 (2), S. 161–171.

41 Mi, Y.; Aliabadi, M. H. (1994): Three-dimensional crack growth simulation using BEM. In: *Computers & Structures* 52 (5), S. 871–878.

42 Michel, Marzin (2012): CASE STUDIES OF CRACK PROPAGATION IN WELDED COMPONENTS.

43 Motarjemi, A.Khodadad; Kokabi, A. H.; Ziaie, A. A.; Manteghi, S.; Burdekin, F. M. (2000): Comparison of the stress intensity factor of T and cruciform welded joints with different main and attachment plate thickness. In: *Engineering Fracture Mechanics* 65 (1), S. 55–66.

44 Newman, J. C.; Raju, I. S. (1983): Stress-Intensity Factor Equations for Cracks in Three-Dimensional Finite Bodies, ASTM STP 791. In: J. C. Lewis und G. Sines (Hg.): Fracture Mechanics: Fourteenth Symposium - Volume I: Theory and Analysis: ASTM International, S. I238-I265.

45 Newman, J. C.; Yamada, Y. (2010): Compression precracking methods to generate near-threshold fatigue-crack-growth-rate data. In: *International Journal of Fatigue* 32 (6), S. 879–885.

46 Niu, X.; Glinka, G. (1989): Stress-intensity factors for semi-elliptical surface cracks in welded joints. In: *Int J Fract* 40 (4), S. 255–270.

47 Nykänen, Timo; Li, Xiaoyan; Björk, Timo; Marquis, Gary (2005): A parametric fracture mechanics study of welded joints with toe cracks and lack of penetration. In: *Engineering Fracture Mechanics* 72 (10), S. 1580–1609.

48 Orowan, E. (1948): Fracture and Strength of Solids. Reports on Progress in Physics, Vol. XII.

49 Ozelo, R R; Sollero, P; Sato, M; Barros, R S.V (2009): Monitoring crack propagation using digital image correlation and cod technique.

50 Paris, c Paul; Gomez, p Mario; Anderson, E William (1961): Paris-Gomez-Anderson1961-A-RationalAnalyticTheory-of-Fatigue.

51 Portela, A.; Aliabadi, M. H.; Rooke, D. P. (1992): The dual boundary element method: Effective implementation for crack problems. In: *Int. J. Numer. Meth. Engng.* 33 (6), S. 1269–1287.

52 PROBST, E. P.; HILLBERRY, B. M. (1974): Fatigue Crack Delay and Arrest Due to Single Peak Tensile Overloads. In: *AIAA Journal* 12 (3), S. 330–335.

53 Radaj, D. (1996): Review of fatigue strength assessment of nonwelded and welded structures based on local parameters. In: *International Journal of Fatigue* 18 (3), S. 153–170.

54 Rice, J. R. (1968): A Path Independent Integral and the Approximate Analysis of Strain Concentration by Notches and Crack. Journal of Applied Mechanics, Division of engineering Brown university providence,R.I.

55 Rice, J. R.; Rosengren, G. F. (1967): Plane Strain Deformation near a Crack Tip in a Power-Law Hardening Material. Journal of the Mechanics and Physics of Solids. Hg. v. Brown univ providenced RI DIV of engineering.

56 Richards, C E; Deans, W F: The Measurement of Crack Length and Load Using Strain Gauges.

57 ROOKE, David Percy; Cartwright, D. J. (1976): Compendium of stress intensity factors. London: H.M.S.O.

58 Saguy, H.; Rittel, D. (2005): Bridging thin and thick skin solutions for alternating currents in cracked conductors. In: *Appl. Phys. Lett.* 87 (8), S. 084103.

59 Saguy, H.; Rittel, D. (2007): Flaw detection in metals by the ACPD technique: Theory and experiments. In: *NDT & E International* 40 (7), S. 505–509.

60 Schijve, Jaap (2015): The application of small overloads for fractography of small fatigue cracks initiated under constant-amplitude loading. In: *International Journal of Fatigue* 70, S. 63–72.

61 Schmid, Steven R. (2013): Fundamentals of Machine Elements, Third Edition: Taylor & Francis Group.

62 Shaw, R. D.; Pitchen, R. G. (1978): Modification to the Suhara-Fukuda method of network generation. In: *Int. J. Numer. Meth. Engng.* 12 (1), S. 93–99.

63 Shukla, Arun (2005): Practical fracture mechanics in design. 2nd ed., rev. and expanded. New York: Dekker (Mechanical engineering, 183).

64 Singh, Krishna Lok; Keswani, Kamal; Mallikarjun, Vaggar (2012): Crack growth simulation of stiffened fuselage panels using XFEM techniques.

65 Soheil, Mohammadi (2007): Extended Finite Element Method: Wiley-Blackwell.

66 Stoschka, Michael; Leitner, Martin; Posch, Gerhard; Eichlseder, Wilfried (2013): Effect of high-strength filler metals on the fatigue behaviour of butt joints. In: *Weld World* 57 (1), S. 85–96.

67 Sukumar, N.; Prévost, J.-H (2003): Modeling quasi-static crack growth with the extended finite element method Part I: Computer implementation. In: *International Journal of Solids and Structures* 40 (26), S. 7513–7537.

68 Sukumar., N; Moes, N.; Moran, B; Belytschko, T (2009): Extended finite element method for three-dimensional crack modelling.

69 Sullivan, A. M.; Crooker, T. W. (1977): A crack-opening-displacement technique for crack length measurement in fatigue crack growth rate testing—development and evaluation. In: *Engineering Fracture Mechanics* 9 (1), S. 159–166.

70 Sutton, M. A.; Wolters, W. J.; Peters, W. H.; Ranson, W. F.; McNeill, SR (1983): Determination of displacements using an improved digital correlation method. In: *Image and Vision Computing* 1 (3), S. 133–139.

71 Vanlanduit, Steve; Vanherzeele, Joris; Longo, Roberto; Guillaume, Patrick (2009): A digital image correlation method for fatigue test experiments. In: *Optics and Lasers in Engineering* 47 (3-4), S. 371–378.

72 Vendroux, G.; Knauss, W.G (1994): deformation measurements at the sub-micro size scale.

73 Wang, C H (1996): Introduction ot fracture mechanics ,DSTO-GD-0103 ;PRDSTO Aeronautical and Maritime Research Laboratory.

74 Wells, A.A (Hg.) (1961): Unstable Crack Propagation in Metals:, Cleavage and Fast Fracture. Cranfield, UK, Royal Society.

75 Wells, A.A (1963): Application of fracture mechanics at and beyond general yield. Hg. v. British Welding Research Association Report 01/1963 und 10:563--570.